Unified Differentially Private Stochastic Gradient Descent with Tail-Aware Discriminative Clipping

Paper ID: 56

Abstract

Differentially Private Stochastic Gradient Descent (DPSGD) is a *de facto* and principled approach for training deep models with formal privacy guarantees, where per-sample gradient clipping is a key technique that shrinks the L_2 norm of each sample's gradient into a specific threshold to stabilize training. Most prior works assume that the stochastic gradient variability (GV) follows a light-tailed distribution (e.g., sub-Gaussian) to determine optimal clipping thresholds. However, recent studies show that GV in deep learning often exhibits heavy-tailed behavior, leading to excessive clipping loss and degraded performance. While several approaches consider heavy-tailed settings, they lack analytical guidance for threshold selection and are limited to specific heavy-tailed distributions.

In this paper, we present a novel clipping mechanism for DPSGD under a generalized sub-Weibull GV assumption. We first establish unified high-probability optimization guarantees that achieve the best-known convergence rates in heavy-tailed settings while retaining optimal rates in light-tailed settings. Building on this, we propose a tail-aware clipping mechanism DC-DPSGD, which privately distinguishes body and tail gradients, and applies discriminative clipping to clip them with different thresholds, thereby balancing clipping loss and DP noise. Further, we theoretically analyze the convergence of DC-DPSGD and provide tighter optimization guarantees. Extensive experiments on twelve real-world datasets demonstrate that our approach outperforms four baselines by up to 3.40%, 4.76%, 3.39% and 5.80% in terms of accuracy, respectively.

CCS Concepts

• **Security and privacy → Privacy protections**.

Keywords

Differential Privacy, Heavy-Tailed Gradient, Gradient Clipping

ACM Reference Format:

Paper ID: 56. 2027. Unified Differentially Private Stochastic Gradient Descent with Tail-Aware Discriminative Clipping. In *Proceedings of ACM International Conference on Management of Data (SIGMOD '27).* ACM, New York, NY, USA, 49 pages. https://doi.org/XXXXXXX.XXXXXXX

1 Introduction

Data privacy has become a critical concern in modern deep learning, as models are often trained on sensitive data from diverse sources, ranging from structured records with personally identifiable attributes to unstructured data containing implicit sensitive information. Differentially Private Stochastic Gradient Descent (DPSGD) is a *de facto* and principled approach to training deep models with formal privacy guarantees [1]. It adds calibrated noise to aggregated gradients during training to obscure individual contributions. To ensure stability and control the privacy loss, DPSGD typically employs per-sample gradient clipping, which bounds each sample's gradient by a specified L_2 norm threshold before noise injection.

Recently, a number of works [11, 19, 29, 40, 51, 73, 75, 77] have been proposed to optimize the clipping mechanisms for DPSGD with per-sample gradient clipping (aka. clipped DPSGD). Most existing works assume that the stochastic gradient variability (GV)—the deviation between the randomly sampled gradient and the average gradient estimated on the full training dataset—follows a light-tailed distribution, such as sub-Gaussian. For instance, [11, 73, 77] focus on concentrated gradients near the center of the light-tailed GV distribution and uniformly trim the tail region for efficient clipping, while [3, 29, 40, 75, 82] leverage the boundedness of GV under the light-tailed distribution to determine the clipping thresholds and derive (near) optimal convergence rates.

Nevertheless, these light-tailed GV assumptions do not align with empirical findings, as extensive studies [9, 13, 60, 61, 80] have shown that the GV of SGD in deep learning often exhibits a heavy-tailed distribution. This occurs even when the dataset originates from a light-tailed distribution, the GV still diverges to a heavy-tailed distribution with unbounded variance [33]. This heavy-tailed behavior, reflecting the presence of hard-to-learn samples with large gradient deviations, typically slows down the convergence rate and impairs training performance [32, 45, 46, 52]. To mitigate this problem, several approaches [19, 51] analyze clipped DPSGD in heavy-tailed settings and derive expectation-based convergence bounds based on specific heavy-tailed Lipschitz assumptions. However, they offer only empirical guidance in convex settings, e.g., suggesting that the clipping threshold be smaller than the minimum gradient norm. Also, they provide no analytical guidance for determining the optimal clipping threshold in non-convex settings, as solving the nonlinear clipping function is intractable. Moreover, the heavy-tailed Lipschitz assumptions restrict their applicability and do not extend to more severe heavy-tailed settings.

Our goal is to design a unified clipped DPSGD mechanism that effectively handles general heavy-tailed GV scenarios and provides analytical guidance for clipping threshold selection. However, there are two main challenges. First, heavy-tailed GV is characterized by unconstrained tails, under which extreme gradient values cannot be effectively bounded. In this case, expectation-based tools commonly adopted in existing studies are no longer applicable to solving an optimal clipping threshold for differentially private optimization. Consequently, convergence guarantees built on sub-Gaussian assumptions or bounded gradients become suboptimal or may even

SIGMOD '27, Huntington Beach, CA, USA

ACM ISBN 978-x-xxxx-xxxx-x/YYYY/MM
https://doi.org/XXXXXXX.XXXXXXX

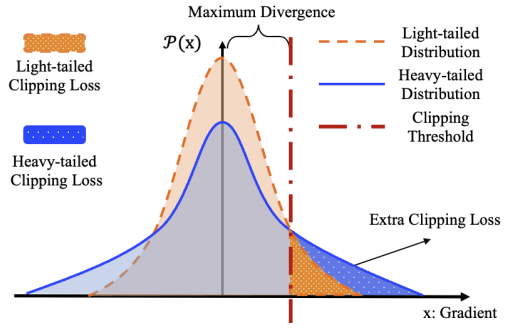

Figure 1: The trade-off comparison between light-tailed and heavy-tailed GV induced by different tail decay rates.

fail. Second, it is challenging to balance the magnitude of random perturbations added to the gradients, i.e., differential privacy (DP) noise, and the clipping loss that is tied to the clipping operation, under the heavy-tail GV setting. Figure 1 shows an example of this trade-off under light-tailed and heavy-tailed GV distributions. On the one hand, as the clipping threshold increases (i.e., when the red dotted line moves to the right), the clipping loss decreases, while the scale of DP noise increases as the maximum divergence (i.e., DP sensitivity) is larger. This could lead to a high-dimensional catastrophe [84] and negatively impact model performance. On the other hand, under the same DP noise magnitude (i.e., when fixing the red dotted line), the slower decay rate of the heavy-tailed distribution (blue line) will introduce extra clipping loss compared to the light-tailed distribution (orange line). It means that aggressive clipping on the tail region can severely distort gradient information under heavy-tailed GV, leading to substantial gradient bias.

In this paper, we present a novel clipping mechanism that achieves the goal above. We address the first challenge by modeling GV using a unified heavy-tailed distribution and employing high-probability analytical tools in place of the expectation tools. This allows us to rigorously characterize tail behaviors and bound the convergence rate of clipped DPSGD under heavy-tailed GV. Specifically, we adopt the sub-Weibull distribution, which generalizes both light-tailed and heavy-tailed distributions through a single form parameterized with a tail index θ (Definition 2.2). For instance, $\theta = 1/2$ corresponds to the light-tailed sub-Gaussian distribution, $1/2 < \theta < 1$ to the heavy-tailed Lipschitz distribution, and $\theta \geq 1$ to even heavier tails. Building on this, we derive unified optimization guarantees for clipped DPSGD that achieve the best-known convergence rates in heavy-tailed GV settings while retaining optimal convergence rates in light-tailed GV settings. To our knowledge, this is the first unified optimization guarantee for clipped DPSGD under both light-tailed and heavy-tailed GV assumptions. Our theoretical analysis further reveals that the convergence performance deteriorates as θ increases, motivating us to establish a principled relationship between the clipping threshold and the tail index.

We address the second challenge by proposing a tail-aware approach, named **Discriminative Clipping (DC)-DPSGD**, which effectively balances the extra clipping loss and required DP noise. We observe that the central body of heavy-tailed GV distributions behaves similarly to light-tailed distributions, while their tails decay much more slowly. Therefore, our key idea is to decompose the gradients into a light-body region and a heavy-tail region, and to use a larger clipping threshold for the heavy tail region, so as to retain more information from tail gradients while preventing unnecessary noise perturbation of body gradients. Specifically, we design a private subspace identification technique to detect tail gradients, and devise a discriminative clipping method with two different thresholds for body and tail gradients, respectively. We theoretically analyze the choice of these two clipping thresholds and provide tighter optimization guarantees for DC-DPSGD.

We compare DC-DPSGD against four differentially private baselines on twelve real-world datasets. The experimental results show that DC-DPSGD consistently outperforms the baselines. In particular, it achieves up to 3.40%, 4.76%, 3.39% and 5.80% improvements in accuracy over standard DPSGD, Auto-S, DP-PSAC and DPSGD-HL, respectively, demonstrating the effectiveness of our approach.

In summary, we make the following contributions in this paper.

- We provide high-probability optimization guarantees for clipped DPSGD under the sub-Weibull GV assumption, achieving the best-known convergence rates in heavy-tailed settings while preserving optimal rates in light-tailed cases. To our knowledge, this is the first unified theoretical guarantee for clipped DPSGD across both light-tailed and heavy-tailed GV settings.
- We propose a tail-aware clipping mechanism DC-DPSGD with a private subspace identification technique and a stair-wise discriminative clipping method to optimize clipped DPSGD under generalized heavy-tailed GV settings. We further analyze the convergence of DC-DPSGD and provide tighter optimization guarantees.
- We conduct extensive experiments on twelve real-world datasets, where DC-DPSGD consistently outperforms four differentially private baselines, achieving up to 3.40%, 4.76%, 3.39% and 5.80% accuracy improvements respectively, demonstrating the effectiveness of our proposed approach.

The remainder of the paper is structured as follows. Section 2 introduces the preliminaries. Section 3 presents our unified optimization guarantees for clipped DPSGD. Section 4 details the proposed discriminative clipping DPSGD approach. Section 5 describes the experimental evaluation. Section 6 reviews the related works, followed by the conclusion in Section 7.

2 Preliminaries

2.1 Differentially Private Optimization

Let S be a private training dataset, which consists of n training data $S = \{z_1, ..., z_n\}$ with a sample domain Z drawn i.i.d. from an underlying distribution $\mathcal{P}$. We aim to train a private model parameterized with $\mathbf{w} \in W \subseteq \mathbb{R}^d$, where W represents the model parameter space. Since the underlying distribution $\mathcal{P}$ is unknown and inaccessible in practice, we instead minimize the empirical risk in a differentially private manner:

$$L_S(\mathbf{w}) := \frac{1}{n} \sum_{i=1}^{n} \ell(\mathbf{w}, z_i), \tag{1}$$

where the loss function $\ell : W \times Z \to \mathbb{R}$ is typically non-convex. We denote by $\nabla \ell(\mathbf{w}, z_i)$ the gradient of the loss $\ell(\mathbf{w}, z_i)$ with respect to $\mathbf{w}$, evaluated at sample z_i. At every iteration t, we randomly sample a mini-batch $B_t \subseteq S$ by drawing j_t uniformly from the set $\{j : j \in$

$[n]\}$, and define the stochastic gradient as $\nabla\ell(\mathbf{w}, z_i)$, $z_i \in B_t$ and the average empirical gradient as$\nabla L_S(\mathbf{w}_t) := \frac{1}{n}\sum_{i=1}^{n}\nabla\ell(\mathbf{w}_t, z_i)$.

DPSGD [1] is widely used to preserve training data privacy in deep learning with SGD. In each iteration, it first clips the gradients with a specified threshold c and then adds random perturbation noise proportional to c. As a result, the overall training process ensures differential privacy (DP) based on composition theorems and post-processing properties [7, 8, 12, 25, 26, 54, 69].

*Definition 2.1 (**Differential Privacy**).* A randomized algorithm M is (ε, δ)-differentially private if for any two neighboring datasets S, S' differ in exactly one data point and any event Y, we have

$$\mathbb{P}(M(S) \in Y) \leq \exp(\varepsilon) \cdot \mathbb{P}(M(S') \in Y) + \delta, \tag{2}$$

where ε is the privacy budget and δ is a small probability.

Given Definition 2.1 of DP, we characterize our convergence rates in terms of the following key quantity:

$$\varphi = \frac{\sqrt{d\log(T/\delta)}}{n\varepsilon}, \tag{3}$$

where T is the number of iterations and d is the number of model parameters. Throughout this paper, our convergence rate $\mathcal{C}(\cdot)$ is measured by $\frac{1}{T}\sum_{t=1}^{T}\min\{\|\nabla L_S(\mathbf{w}_t)\|_2, \|\nabla L_S(\mathbf{w}_t)\|_2^2\}$.

Throughout the paper, we use $\mathbb{O}(\cdot)$ to represent dominant higher-order terms and $\|v\|_p$ to denote the L_p norm for any vector v. For ease of reference, we summarize the frequently used notations in Appendix A.2 of the full paper [4].

2.2 Sub-Weibull Distribution

We employ the sub-Weibull distribution (see Definition 2.2) to model the gradient variability as it unifies light-tailed and heavy-tailed behaviors within a single analytical form.

Definition 2.2 (Sub-Weibull Distribution [66]). A random variable X is said to follow a *sub-Weibull distribution* with tail index $\theta > 0$ and scale parameter $K > 0$, denoted by $X \sim subW(\theta, K)$, if

$$\mathbb{E}_X\left[\exp\left(|X/K|^{1/\theta}\right)\right] \leq 2. \tag{4}$$

In particular, the sub-Weibull distribution corresponds to light-tailed sub-Gaussian variables when $\theta = 1/2$, and sub-Exponential variables when $\theta = 1$. Larger values with $\theta > 1$ indicate heavier tails. In this paper, we refer to stochastic gradient variability as heavy-tailed when $\theta > 1/2$, and as light-tailed when $\theta = 1/2$.

2.3 Assumptions

We now introduce the assumption of sub-Weibull gradient variability and other assumptions commonly used in DPSGD.

Assumption 2.1 (**Sub-Weibull gradient variability** [45]). *Conditioned on the iterative parameter $\mathbf{w}_t$, the gradient variability $\mathcal{G}_t := \nabla\ell(\mathbf{w}_t, z_{j_t}) - \nabla L_S(\mathbf{w}_t)$ satisfies $\mathbb{E}[\nabla\ell(\mathbf{w}_t, z_{j_t}) - \nabla L_S(\mathbf{w}_t)] = 0$ and $\|\nabla\ell(\mathbf{w}_t, z_{j_t}) - \nabla L_S(\mathbf{w}_t)\|_2 \sim subW(\theta, K)$, where $subW(\theta, K)$ denotes a Sub-Weibull distribution with tail index θ and positive scale parameter K, such that $\theta \geq \frac{1}{2}$, and we have*

$$\mathbb{E}_{z_{j_t}\sim S}[\exp((\|\nabla\ell(\mathbf{w}_t, z_{j_t}) - \nabla L_S(\mathbf{w}_t)\|_2/K)^{\frac{1}{\theta}})] \leq 2. \tag{5}$$

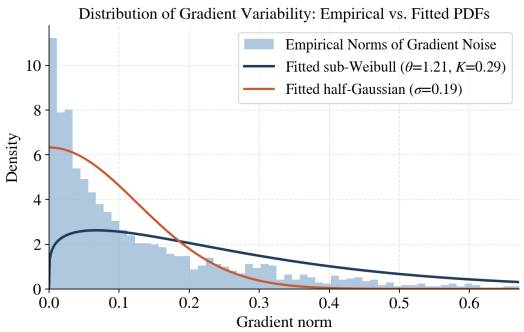

Figure 2: Sub-Weibull simulation of gradient variability on MNLI dataset using full fine-tuning with RoBERTa.

Assumption 2.1 is a relaxed version of gradient variability following sub-Gaussian distributions, that is, $\mathbb{E}_t[\exp((\|\nabla\ell(\mathbf{w}_t, z_{j_t}) - \nabla L(\mathbf{w}_t)\|_2/K)^2)] \leq 2$. It implies that finding upper bounds for moment generating function under Assumption 2.1 is impracticable by standard tools [66]. Therefore, we use the truncated tail theory [5] and martingale difference inequality [52] to address this problem in our analysis. To validate this assumption, we conduct a simulation experiment to examine the empirical distribution of gradient variability $\|\nabla\ell(\mathbf{w}_t, z_{j_t}) - \nabla L_S(\mathbf{w}_t)\|_2$ on real-world datasets. As shown by the results on MNLI dataset in Figure 2, the distribution is centrally concentrated and closely matches a sub-Gaussian fit, but exhibits clear tail deviations. These heavy tails are better captured by a sub-Weibull distribution with $\theta > 1$. Consistent observations on more datasets and architectures are reported in Appendix H.5.

Assumption 2.2 (β-**Smoothness**). *The loss function ℓ is β-smooth, for any sample $z \in Z$ $\mathbf{w}_t, \mathbf{w}_t' \in W$, we have*

$$\|\nabla\ell(\mathbf{w}_t, z) - \nabla\ell(\mathbf{w}_t', z)\|_2 \leq \beta\|\mathbf{w}_t - \mathbf{w}_t'\|_2. \tag{6}$$

Assumption 2.3 (**G-Bounded**). *For any $\mathbf{w}_t \in \mathbb{R}^d$, there exists a positive real number $G > 0$, and the expectation gradient satisfies*

$$\|\nabla L_S(\mathbf{w}_t)\|_2^2 \leq G. \tag{7}$$

Assumption 2.2 is widely used in optimization literature [30, 45, 84] and is essential for ensuring the convergence of gradients to zero [47]. Assumption 2.3 is milder compared to the bounded stochastic gradient assumption [45, 46, 84], i.e., $\|\nabla\ell(\mathbf{w}_t, z_i)\|_2^2 \leq G$. Note that Assumption 2.3 constrains the L_2 norm of the average gradient under the objective [45, 52], while Assumption 2.1 characterizes the randomness of individual gradients by quantifying their deviation from the empirical average over private training data. These assumptions provide a complementary view of the gradient behavior during optimization. We include other lemmas and theoretical tools in Appendix B.

3 Unified Optimization Guarantees for Clipped DPSGD under Heavy-tailed GV

In this section, we first revisit existing optimization guarantees for clipped DPSGD and establish a unified guarantee under heavy-tailed gradient variability. We then discuss the theoretical insights that motivate our approach. Due to space limitations, we provide only the main results here, while the detailed proofs and extended discussions are included in Appendix C of the full paper [4].

3.1 Optimization Guarantees

Most existing analyses of clipped DPSGD focus on light-tailed sub-Gaussian gradient variability (GV) and rely on strong symmetry assumptions to handle clipping loss [11, 16]. However, GV often exhibits heavy-tailed behaviors. Recent approaches [19, 51] analyze optimization guarantees by assuming that gradients satisfy a specific heavy-tailed Lipschitz condition, that is, the per-sample gradient has unbounded upper constants. Nevertheless, they could not provide analytical guidance on selecting the clipping threshold.

In this paper, we derive unified optimization guarantees under a more general assumption that GV follows a sub-Weibull distribution. This assumption subsumes the light-tailed sub-Gaussian and heavy-tailed Lipschitz assumptions (see Lemma 22 of [52]), which correspond to $\theta = 1/2$ and $1/2 < \theta < 1$ in Definition 2.2, respectively. Hence, prior results [11, 77] become special cases of ours with $\theta = 1/2$, while other results [19] fall into the regime $\theta < 1$ and our results naturally extend to even heavier tails with $\theta \geq 1$. Our unified optimization guarantee for clipped DPSGD under the sub-Weibull GV assumption is presented in the following theorem. We follow the outline of Abadi's clipped DPSGD scheme [1], as summarized in Algorithm 1. The clipping mechanism is defined as $\overline{\mathbf{g}}_t(z_i) = \mathbf{g}_t(z_i)/\max(1, \frac{\|\mathbf{g}_t(z_i)\|_2}{c})$, where $\mathbf{g}_t(z_i) = \nabla\ell(\mathbf{w}_t, z_i)$ and c denotes the clipping threshold, serving as a biased estimate.

Theorem 3.1 (**Convergence Rate of Clipped DPSGD under Sub-Weibull gradient variability Assumption**). *Let $\mathbf{w}_t$ be the iterative parameter $\mathbf{w}_t$ produced by Algorithm 1 with learning rate $\eta_t = \frac{1}{\sqrt{T}}$, where $T = \mathbb{O}(\frac{n\varepsilon}{\sqrt{d\log(1/\delta)}})$, $T \geq 1$, and d is the number of model parameters. Under Assumptions 2.1 and 2.2, given that the clipping threshold $c = \max\left(4K\log^{\theta}(\sqrt{T}), 39K\log^{\theta}(2/\delta)\right)$, for any $\delta \in (0,1)$, with probability $1-\delta$, we have:*

$$C_{\text{clipped-DPSGD}}(c) \leq \mathbb{O}\left(\log^{\max(1,\theta)}(T/\delta)\log^{2\theta}(\sqrt{T})\varphi^{\frac{1}{2}}\right). \quad (8)$$

Proof Sketch. We give a proof sketch and provide the complete proof in Appendix C of our full paper [4]. In the derivation process, a key quantity is the first-order term $\langle\overline{\mathbf{g}}_t(z_i) - \nabla L_S(\mathbf{w}_t), \nabla L_S(\mathbf{w}_t)\rangle$. We split it into two components, i.e.,

$$\langle\overline{\mathbf{g}}_t(z_i) - \nabla L_S(\mathbf{w}_t), \nabla L_S(\mathbf{w}_t)\rangle = \quad (9)$$
$$\langle\overline{\mathbf{g}}_t(z_i) - \mathbb{E}_t[\overline{\mathbf{g}}_t(z_i)], \nabla L_S(\mathbf{w}_t)\rangle + \langle\mathbb{E}_t[\overline{\mathbf{g}}_t(z_i)] - \nabla L_S(\mathbf{w}_t), \nabla L_S(\mathbf{w}_t)\rangle.$$

We first derive high-probability bounds by constructing martingale difference sequences $\sum_{t=1}^{T}(\langle\overline{\mathbf{g}}_t(z_i) - \mathbb{E}_t[\overline{\mathbf{g}}_t(z_i)], \nabla L_S(\mathbf{w}_t)\rangle)$ and applying advanced concentration inequalities to bound the term. Then, we utilize the sub-Weibull properties to obtain an upper bound of the second term $\langle\mathbb{E}_t[\overline{\mathbf{g}}_t(z_i)] - \nabla L_S(\mathbf{w}_t), \nabla L_S(\mathbf{w}_t)\rangle$. □

From this theorem, we observe that the convergence rate degrades as θ increases, since both $\log^{\max(1,\theta)}(T/\delta)$ and $\log^{2\theta}(\sqrt{T})$ grow with θ. This insight motivates the need to establish a relationship between the clipping threshold c and the heavy-tail index θ, which we will elaborate on in Section 3.2. We further compare our result in Theorem 3.1 with the current optimization guarantees of clipped DPSGD under light-tailed and heavy-tailed settings [11, 19, 51, 77], as summarized in Appendix A.1. There are two main findings. First, when $\theta = 1/2$, corresponding to the light-tailed sub-Gaussian GV setting, our optimization guarantees

Algorithm 1 Outline of Clipped DPSGD [1]

Input: sample size n, mini-batch size B, clipping threshold c, learning rate η_t, noise scale σ, the number of iterations T.
Output: trained model parameters $\mathbf{w}_T$.

```
Initialize w_0 randomly.
for iteration t = 1, ..., T do
    Take a random mini-batch B_t with sampling ratio B/n.
    g̃_t = Clip_and_Perturbation(c, B_t).
    Update model parameters: w_{t+1} = w_t − η_t g̃_t.
end for
return w_T

Function Clip_and_Perturbation(c, π):
    for every sample z_i in π do
        Compute per-sample gradient: g_t(z_i) = ∇ℓ(w_t, z_i).
        Abadi's clipping: ḡ_t(z_i) = g_t(z_i)/max(1, ||g_t(z_i)||_2 / c).
    end for
    Compute the weighted average of the gradients: ḡ_t = Σ_{i=1}^{|π|} ḡ_t(z_i).
    Add the corresponding noise: g̃_t = 1/|π| (ḡ_t + N(0, c^2 σ^2 I_d)).
return g̃_t
```

$\mathbb{O}(\log(T/\delta)\log(\sqrt{T})\varphi^{\frac{1}{2}})$ aligns with the current optimal rates without the gradient symmetry assumption [77], except for extra high probability terms. Second, the convergence rates in [19] depend on θ through φ and δ, which deteriorate rapidly as the tail becomes heavier. Their approach also fails to extend to sub-Exponential or heavier-tailed distributions ($\theta \geq 1$), where the rates degenerate to $\mathbb{O}(1)$, meaning that their training algorithm cannot converge in this setting. In contrast, θ is only related to the logarithmic terms in our result, which remains valid with heavier tails when $\theta \geq 1$.

3.2 Theoretical Insights

As discussed in Section 1, extreme samples that deviate significantly from the mean occur more frequently under heavy-tailed distributions, resulting in gradient variability with unbounded L_2 norms and thus more severe clipping loss. To analyze the clipping loss of DPSGD, we need to estimate the deviation between the clipped gradient and the true mean gradient, denoted by $\|\bar{\mathbf{g}}_t - \nabla L_S(\mathbf{w}_t)\|_2$. Unlike the light-tailed case, this deviation cannot be easily bounded by its expectation over t iterations, necessitating alternative theoretical analysis. To address this problem, we decompose the deviation term to explicitly isolate the gradient variability component $\|\mathbf{g}_t - \nabla L_S(\mathbf{w}_t)\|_2$ that dominates the clipping loss:

$$\begin{aligned}\|\mathbb{E}_t[\bar{\mathbf{g}}_t] - \nabla L_S(\mathbf{w}_t)\|_2 &= \|\mathbb{E}_t[(\mathbf{g}_t - \nabla L_S(\mathbf{w}_t))b_t]\|_2 \\ &\leq \sqrt{\mathbb{E}_t[\|\mathbf{g}_t - \nabla L_S(\mathbf{w}_t)\|_2^2]\,\mathbb{E}_t[b_t^2]}. \end{aligned} \quad (10)$$

Intuitively, when the stochastic gradient $\mathbf{g}_t$ is close to the true mean gradient $\nabla L_S(\mathbf{w}_t)$, it contributes little to the final error. Thus, the upper bound of the deviation term is mainly determined by cases where the stochastic gradient deviates substantially from the true mean. To capture such cases, we define the indicator $b_t = \mathbb{I}_{\|\mathbf{g}_t - \nabla L_S(\mathbf{w}_t)\|_2 > \frac{c}{2}}$, which identifies large-deviation gradient variability that dominates the clipping loss. The constant $\frac{1}{2}$ is chosen for analytical tractability and can be replaced by any constant in the interval of $(0,1)$ without loss of generality. Then, according

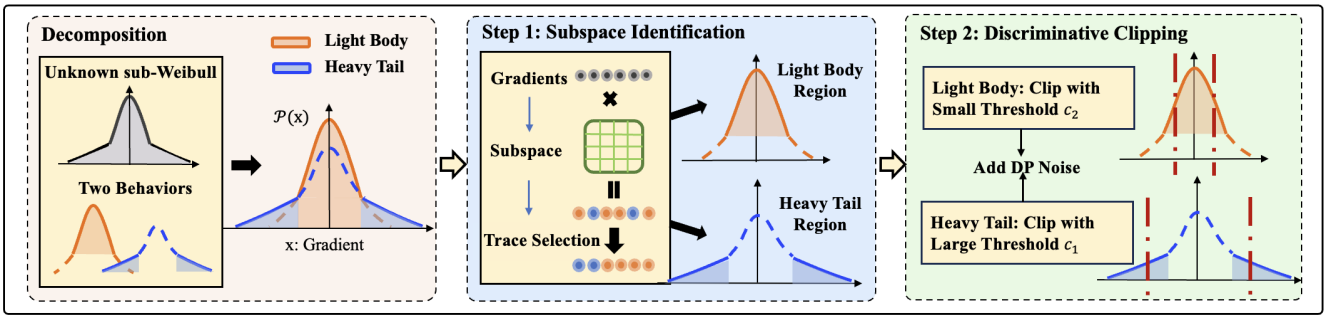

Figure 3: Overview of our DC-DPSGD mechanism.

to Assumption 2.1, we have:

$$\mathbb{E}_t[b_t^2] = \mathbb{P}(\|\mathbf{g}_t - \nabla L_S(\mathbf{w}_t)\|_2 > \frac{c}{2}) \leq 2\exp(-(\frac{c}{4K})^{\frac{1}{\theta}}). \quad (11)$$

From Eq. 11, the optimal clipping threshold increases with the tail index θ, as heavier tails require a larger c for optimality. Thus, directly adopting the same clipping threshold c as used in light-tailed settings tends to exacerbate the extra error $\mathbb{O}(\varphi^{-1/2})$ in $\mathbb{E}_t[b_t^2]$, since the clipping threshold is insufficient to accommodate the heavier-tailed gradients. Compared with the error introduced by DP noise, the effect of clipping is more severe, and the optimization guarantee of clipped DPSGD may become suboptimal or even collapse due to the extra clipping loss.

Optimal clipping threshold under heavy-tailed GV. Our unified optimization guarantee in Theorem 3.1 provides an important insight that the ideal clipping threshold c should scale up as the tail index θ increases because the theoretical value of c is positively correlated to θ. Specifically, as derived in Theorem 3.1, the optimal clipping threshold is given by $c = \max\left(\mathbb{O}\left(\log^{\theta}(1/\delta), \log^{\theta}(\sqrt{T})\right)\right)$. The two logarithmic terms originate from distinct factors. The term $\mathbb{O}(\log^{\theta}(1/\delta))$ arises from the high-probability concentration under the heavy-tailed assumption, ensuring that the deviation bound holds with high confidence $1-\delta$. The term $\log^{\theta}(\sqrt{T})$ accounts for the cumulative clipping loss across T iterations. When c deviates from its optimal value, the deviation bound deteriorates in opposite directions. A smaller c enlarges the probability term $\mathbb{P}(\|\mathbf{g}_t - \nabla L_S(\mathbf{w}_t)\|_2 > c/2)$, slowing the exponential decay term $\exp(-(\frac{c}{4K})^{1/\theta})$ and inducing the extra error $\mathbb{O}(\varphi^{-1/2})$ in the upper bound. Conversely, an excessively large c reduces clipping loss but amplifies the variance of the injected DP noise, which scales as c^2 (see line 14 in Algorithm 1), thereby loosening the overall error bound. Hence, the clipping mechanism must strike a balance between clipping loss and injected DP noise to ensure tighter optimization guarantees in the heavy-tailed setting.

4 Discriminative Clipping DPSGD

In this section, we first present our rationale and give an overview of the proposed mechanism DC-DPSGD. Then, we detail the private subspace identification and tail-aware discriminative clipping steps in DC-DPSGD. Finally, we provide a theoretical analysis of the optimization guarantee and privacy guarantee.

4.1 Rationale and Overview

Rationale. According to the optimization guarantee and theoretical insights presented in Section 3, the clipping threshold shall scale with the heavy-tail index θ to balance the trade-off between clipping loss and DP noise. In practice, most values in GV settings remain small and concentrated around the mean of the distribution; hence, it is desirable to maintain a low DP noise level for these gradients while selectively mitigating clipping loss for those with large magnitudes. Owing to its intrinsic structural properties, the sub-Weibull distribution is well suited for modeling GV in differentially private optimization: its concentration is characterized by small deviations whose decay can be well captured by a sub-Gaussian distribution, while its tail region exhibits large deviations that can be independently observed. Motivated by this natural property, our key idea is to exploit the sub-Weibull geometry of GV to partition DPSGD training into two regions: a *light-body* region that behaves similarly to a sub-Gaussian distribution, and a *heavy-tail* region with large deviations. Such a design enables tail-aware clipping and imposes localized intervention for DP optimization, where a smaller clipping threshold is applied to the light-body region to control DP noise, while a larger threshold is reserved for the heavy-tail region to mitigate excessive clipping loss.

Overview. Figure 3 illustrates an overview of DC-DPSGD, which consists of two steps. In the first step (Section 4.2), we propose a private subspace identification technique to distinguish gradients from light body and heavy tail, where we estimate distributional properties of per-sample gradients by computing and selecting their traces under a specific subspace. To make the trace identification satisfy DP, we adopt a private selection mechanism with privacy budget ε_{tr} to this step, and provide the corresponding utility guarantees (Theorem 4.1). In the second step (Section 4.3), we present a discriminative clipping method that applies different clipping thresholds for gradients in the two regions and adds DP noise with privacy budget ε_{gp} for gradient perturbation. To establish the comprehensive theoretical guarantees of our differentially private optimization method, we utilize the sharp sub-Weibull concentration tools [5] to derive high-probability guarantees (Theorem 4.2) for the light-body and heavy-tail regions, respectively. Moreover, we combine the results of the two steps to obtain a complete optimization guarantee (Theorem 4.3) for DC-DPSGD (Section 4.4). At last, we rigorously analyze the privacy guarantee of DC-DPSGD (Theorem 4.5) and provide the privacy budget allocation for the two steps (Section 4.5). Algorithm 2 presents the detailed steps of DC-DPSGD.

Algorithm 2 Discriminative Clipping DPSGD

Input: tail proportion p; learning rate η_t; number of iterations T; tail index θ; heavy-tailed and light-tailed clipping thresholds c_1, c_2.
Output: model parameters $\mathbf{w}_T$.

1: Initialize $\mathbf{w}_0$ randomly and initialize $V_{t,k}$ to None.
2: **for** each iteration $t = 1 \dots T$ **do**
3: **if** `Strategy_trigger` **then**
4: **Step 1: Private Subspace Identification**
5: Private selection: $(S^{\text{tail}}, S^{\text{body}}) \leftarrow$ Algorithm 3,
6: where $S^{\text{tail}} = \{\widetilde{z}_i\}_{i=1}^{pn}$, $S^{\text{body}} = \{\widetilde{z}_i\}_{i=1}^{(1-p)n}$, and $i \in S$.
7: Sample mini-batches with rates q_1 and q_2:
8: $S^{\text{tail}} \leftarrow \{B_1^{\text{tail}}, \dots, B_{q_1 pn}^{\text{tail}}\}$,
9: $S^{\text{body}} \leftarrow \{B_1^{\text{body}}, \dots, B_{q_2(1-p)n}^{\text{body}}\}$.
10: Apply random permutation:
11: $\Pi \leftarrow \text{Perm}\Big(B_1^{\text{body}}, \dots, B_{q_2(1-p)n}^{\text{body}}, B_1^{\text{tail}}, \dots, B_{q_1 pn}^{\text{tail}}\Big)$.
12: **end if**
13: **Step 2: Discriminative Clipping**
14: **for** each batch $\pi \in \Pi$ **do**
15: **if** $\pi \in S^{\text{tail}}$ **then**
16: $\widetilde{\mathbf{g}}_t \leftarrow$ Clip_and_Perturbation(c_1, π)
17: **else if** $\pi \in S^{\text{body}}$ **then**
18: $\widetilde{\mathbf{g}}_t \leftarrow$ Clip_and_Perturbation(c_2, π)
19: **end if**
20: Update parameters: $\mathbf{w}_{t+1} \leftarrow \mathbf{w}_t - \eta_t \widetilde{\mathbf{g}}_t$
21: **end for**
22: **end for**

4.2 Private Subspace Identification

We now introduce our private subspace identification technique in the first step. We note that numerous studies [49, 84] leverage in-distribution public subspaces to preserve the low-rank private training information. This implies that gradients tend to exhibit more pronounced eigen signals in similar subspaces due to shared eigenvector directions. In light of this, samples from the light-body region are expected to generate stronger responses within subspaces characterized by sub-Gaussian distributions, while heavy-tail samples tend to be more active in subspaces associated with heavier sub-Weibull distributions with $\theta > 1/2$. In addition, due to the high-dimensional nature of gradients in DP stochastic learning, their normalized versions can act as mutually orthogonal directional eigenvectors [67] and provide effective information for model optimization [11, 77]. Given that normalized gradients have bounded L_2 sensitivity, we can bypass the unbounded norm of heavy-tailed gradients and avoid impracticable DP estimation. Based on the above two points, we use the inner product between the normalized gradients and the constructed heavy-tailed subspace as a measure of linear transformation similarity, where higher similarity indicates closer alignment with the heavy-tail region, while conversely lower value suggests membership in the light-body region.

Private selection by SVT. To capture these properties, we project each per-sample gradient onto a designated subspace and use the resulting trace as a signal score to characterize sample behavior. Then, we apply the *sparse vector technique* (SVT), a standard private selection mechanism [23, 63], to identify the first query whose score exceeds a privatized threshold as one positive outcome in each execution. In this paper, we use SVT to identify samples exhibiting heavy-tailed behavior. Note that when SVT is applied to disjoint subsets of the dataset in parallel, the privacy loss does not accumulate, and the composed mechanism remains (ε, δ)-DP by the parallel composition theorem [22, 53]. Therefore, we randomly partition the training set S into n^* disjoint subset domains, where $n^* = \lceil pn \rceil$ and p denotes the portion of heavy-tailed samples, to perform SVT in parallel across these domains.

To be concrete, in the private subspace identification step of iteration t, we first construct a projection matrix composed of k random orthogonal unit vectors $V_{t,k} = [v_{t,1}, ..., v_{t,k}] \in \mathbb{R}^{d \times k}$, which is sampled from the sub-Weibull distributions with different candidate tail indices $\theta = [1/2, 1, 2]$. These tail indices are selected to span a representative spectrum of tail behaviors, ranging from sub-Gaussian ($\theta = 1/2$) to sub-Exponential ($\theta = 1$), and heavier-tailed regimes ($\theta = 2$). This enables the subspace to capture diverse gradient variability patterns. Secondly, we compute the per-sample projected trace by $\lambda_{t,i}^{\text{tr}} = \text{tr}(V_{t,k}^\top \hat{\mathbf{g}}_t(z_i) \hat{\mathbf{g}}_t^\top(z_i) V_{t,k})$, where $\hat{\mathbf{g}}_t(z_i)$ is the normalized version of $\mathbf{g}_t(z_i)$ with bounded directional information and $V_{t,k}^\top$ is the transpose of $V_{t,k}$. Thirdly, we employ an SVT mechanism with Gaussian noise to perturb the normalized traces.

Algorithm 3 describes our SVT-based private selection method. The threshold perturbation uses privacy budget ε_1 with noise multiplier σ_1, while each query is perturbed by ν_i using budget ε_2 with scale σ_2, where a total privacy budget $\varepsilon_{\text{tr}} = \varepsilon_1 + \varepsilon_2$. This mechanism enables larger traces with higher similarity to the target subspace to be selected with high probability while preserving differential privacy. Ultimately, among the n^* noisy traces $\widetilde{\lambda}_t^{\text{tr}}$, those scores that exceed the noisy threshold $\widetilde{\mathcal{T}}$ are selected and assigned to the region corresponding to the candidate tail index θ. For instance, if $\theta > 1/2$, the threshold-exceeding samples are assigned to the heavy-tail region, whereas the remaining samples whose traces fall below the threshold are classified into the light-body region.

Building on Algorithm 3, lines 3-12 in Algorithm 2 summarize the execution of the private subspace identification step. The `strategy_trigger` flag (line 3) controls the frequency of private subspace identification. It can be executed only once at the beginning or periodically every few iterations, which effectively balances the stability of subspace and privacy guarantees.

Utility analysis of private subspace identification. We first analyze the utility guarantee of the subspace identification, for which we need to bound the skewing between the empirical and the population second moment, i.e., $\|V_{t,k}V_{t,k}^\top - \mathbb{E}_{V_{t,k}\sim\mathcal{P}}[V_{t,k}V_{t,k}^\top]\|_2$, where $V_{t,k}V_{t,k}^\top = \frac{1}{k}\sum_{i=1}^k v_{t,i}v_{t,i}^\top$. We analyze the error caused by the skewing based on Ahlswede-Winter Inequality [67]. In addition, since extra DP noise is injected through the SVT mechanism during private trace selection, the accuracy of identification could be affected. Thus, we also need to constrain the error introduced by the SVT. Consequently, we derive the high-probability bound for private subspace identification in Theorem 4.1.

Theorem 4.1 (**Utility Bound for Heavy-Tail Identification**). *Under the empirical projection subspace $M = V_{t,k}V_{t,k}^\top \in \mathbb{R}^{d\times d}$ and $\lambda_{t,i}^{\text{tr}} = \text{tr}(V_{t,k}^\top \hat{\mathbf{g}}_t(z_i)\hat{\mathbf{g}}_t^\top(z_i)V_{t,k})$, for the error $\mathcal{E}_{\text{trace}}$ of the SVT-based heavy-tail selection, with probability $1-\delta_{\text{tr}}$, we have*

$$\mathcal{E}_{\text{trace}} \leq \mathbb{O}\left(\frac{\log(d/\delta_{\text{tr}})\sqrt{\log(1/\delta_{\text{tr}})\log(n^*/\delta_{\text{tr}})}}{k\varepsilon_{\text{tr}}}\right).$$

Algorithm 3 SVT-based Private Selection

Input: samples $\{z_i\}_{i=1}^n$; subspace dimension k; trace sensitivity Δ; noise multiplier (σ_1, σ_2); cutoff $n^* = \lceil pn \rceil$; selection threshold $\mathcal{T}$.
Output: discriminative sample set $(S^{\text{tail}}, S^{\text{body}})$.

1: Partition the training set $S = \{z_i\}_{i=1}^n$ into disjoint subsets $\{S_j\}_{j=1}^{n^*}$, where $\bigcup_{j=1}^{n^*} S_j = S$ and $S_j \cap S_{j'} = \emptyset$ for $j \neq j'$.
2: Extract orthogonal vectors $[v_1, \ldots, v_k]$ from a sub-Weibull distribution with shape parameter θ, and construct the projection subspace $V_{t,k}V_{t,k}^\top = \frac{1}{k}\sum_{j=1}^k v_j v_j^\top$.
3: Initialize $S^{\text{tail}} \leftarrow \emptyset$.
4: Sample selection threshold noise $\rho \sim \mathbb{N}\left(0, \Delta^2\sigma_1^2\mathbb{I}\right)$.
5: Set noisy selection threshold $\widetilde{\mathcal{T}} = \mathcal{T} + \rho$.
6: **for** each $j \in [n^*]$ **in parallel do**
7: **for** per-sample $i \in S_j$ **do**
8: Normalize per-sample gradient: $\hat{\mathbf{g}}_t(z_i) = \frac{\mathbf{g}_t(z_i)}{\|\mathbf{g}_t(z_i)\|_2}$.
9: Compute trace score: $\lambda_{t,i}^{\text{tr}} = \text{tr}\left(V_{t,k}^\top \hat{\mathbf{g}}_t(z_i)\hat{\mathbf{g}}_t^\top(z_i)V_{t,k}\right)$.
10: Sample query noise $\nu_i \sim \mathbb{N}\left(0, 4\Delta^2\sigma_2^2\mathbb{I}\right)$.
11: Set $\widetilde{\lambda}_{t,i}^{\text{tr}} = \lambda_{t,i}^{\text{tr}} + \nu_i$.
12: **if** $\widetilde{\lambda}_{t,i}^{\text{tr}} \geq \widetilde{\mathcal{T}}$ **then**
13: Add z_i to S^{tail} and label it as heavy-tail sample $\overline{z}_i$.
14: **break**
15: **end if**
16: **end for**
17: **end for**
18: Assign remaining samples to $S^{\text{body}} = \{z_i\}_{i=1}^n \setminus S^{\text{tail}}$ and label them as light-body samples $\widetilde{z}_i$.

The detailed proof is provided in Appendix D of the full paper [4]. The utility bound is primarily governed by the projection dimension k and the privacy budget ε_{tr} due to the factor $\frac{1}{k\varepsilon_{\text{tr}}}$. When k is moderately large relative to the model dimension, e.g., $k \geq \log(d/\delta_{\text{tr}})$, the resulting error introduced by the projection remains mild. Moreover, since the dimension d grows for LLM architectures, a larger projection dimension k is required in practice. Meanwhile, the accuracy of the SVT-based procedure is affected by the number of selected heavy-tailed samples n^*: selecting more samples requires partitioning more domains, which amplifies per-domain variance and introduces logarithmic error $\sqrt{\log n^*}$. Theorem 4.1 applies to a single run, with ε_{tr} proportionally split when the `strategy_trigger` is greater than one. Overall, by choosing a sufficiently large projection dimension k and appropriate n^*, the SVT-based heavy-tail selection achieves effective utility guarantees.

4.3 Tail-aware Discriminative Clipping

Next, we present our tail-aware discriminative clipping strategy in the second step. In practice, gradients from the heavy-tail region often exhibit larger deviations from the mean, resulting in larger L_2 norms. In contrast, the light-body gradients tend to be more concentrated and exhibit smaller norms. Under the same clipping threshold, heavy-tailed gradients suffer from more severe clipping loss than light-tailed gradients, which ultimately degrades the utility of the privatized algorithm. This necessitates stair-wise clipping strategies for heavy-tailed and light-tailed gradients, respectively.

However, existing adaptive approaches [11, 73, 77] can be viewed as an approximated version of Abadi's clipping function (Algorithm 1) under small clipping threshold regimes. They primarily allocate more weights to scale concentrated gradients with relatively small norms. For example, Auto-S [11] and NSGD [77] employ a normalized clipping strategy with the form $\frac{\mathbf{g}_t(z_i)}{\|\mathbf{g}_t(z_i)\|_2+\gamma}$, where γ is a regularization term and is often set to a small positive value. DP-PSAC [73] adopts a conservative clipping strategy to control the amplification using the weight function $\frac{\mathbf{g}_t(z_i)}{\|\mathbf{g}_t(z_i)\|_2+\frac{\gamma}{\|\mathbf{g}_t(z_i)\|_2+\gamma}}$. These methods overlook the optimization for heavy-tailed gradients and weaken their contributions after clipping, whose large deviations are more susceptible to information loss under uniform clipping. As shown in Figure 4, Auto-S and NSGD achieve intense amplification as the gradient norm decreases, imposing excessive weight on small-norm gradients. DP-PSAC mitigates the amplification of small-norm gradients by employing a non-monotonic adaptive weight function, which estimates the true averaged gradient better. Moreover, these methods rely on the assumption of light-tailed GV, which are inapplicable in heavy-tailed settings.

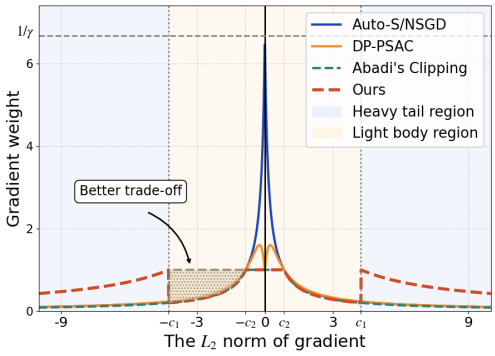

Figure 4: The gradient weight under different per-sample clipping functions, and $\gamma = 0.15$, $c_2 = 1 - \gamma$ and $c_1 = 5c_2$.

To tackle this problem, we propose a stair-wise discriminative clipping mechanism. After identification, the partitioned samples are randomly permuted and divided into batches, where an equivalent level of privacy amplification can be achieved by adopting a smaller batch size (we provide a detailed privacy analysis of this process in Section 4.5). Then, as shown in line 9 of Algorithm 2, we tailor two different clipping thresholds (denoted as c_1 and c_2) for the tail and body gradients classified in the subspace identification step, and perturb the clipped gradients scaled with corresponding clipping thresholds. To make a clear comparison, we set the threshold in Abadi's clipping by $c_2 = 1 - \gamma$. Taking $c_1 = 5c_2$ as an example, we define the light-body region as gradients with norms less than c_1 and present the gradient weights assigned by our discriminative clipping. As illustrated in Figure 4, we assign more weights to large-norm gradients in the heavy-tail region while preserving the original scale of concentrated gradients in the light-body region. Especially, the 'Better trade-off' in the figure shows that our approach is not a simple reparameterization of DPSGD: it injects less noise than DPSGD with $c = c_1$, while retaining more heavy-tailed information than DPSGD with $c = c_2$.

To characterize the convergence behaviors for the two regions, we assume that the gradients are classified into the correct heavy-tail and light-body regions. In this way, we conduct separate analyses for the two regions, each accompanied by the respective high-probability guarantee. Next, to establish the optimization guarantee

for the two regions, we generalize the sharp heavy-tailed concentration [5] and sub-Weibull Freedman inequality [52] to truncate the heavy-tailed distribution and find the optimal clipping threshold for each region. As a result, we have the following theorem.

Theorem 4.2 (**Convergence Rate of DC-DPSGD**). *Let* $\mathbf{w}_t$ *be the iterative parameter produced by discriminative clipping with* $T = \mathbb{O}(\frac{n\varepsilon_{\text{gp}}}{\sqrt{d\log(1/\delta)}}), T \geq 1$ *and* $\eta_t = \frac{1}{\sqrt{T}}$. *Define* $\Gamma(x) := \int_0^\infty t^{x-1}e^{-t}dt$, $a = 2$ *if* $\theta = \frac{1}{2}$, $a = (4\theta)^{2\theta}e^2$ *if* $\theta \in (\frac{1}{2}, 1]$, *and* $a = (2^{2\theta+1}+2)\Gamma(2\theta+1) + 2^{3\theta}\Gamma(3\theta+1)/3$ *if* $\theta > 1$. *Under Assumptions 2.1, 2.2 and 2.3, for any* $\delta \in (0,1)$, *we have:*

(i) **In the heavy-tail region**:
suppose that $c_1 = \max\left(4^\theta 2K\log^\theta(\sqrt{T}), 4^\theta 33K\log^\theta(2/\delta)\right)$,

$$C_{\text{tail}}(c_1) \leq \mathbb{O}\left(\log^{\max(1,\theta)}(T/\delta)\log^{2\theta}(\sqrt{T})\varphi^{\frac{1}{2}}\right). \tag{12}$$

(ii) **In the light-body region**:
suppose that $c_2 = \max\left(2\sqrt{2a}K\log^{\frac{1}{2}}(\sqrt{T}), 33\sqrt{2a}K\log^{\frac{1}{2}}(2/\delta)\right)$,

$$C_{\text{body}}(c_2) \leq \mathbb{O}\left(\log(T/\delta)\log(\sqrt{T})\varphi^{\frac{1}{2}}\right). \tag{13}$$

Proof Sketch. In Theorem 4.2, the convergence rates for the two regions correspond to the discriminative clipping thresholds c_1 and c_2, denoted by $C_{\text{tail}}(c_1)$ and $C_{\text{body}}(c_2)$ respectively. First, we optimize the theoretical tools by transforming the concentration inequalities for the sum of sub-Weibull random variables X into two-region versions distinguished by the tail probability $\mathbb{P}(|X| > x)$, namely sub-Gaussian tail decay rate $\exp(-x^2)$ and heavy-tailed decay rate $\exp(-x^{1/\theta})$, $\theta > \frac{1}{2}$. Then, we analyze the high-probability bounds for the gradient variability of clipped DPSGD in each region. In the heavy-tail region, we make the inequality $\mathbb{P}(\|\mathbf{g}_t - \nabla L_S(\mathbf{w}_t)\|_2 > c_1) \leq 2\exp(-c_1^{1/\theta})$ hold and derive the dependence of factor $\log^\theta(1/\delta)$ for c_1. In the light-body region, we have $\mathbb{P}(\|\mathbf{g}_t - \nabla L_S(\mathbf{w}_t)\|_2 > c_2) \leq 2\exp(-c_2^2)$, resulting in the factor $\log^{1/2}(1/\delta)$ of c_2. Next, we investigate the high-probability error on the unbounded DP noise using Gaussian distribution properties. Finally, we integrate the results regarding gradient variability and privacy noise to determine the optimal clipping thresholds for both regions and achieve faster convergence rates for the optimization guarantee. We provide the full proof in Appendix E [4]. □

From Theorem 4.2, we can observe that when the gradients fall into the light-body region, our rate $C_{\text{body}}(c_2)$ does not contain the heavy-tail index θ, implying that the optimization guarantee is not affected by θ and always converges with respect to the light-tailed sub-Gaussian behavior. Moreover, the bound $C_{\text{tail}}(c_1)$ reveals the influence of the tail index θ in the heavy-tail region, which becomes deteriorated as θ increases and leads to a slower convergence rate compared to the light-body region. However, since the θ-dependent effect is confined to the heavy-tail region rather than the full gradients, the result that combines the two-behavior rates can yield significantly better performance than that of the classical heavy-tailed clipped DPSGD in Theorem 3.1.

Guidance for clipping threshold selection. Existing adaptive methods implicitly couple the clipping threshold c with the learning rate η_t, forming one single tunable parameter that ultimately guides the gradient clipping. Notably, Abadi's clipping can also be transformed as a form of adaptive clipping Auto-S [11], provided a sufficiently small clipping threshold is used with a large learning rate. The guidance stated in [11] has been widely applied in practice and proven in theory [16, 59]. Prior works [11, 16] have theoretically shown that both Abadi's clipping and the adaptive clipping can achieve the same optimal order of convergence rate. However, their results cannot be extended to heavy-tailed scenarios. Here, we provide a simplified explanation for the transformation: $\eta_t\mathbf{g}_t(z_i)/\max(1, \frac{\|\mathbf{g}_t(z_i)\|_2}{c}) \overset{c\to 0}{\approx} c\eta_t\mathbf{g}_t(z_i)/(\|\mathbf{g}_t(z_i)\|_2+\gamma)$, where γ is a small constant. Consequently, our discriminative clipping does not conflict with the majority of clipping guidance. Accordingly, for gradients in the light-body region, we can follow the existing practice in Abadi's clipping and set c_2 by a sufficiently small threshold to guarantee the proven optimality of Abadi's clipping. Furthermore, to achieve optimality in the heavy-tail region, we design a more relaxed threshold based on our theoretical analysis in Theorem 4.2, which shows that the clipping threshold c_1 should be about $\log^{(\theta-1/2)}(1/\delta)$ times greater than c_2. When $\theta = 1/2$, we have $c_1 = c_2$, recovering standard Abadi's clipping.

4.4 Optimization Guarantee for DC-DPSGD

In this subsection, we provide the formal optimization guarantees for DC-DPSGD. Note that the boundary derived in Section 4.3 is based on the assumption of perfectly classifying each sample into its corresponding region. In practice, the private subspace identification may incur utility errors by misidentification, which are jointly determined by the subspace skewing and the tail proportion p, as analyzed in Section 4.2. Since the subspace skewing of $\mathbb{O}(\log d/k)$ is non-dominant compared to the optimization guarantee in Theorem 4.2, we only consider its impact guaranteed by the high-probability term $1-\delta_{\text{tr}}$. Then, the parameter p is theoretically determined by the tail index θ and scale K of the sub-Weibull distribution. Nevertheless, estimating its true value is generally intractable. Therefore, we treat p as a tunable hyperparameter in our method. In practice, we consider values of p typically ranging in the interval refer to $[0.05, 0.1]$ [65].

Suppose that p is the proportion of heavy-tailed gradients in the mini-batch and each gradient is correctly identified into the corresponding region with probability at least $1-\delta_{\text{tr}}$ according to Theorem 4.1. For a mini-batch, the expected fraction of correctly identified heavy-tailed gradients is $p*(1-\delta_{\text{tr}})$. Thus, we can analyze the convergence rate by combining Theorems 4.1 and 4.2 to derive the formal bound for DC-DPSGD, as stated in Corollary 4.3.

Corollary 4.3 (**Optimization Guarantee for DC-DPSGD**). *Let* $\mathbf{w}_t$ *be the parameter produced by DC-DPSGD. Given Assumptions 2.1, 2.2, 2.3, and Theorem 4.2, for any* $\delta' \in (0,1)$:

$$\begin{aligned} C_{\text{m}}(c_1, c_2) \leq\ & p * \mathbb{O}\left(\log^{\max(1,\theta)}(T/\delta')\log^{2\theta}(\sqrt{T})\varphi^{\frac{1}{2}}\right) \\ & + (1-p) * \mathbb{O}\left(\log(T/\delta')\log(\sqrt{T})\varphi^{\frac{1}{2}}\right), \end{aligned} \tag{14}$$

with probability $1-\delta'$, *where* $\delta' = \delta_{\text{tr}} + \delta$, *with* δ_{tr} *being the error of subspace identification, and* δ *being the convergence probability.*

Proof Sketch. The bound $C_{\text{m}}(c_1, c_2)$ includes three parts: (i) the convergence rate $C_{\text{tail}}(c_1)$ from correctly identified heavy-tailed

gradients with proportion p and probability $1-\delta_{\text{tr}}$; (ii) the convergence rate $C_{\text{body}}(c_2)$ from correctly identified light-body gradients with proportion $1-p$ and probability $1-\delta_{\text{tr}}$; and (iii) an ignorable misidentification error $\delta_{\text{tr}}\left|C_{\text{tail}}(c_1) - C_{\text{body}}(c_2)\right|$ due to the small probability δ_{tr}, reflecting the worst-case gap caused by applying incorrect clipping thresholds to misclassified gradients. The full proof is provided in Appendix F [4]. □

Corollary 4.3 indicates that the optimization guarantee of DC-DPSGD is composed of p-weighted average bounds, where the heavy-tailed convergence rate merely accounts for the portion of p, with the rest made up of the light-body rate. Therefore, our bound is tighter than Theorem 3.1 owing to the value of p being always less than 1. Moreover, even for large tail indices θ, the tail proportion p can be restricted with a sufficiently small variance K [66]. Especially, if $p \leq 1/(\frac{C_{\text{tail}}(c_1)}{C_{\text{body}}(c_2)} + 1)$, it enables us to achieve θ-independent rates of $(1-p) * \mathbb{O}\left(\log(T/\delta')\log(\sqrt{T})\varphi^{1/2}\right)$.

4.5 Privacy Analysis

Given partitioned sampling with heterogeneous subsampling rates, the required noise must be rescaled to maintain an equivalent privacy level. In Algorithm 2, we partition the dataset into a heavy-tail region and a light-body region with proportions p and $1-p$, and corresponding sampling rates q_1 and q_2. Let $\bar{q} = pq_1 + (1-p)q_2$ denote the average sampling rate. We study the noise multiplier σ_{gp} of the discriminative mechanism with the partitioned sampling.

Theorem 4.4 (Noise scaling under partitioned sampling). *Under the same privacy budget ε, the partitioned mechanism requires a noise multiplier that requires*

$$\sigma_{\text{gp}} \approx \sqrt{\frac{pq_1^2 + (1-p)q_2^2}{\bar{q}^2}}\sigma_{\text{Pois}}. \tag{15}$$

Equality holds if and only if $q_1 = q_2 = \bar{q}$.

Theorem 4.4 formalizes this relation between the noise multiplier σ_{gp} in DC-DPSGD and σ_{Pois} in standard clipped DPSGD. The proof is provided in Appendix G.1.

Finally, we analyze the privacy guarantee of DC-DPSGD. For a fair comparison to existing clipped DPSGD works, the total privacy budget allocated by DC-DPSGD to ε_{tr} and ε_{gp} is equal to the privacy budget ε in DPSGD variants, i.e., $\varepsilon = \varepsilon_{\text{tr}} + \varepsilon_{\text{gp}}$. Theorem 4.5 gives the privacy guarantee of our DC-DPSGD approach.

Theorem 4.5 (**Privacy Guarantee**). *There exist constants m_1 and m_2 such that for any $\varepsilon_{\text{tr}} \leq m_1 T$, $\varepsilon_{\text{gp}} \leq m_1 q^2 T$, $\delta > 0$ and the noise multiplier $\sigma_{\text{gp}}^2 = \frac{m_2 T \bar{q}^2 \ln\frac{1}{\delta}}{\varepsilon_{\text{gp}}^2}$ over T iterations, where $\bar{q} = pq_1 + (1-p)q_2$, and we have the SVT-based identification is $(\varepsilon_{\text{tr}}, \delta_{\text{tr}})$-DP and DC-DPSGD (Algorithm 2) is $(\varepsilon_{\text{tr}} + \varepsilon_{\text{gp}}, \delta)$-DP.*

Proof Sketch. Our private subspace identification technique follows the proof of the SVT mechanism in [26, 85] with parallel composition [22]. For the discriminative clipping mechanism, since it uses two clipping thresholds to separately handle gradients from different parts of the mini-batch, we reanalyze the gradient perturbation with the Gaussian mechanism [1] and subsampling. The detailed privacy proof is provided in Appendix G [4]. □

5 Experiments

In this section, we evaluate the performance of our DC-DPSGD approach and compare it with state-of-the-art clipping mechanisms on a wide range of datasets. We first introduce the experimental setup and then report the evaluation results.

5.1 Experimental Setup

Datasets. We evaluate DC-DPSGD on twelve real-world datasets, including four image datasets, two natural language datasets, and six tabular datasets.

- **Image datasets:** *MNIST* [43] contains 60,000 training images and 10,000 testing images of handwritten digits from 10 classes. *FMNIST* [74] contains 60,000 training images and 10,000 testing images of fashion products from 10 categories. *CIFAR10* [41] contains 60,000 color images of size 32×32 from 10 object categories, with 50,000 for training and 10,000 for testing. *ImageNette* [20] is a curated subset of ImageNet containing 10 classifiable categories with a total of 13,394 images.
- **Language datasets:** *E2E* [24] is a natural language generation dataset for end-to-end dialogue systems, containing over 42,000 instances describing restaurant information in natural language. *MNLI* [71] is a large-scale natural language inference dataset that classifies the semantic relationship between a premise and a hypothesis across multiple text genres.
- **Tabular datasets:** *Product* [2] contains 35,311 samples with 7 attributes. The task is to distinguish products from 10 classes. *Breast Cancer* [72] contains 569 samples with 30 attributes. The task is to distinguish malignant from benign tumors. *Android Malware* [10] contains 4,464 samples extracted from Android applications, labeled as benign or malicious. *Adult* [39] contains 48,842 samples. The task is to predict whether an individual belongs to the higher-income group. *Bank Marketing* [55] contains 45,211 samples with 16 attributes. The task predicts whether a customer will subscribe. *Credit Card* [78] contains 30,000 samples with 23 attributes. The task is to predict whether a customer will default on credit card payments in the following month.

Following [14, 58], we further construct two heavy-tailed datasets, namely *CIFAR10-HT* [14] (a heavy-tailed version of CIFAR10) and *ImageNette-HT* (modified on [58]) to evaluate the performance in heavier-tail settings. We construct these two datasets via class-imbalanced sampling, as imbalanced label distributions are known to induce markedly heavy-tailed gradient behavior [42].

Models. For MNIST and FMNIST, we train a two-layer CNN model from scratch. For CIFAR10 and CIFAR10-HT, we fine-tune SimCLRv2 pre-trained by unlabeled ImageNet and ResNeXt-29 pre-trained by CIFAR100 [64] with a linear classifier, respectively. For ImageNette and ImageNette-HT, we adopt the same setting as [11] and ResNet9 without pre-training. For E2E and MNLI, wefine-tune transformer-based large language models (LLMs), namely GPT-2 (163M) and RoBERTa (355M). For tabular tasks, we train MLP models equipped with ReLU activations and a two-unit output layer from scratch for binary and multi-label classification.

We evaluate classification tasks using accuracy that measures the portion of correct predictions, and natural language generation tasks using the BLEU score [57] that measures the quality of generated data with a modified n-gram score.

Table 1: Test accuracy (%) comparison between DC-DPSGD and baselines on image datasets.

Algorithm	Privacy	MNIST	FMNIST	CIFAR10	ImageNette	CIFAR10-HT / ImageNette-HT
DPSGD	$\varepsilon = 8, \delta = 1/n^{1.1}$	97.65±0.09	83.63±0.12	93.31±0.01	66.81±0.42	57.98±0.59 / 34.98±1.47
Auto-S		97.55±0.16	83.38±0.09	93.28±0.06	65.57±0.85	58.30±0.61 / 31.96±2.39
DP-PSAC		97.67±0.06	83.75±0.21	93.30±0.03	65.68±1.71	57.99±0.58 / 34.07±1.55
DPSGD-HL		97.31±0.22	83.02±0.25	93.14±0.10	64.33±0.45	56.08±0.42 / 32.54±0.83
Ours (DC-DPSGD)		**98.14±0.13**	**84.76±0.34**	**93.80±0.03**	**67.66±0.29**	**61.38±1.00 / 36.72±0.91**
DPSGD	$\varepsilon = 4, \delta = 1/n^{1.1}$	96.82±0.05	83.32±0.33	93.06±0.09	65.67±0.58	56.81±0.69 / 31.05±1.67
Auto-S		96.68±0.34	83.08±0.12	93.08±0.06	64.20±0.95	56.63±0.62 / 30.99±1.69
DP-PSAC		96.35±0.51	83.13±0.20	93.11±0.08	64.15±1.14	56.62±0.63 / 31.37±2.33
DPSGD-HL		95.48±0.17	82.52±0.13	92.79±0.06	62.05±0.84	53.79±1.02 / 30.12±1.55
Ours (DC-DPSGD)		**97.92±0.11**	**84.07±0.25**	**93.36±0.14**	**66.09±0.82**	**59.03±0.81 / 33.58±1.37**

Table 2: BLEU (%) and test accuracy (%) of DC-DPSGD on natural language dataset.

Algorithm	Privacy	E2E Full	E2E LoRA	MNLI Full
DPSGD	$\varepsilon = 8$, $\delta = \frac{1}{n^{1.1}}$	63.189	63.389	76.90
Auto-S		63.600	63.518	76.92
DP-PSAC		63.627	63.502	76.92
DPSGD-HL		62.824	63.002	75.20
Ours		**64.180**	**63.920**	**78.00**
DPSGD	$\varepsilon = 3$, $\delta = \frac{1}{n^{1.1}}$	61.519	61.220	73.60
Auto-S		61.340	61.220	73.80
DP-PSAC		61.340	61.263	73.82
DPSGD-HL		60.120	60.200	69.30
Ours		**61.732**	**61.563**	**75.10**

Table 3: Test accuracy (%) comparison between DC-DPSGD and baselines on tabular datasets.

Algorithm	Privacy	Product	Malware	Cancer	Adult	Bank	Credit
DPSGD	$\varepsilon = 0.8$, $\delta = \frac{1}{n^{1.1}}$	83.22	96.86	94.74	85.12	88.62	80.90
Auto-S		82.22	96.86	94.74	85.20	88.51	80.95
DP-PSAC		83.69	96.75	95.09	85.15	88.51	80.92
DPSGD-HL		81.97	94.51	92.36	82.70	88.09	78.75
Ours (DC-DPSGD)		**85.90**	**97.49**	**95.52**	**85.61**	**88.73**	**81.28**
DPSGD	$\varepsilon = 0.5$, $\delta = \frac{1}{n^{1.1}}$	78.06	93.06	85.09	81.94	86.63	77.95
Auto-S		77.37	93.39	85.96	82.17	86.62	78.45
DP-PSAC		78.45	93.06	84.21	81.86	86.51	77.60
DPSGD-HL		74.88	90.43	81.35	79.28	85.03	75.16
Ours (DC-DPSGD)		**80.03**	**93.58**	**86.32**	**82.30**	**86.72**	**78.63**

Baselines. We compare DC-DPSGD with four DP baselines:

- **DPSGD** [1], which adopts Abadi's clipping mechanism. It clips gradients with norms exceeding c onto the L_2-ball of radius c.
- **Auto-S/NSGD** [11, 77], which is the DPSGD equipped with an automatic clipping mechanism that adaptively normalizes per-sample gradient norms.
- **DP-PSAC** [73], which extends DPSGD with a controlled clipping mechanism to mitigate the unbounded amplification of small-norm gradients often induced by automatic clipping.
- **DPSGD-HL** [19], which selects a clipping threshold below the minimum gradient norm by Report Noisy Max [26] under the heavy-tailed Lipschitz assumption.

Implementation details. We implement pre-sample clipping by BackPACK [18]. All experiments are conducted on a server with an Intel(R) Xeon(R) E5-2640 v4 CPU at 2.40GHz and a NVIDIA Tesla P40 GPU running on Ubuntu. By default, we set the subspace dimension to $k = 200$, and scale up to $k = 2,000$ for LLMs. $\varepsilon = \varepsilon_{\text{tr}} + \varepsilon_{\text{gp}}$ with $\varepsilon_{\text{tr}}/\varepsilon = 0.05$, $p = 0.1$, and sub-Weibull index $\theta = 2$ for experiments. More details are presented in Appendix H.1.

5.2 Effectiveness Comparison with Baselines

We compare the performance of DC-DPSGD with four DP baselines on twelve datasets under various DP constraints. Tables 1, 2, and 3 summarize the results on image, natural language, and tabular datasets. We analyze non-DP comparison results in Appendix H.3.

Results on image datasets. From Table 1, we observe that on normal datasets in high privacy regimes, DC-DPSGD outperforms DPSGD, Auto-S, DP-PSAC and DPSGD-HL by up to 1.71%, 2.09%, 2.43% and 4.04%, respectively. While on heavy-tailed datasets (i.e., CIFAR10-HT and ImageNette-HT), the corresponding improvements are 3.40%, 4.76%, 3.39% and 5.80%. For light-tailed baselines, including DPSGD with Abadi's clipping and adaptive variants, their methods adopt relatively small clipping thresholds and exhibit similar empirical behavior. Nevertheless, they fundamentally overweight small-norm gradients while neglecting large-norm gradients, which is not optimal in practice. For the heavy-tailed baseline, DPSGD-HL uses a clipping threshold based on the minimum gradient norm, which is orders of magnitude larger than that of light-tailed methods. Although this method aims to reduce clipping bias, the setting of a uniform clipping threshold prevents DPSGD-HL from achieving a better balance between body gradients and tail gradients. Then, these methods degrade notably on complex datasets (e.g., ImageNette) and those with heavier-tailed gradient variability characteristics (e.g., CIFAR10-HT and ImageNette-HT). In contrast, DC-DPSGD consistently improves accuracy on normal datasets while remaining robust under heavy-tailed settings due to our tail-aware discriminative clipping strategy. In contrast, under heavier-tailed regimes, existing methods either suffer from increased clipping loss due to small clipping thresholds or introduce excessive DP noise because of uniform thresholding.

Results on natural language dataset. Table 2 presents the results on text generation tasks. We evaluate DC-DPSGD on the E2E dataset under both full fine-tuning and parameter-efficient fine-tuning (LoRA), and on the MNLI dataset with a larger model

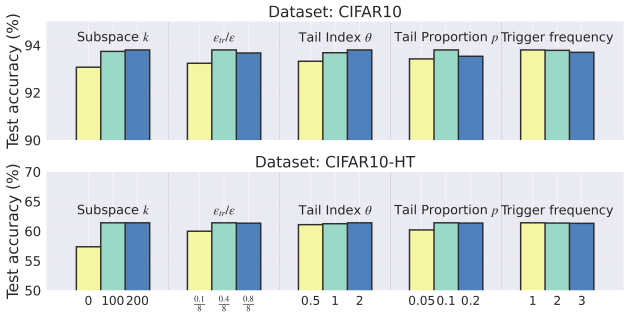

Figure 5: Effects of different parameters on test accuracy.

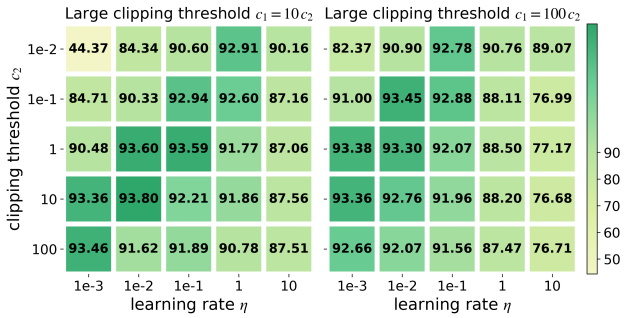

Figure 6: Test accuracy heatmap on CIFAR10 with c_1, c_2 and η.

architecture. The results demonstrate that DC-DPSGD consistently achieves superior test performance compared with baselines, indicating better preservation of linguistic fluency and content fidelity under various privacy constraints. Moreover, these improvements on transformer–based text generation suggest that our method remains scalable and effective even in large-scale architectures.

Results on tabular datasets. As shown in Table 3, under relatively loose privacy constraints (e.g., $\varepsilon = 0.8$), DC-DPSGD achieves superior performance across all tabular datasets, surpassing DPSGD baselines by a clear margin. Even when the privacy budget is reduced to $\varepsilon = 0.5$, the performance degradation of DC-DPSGD remains moderate compared to baselines, indicating its strong robustness to injected DP noise. These results demonstrate that DC-DPSGD maintains competitive accuracy in the low-privacy regime.

5.3 Parameter Evaluation

We next investigate the effects of various parameters in DC-DPSGD.

Parameter sensitivity analysis for DC-DPSGD. We first analyze the sensitivity of five parameters on model performance, including the dimension of the subspace k, the allocation of privacy budget ε, the tail index θ of the sub-Weibull distribution, the heavy-tail proportion p and the identification `strategy_trigger` frequency, with other parameters kept at default. The results on CIFAR10 and CIFAR10-HT are shown in Figure 5.

- **Subspace k**: We observe that the test accuracy increases with the value of k, consistent with the theoretical analysis that the trace error scales as $\mathbb{O}(1/k)$ and has a small impact on the results.
- **$\varepsilon_{tr}/\varepsilon$**: For the allocation of privacy budget between ε_{tr} and ε, where $\varepsilon = \varepsilon_{tr} + \varepsilon_{gp}$, we empirically find that a moderate privacy budget of around 5% of the total budget allows subspace identification to maintain acceptable performance.
- **Tail index θ**: Since 'HT' datasets are extracted by sub-Exponential distributions, the gradient exhibits a heavier tail phenomenon. Therefore, adopting a heavier-tailed latent distribution with larger $\theta > 1$ for the identification step tends to yield higher accuracy.
- **Tail proportion p**: We observe that $p = 0.1$ yields the best performance. When p is too small, it fails to sufficiently mitigate clipping loss; when too large, it introduces excessive noise. The identified proportion of heavy-tailed samples aligns with statistical expectations, while assigning larger clipping thresholds to light-body samples unnecessarily amplifies noise.
- **Trigger frequency**: Varying the trigger frequency has only a moderate effect on model performance, consistent with the empirical observation that the subspace remains stable during training. Therefore, subspace identification can be performed infrequently to reduce extra privacy overhead.

The results show that our method is insensitive to parameter choices, remaining stable across a wide range of configurations.

Guidance for clipping threshold and learning rate. We now validate our empirical guidance for the clipping threshold in Theorem 4.2. The results in Figure 6 indicate that the optimal ratio is approximately $c_1 \approx 10c_2$. We note that when $c_1 = 100c_2$, the maximum performance declines noticeably, and when $c_1 = c_2$, it corresponds to standard clipped DPSGD. From a theoretical perspective, given the parameters $\delta = 1e^{-5}$, $\eta/B = 0.04$, and $\theta \approx 2$ (following [27, 33, 66]), we can obtain $c_1 = \mathbb{O}(\log^{\theta}(1/\delta))$, which is roughly $\sqrt{125}$ times larger than $c_2 = \mathbb{O}(\log^{1/2}(1/\delta))$. This implies $c_1 = \log^{3/2}(1/\delta)c_2 \approx 10c_2$, confirming that the empirically observed optimal threshold ratio is theoretically consistent.

Effect of sampling strategies on test accuracy. We further investigate how different sampling strategies affect model performance. Table 4 reports test accuracy under two configurations: (1) equal sampling rates $q_1 = q_2 = q$ ($\sigma_{gp} = \sigma_{Pois}$), and (2) equal batch sizes $B_1 = B_2 = B$ (e.g., $B = 64$, $p = 0.1$, leading to $\sigma_{gp} = 1.3\sigma_{Pois}$ for CIFAR10). The accuracy difference between the two strategies is marginal (within 0.2–0.3%), suggesting that the minor degradation caused by smaller batch sizes is acceptable. Overall, this implies that maintaining consistent sampling rates can preserve privacy amplification in DC-DPSGD without noticeable performance loss.

In addition, we include the training trajectory, algorithm efficiency and ablation study on more datasets in Appendix H.2 [4].

5.4 Evaluation of DP Auditing Guarantees

Finally, we conduct state-of-the-art DP auditing methods to examine whether our algorithm maintains formal privacy guarantees in practice. DP guarantees are described using a theoretical privacy budget ε and a failure probability δ, which can limit the ability of adversary $\mathcal{A}$ to distinguish between $M(S)$ and $M(S')$. This inference can be seen as the adversary's membership inference attack (MIA) attempt, from which both false positive rate (FPR) and false negative rate (FNR) are derived. DP auditing [35] is a tool to verify whether an algorithm satisfies the claimed ε and δ, which leverages MIA [15] to obtain FPR and FNR, thereby deriving the empirical privacy budget ε^*. As demonstrated by [37], the privacy region of any (ε,δ)-DP mechanism is related to μ_{emp}-Gaussian Differential Privacy (GDP) [21] and can be defined as:

$$\mu_{emp} = \Phi^{-1}(1 - \text{FPR}) - \Phi^{-1}(\text{FNR}), \tag{16}$$

Table 4: Effect of sampling strategy on test accuracy.

Task	Fixed Parameter	Test Accuracy
CIFAR10	Sampling rate	93.80%
$\varepsilon = 8$	Batch size	93.69%
CIFAR10-HT	Sampling rate	61.38%
$\varepsilon = 8$	Batch size	60.51%
Malware	Sampling rate	97.49%
$\varepsilon = 0.8$	Batch size	97.42%

Table 5: Empirical ε^* of DC-DPSGD with DP auditing.

Method	O(T) Audit [56]		O(1) Audit [62]	
	$\varepsilon = 4$	$\varepsilon = 8$	$\varepsilon = 4$	$\varepsilon = 8$
DPSGD	2.07	4.02	1.80	3.72
DC-DPSGD	2.15	4.31	1.80	3.88
DC-DPSGD-NSI	4.13	7.87	3.35	7.23

where $\Phi(\cdot)$ is the cumulative distribution function (CDF) of the standard normal distribution. The empirical μ_{emp}-GDP can directly be converted to $(\varepsilon^*, \delta(\varepsilon^*))$-DP by the transformation formula of

$$\delta(\varepsilon^*) = \Phi\left(-\frac{\varepsilon^*}{\mu_{\text{emp}}} + \frac{\mu_{\text{emp}}}{2}\right) - e^{\varepsilon^*}\Phi\left(-\frac{\varepsilon^*}{\mu_{\text{emp}}} - \frac{\mu_{\text{emp}}}{2}\right). \quad (17)$$

This metric provides a convenient bridge between the GDP parameter μ_{emp} and the standard (ε, δ)-DP guarantee. In particular, given an empirical estimate of μ_{emp} obtained from auditing, the above transformation enables one to directly compute the empirical privacy budget ε^* for any target δ. Intuitively, a smaller ε^* indicates stronger empirical privacy preservation, and when ε^* approaches the claimed theoretical ε from below, it implies that the auditing process is stronger in detecting potential privacy leakage. We adopt two state-of-the-art black-box auditing methods in this set of experiments. One is $\mathbb{O}(T)$ auditing that performs T independent training runs for performing membership hypothesis testing. It claims to be nearly tight by pre-training the target model with in-distribution data and inserting out-of-distribution canaries [56] that are easily identifiable. The other is $\mathbb{O}(1)$ auditing, which randomly inserts multiple canaries on one training run to collect membership observations [62]. We evaluate the empirical ε^* of DC-DPSGD and compare it with that of DPSGD. To further justify the effectiveness of our private subspace identification method, we include DC-DPSGD-NSI with non-private subspace identification for comparison, i.e., $\varepsilon_{\text{tr}} = \text{null}$.

Table 5 presents the comparison results on CIFAR10 between our method and standard DPSGD [1] under the above two privacy auditing methods, evaluated at the 95% confidence interval. Under $\mathbb{O}(T)$ auditing, the empirical privacy budget ε^* of DC-DPSGD remains below the theoretically claimed privacy budget ε, demonstrating that the algorithm strictly adheres to differential privacy guarantees in practice. Under $\mathbb{O}(1)$ auditing, DC-DPSGD exhibits a privacy detectability level comparable to that of standard DPSGD, indicating a similarly high level of privacy protection. The slightly reduced audibility may result from the insertion of batched canaries, which can dilute the worst-case privacy signal due to averaging effects across batches. Furthermore, in DC-DPSGD-NSI, where subspace identification is performed without privacy constraints, the audited privacy budget exceeds ε, suggesting potential leakage through non-private identification. This observation validates the necessity of our proposed private subspace identification mechanism, confirming its effectiveness in enforcing privacy guarantees and mitigating the leakage risks in non-private alternatives.

6 Related Work

Heavy-tailed gradient variability and high-probability bounds. Studies of stationary point escape and Langevin dynamics reveal that gradient variability in neural networks exhibits anisotropic and non-Gaussian properties [32, 33, 60, 80]. These studies have identified and characterized specific heavy-tailed phenomena in gradient descent for deep neural networks. Recently, several works have focused on heavy-tailed convex optimization in privacy-preserving deep learning [38, 68]. However, the convergence characteristics of heavy-tailed clipped DPSGD in non-convex learning are not addressed. Meanwhile, due to the ability to capture tail behaviors of stochastic gradients, high probability theoretical tools [45, 46, 52] are widely used in non-private learning such as convex and non-convex optimization. Specifically, under bounded α-th moments assumption, [46] provide a high-probability bound for clipped SGD with adaptive momentum by martingale concentration inequalities. However, these tools remain under-explored in DP learning. Existing works [19, 38, 51] on optimizing clipped DPSGD rely on expectation bounds, which are unsuitable for heavier assumptions.

Gradient clipping. Gradient clipping is a widely adopted technique to ensure the sensitivity of gradients is bounded in both practical implementations and theoretical analysis of DPSGD [16, 31, 40, 70, 75, 79, 83]. Since the tuning parameters in the Abadi's clipping function [1] are complex, various adaptive gradient clipping schemes have been proposed [11, 77]. These schemes scale per-sample gradients based on their norms. In particular, gradients with concentrated norms are amplified infinitely. Building upon this, [73] controls the amplification of gradients with concentrated norms in a finite manner. For the theoretical guidance of clipping thresholds, [19] proposes to set the clipping threshold as a constant strictly smaller than the minimum per-sample gradient norm under the convex heavy-tailed Lipschitz condition. Moreover, Additionally, research on clipping loss has gradually gained importance. [70] and [40] argue for the connection between sampling noise and clipping loss, and mitigate clipping loss through group sampling. However, none of these works can be adapted to gradient clipping under the heavy-tailed GV assumption in DPSGD.

7 Conclusion

In this paper, we present unified high-probability optimization guarantees for clipped DPSGD, achieving the best-known convergence rates under heavy-tailed GV while preserving optimal rates in light-tailed settings. Motivated by these guarantees, we propose a novel tail-aware clipping mechanism DC-DPSGD that applies discriminative clipping thresholds to body and tail gradients, effectively balancing clipping loss and DP noise. We further analyze the convergence of DC-DPSGD and provide tighter optimization guarantees. We conduct extensive experiments on twelve real-world datasets, and the results demonstrate that DC-DPSGD outperforms four state-of-the-art baselines by up to 3.40%, 4.76%, 3.39% and 5.80% accuracy improvements, respectively.

References

[1] Martin Abadi, Andy Chu, Ian Goodfellow, H Brendan McMahan, Ilya Mironov, Kunal Talwar, and Li Zhang. 2016. Deep learning with differential privacy. In *CCS*. 308–318.

[2] Leonidas Akritidis. 2020. Product Classification and Clustering. https://doi.org/10.24432/C5M91Z. UCI Machine Learning Repository.

[3] Galen Andrew, Om Thakkar, Brendan McMahan, and Swaroop Ramaswamy. 2021. Differentially private learning with adaptive clipping. *NeurIPS* 34 (2021), 17455–17466.

[4] Anonymous. 2025. *Unified Differentially Private Stochastic Gradient Descent with Tail-Aware Discriminative Clipping*. https://anonymous.4open.science/r/Discriminative_Clipping_DPSGD-1FE6/full_version_DC_DPSGD.pdf Full Version and Supplementary Materials.

[5] Milad Bakhshizadeh, Arian Maleki, and Victor H De La Pena. 2023. Sharp concentration results for heavy-tailed distributions. *Information and Inference: A Journal of the IMA* 12, 3 (2023), 1655–1685.

[6] Ergute Bao, Yangfan Jiang, Fei Wei, Xiaokui Xiao, Zitao Li, Yaliang Li, and Bolin Ding. 2025. Unlocking the Power of Differentially Private Zeroth-order Optimization for Fine-tuning {LLMs}. In *USENIX Security*. 1569–1588.

[7] Ergute Bao, Fei Wei, Yin Yang, Xiaokui Xiao, Tianyu Pang, and Chao Du. 2025. Towards Learning on Vertically Partitioned Data with Distributed Differential Privacy. In *ICDE*. 2121–2134.

[8] Ergute Bao, Yizheng Zhu, Xiaokui Xiao, Yin Yang, Beng Chin Ooi, Benjamin Hong Meng Tan, and Khin Mi Mi Aung. 2022. Skellam Mixture Mechanism: a Novel Approach to Federated Learning with Differential Privacy. *Proc. VLDB Endow.* 15, 11 (2022), 2348–2360.

[9] Melih Barsbey, Milad Sefidgaran, Murat A Erdogdu, Gael Richard, and Umut Simsekli. 2021. Heavy tails in SGD and compressibility of overparametrized neural networks. *NeurIPS* 34 (2021), 29364–29378.

[10] Parthajit Borah and Dhruba K. Bhattacharyya. 2023. TUANDROMD (Tezpur University Android Malware Dataset). UCI Machine Learning Repository. https://archive.ics.uci.edu/dataset/855/tuandromd+(tezpur+university+android+malware+dataset) 4465 instances, 241 attributes, binary classification (malware vs goodware).

[11] Zhiqi Bu, Yu-Xiang Wang, Sheng Zha, and George Karypis. 2024. Automatic clipping: Differentially private deep learning made easier and stronger. *NeurIPS* 36 (2024).

[12] Kuntai Cai, Xiaokui Xiao, and Graham Cormode. 2023. PrivLava: Synthesizing Relational Data with Foreign Keys under Differential Privacy. *Proc. ACM Manag. Data* 1, 2 (2023), 142:1–142:25.

[13] Alexander Camuto, Xiaoyu Wang, Lingjiong Zhu, Chris Holmes, Mert Gurbuzbalaban, and Umut Simsekli. 2021. Asymmetric heavy tails and implicit bias in gaussian noise injections. In *ICML*. 1249–1260.

[14] Kaidi Cao, Colin Wei, Adrien Gaidon, Nikos Arechiga, and Tengyu Ma. 2019. Learning imbalanced datasets with label-distribution-aware margin loss. *NeurIPS* 32 (2019).

[15] Nicholas Carlini, Steve Chien, Milad Nasr, Shuang Song, Andreas Terzis, and Florian Tramer. 2022. Membership inference attacks from first principles. In *SP*. IEEE, 1897–1914.

[16] Xiangyi Chen, Steven Z Wu, and Mingyi Hong. 2020. Understanding gradient clipping in private sgd: A geometric perspective. *NeurIPS* 33 (2020), 13773–13782.

[17] Ashok Cutkosky and Harsh Mehta. 2020. Momentum improves normalized sgd. In *ICML*. PMLR, 2260–2268.

[18] Felix Dangel, Frederik Kunstner, and Philipp Hennig. 2020. BackPACK: Packing more into Backprop. In *ICLR*. https://openreview.net/forum?id=BJlrF24twB

[19] Rudrajit Das, Satyen Kale, Zheng Xu, Tong Zhang, and Sujay Sanghavi. 2023. Beyond uniform lipschitz condition in differentially private optimization. In *ICML*. PMLR, 7066–7101.

[20] Jia Deng, Wei Dong, Richard Socher, Li-Jia Li, Kai Li, and Li Fei-Fei. 2009. Imagenet: A large-scale hierarchical image database. In *CVPR*. Ieee, 248–255.

[21] Jinshuo Dong, Aaron Roth, and Weijie J Su. 2022. Gaussian differential privacy. *Journal of the Royal Statistical Society: Series B (Statistical Methodology)* 84, 1 (2022), 3–37.

[22] Wei Dong, Qiyao Luo, Giulia Fanti, Elaine Shi, and Ke Yi. 2024. Almost instance-optimal clipping for summation problems in the shuffle model of differential privacy. In *CCS*. 1939–1953.

[23] Wei Dong and Ke Yi. 2021. Residual sensitivity for differentially private multi-way joins. In *SIGMOD*. 432–444.

[24] Ondřej Dušek, Jekaterina Novikova, and Verena Rieser. 2020. Evaluating the state-of-the-art of end-to-end natural language generation: The e2e nlg challenge. *Computer Speech & Language* 59 (2020), 123–156.

[25] Cynthia Dwork, Frank McSherry, Kobbi Nissim, and Adam Smith. 2006. Calibrating noise to sensitivity in private data analysis. In *TCC*. Springer, 265–284.

[26] Cynthia Dwork, Aaron Roth, et al. 2014. The algorithmic foundations of differential privacy. *Foundations and Trends® in Theoretical Computer Science* 9, 3–4 (2014), 211–407.

[27] Khaled Eldowa and Andrea Paudice. 2024. General tail bounds for non-smooth stochastic mirror descent. In *AISTATS*. PMLR, 3205–3213.

[28] Xiequan Fan and Davide Giraudo. 2019. Large deviation inequalities for martingales in Banach spaces. *arXiv preprint arXiv:1909.05584* (2019).

[29] Huang Fang, Xiaoyun Li, Chenglin Fan, and Ping Li. 2022. Improved convergence of differential private sgd with gradient clipping. In *ICLR*.

[30] Dylan J Foster, Ayush Sekhari, and Karthik Sridharan. 2018. Uniform convergence of gradients for non-convex learning and optimization. *NeurIPS* 31 (2018).

[31] Jie Fu, Qingqing Ye, Haibo Hu, Zhili Chen, Lulu Wang, Kuncan Wang, and Xun Ran. 2024. DPSUR: Accelerating Differentially Private Stochastic Gradient Descent Using Selective Update and Release. *Proceedings of the VLDB Endowment* 17, 6 (2024), 1200–1213.

[32] Eduard Gorbunov, Marina Danilova, and Alexander Gasnikov. 2020. Stochastic optimization with heavy-tailed noise via accelerated gradient clipping. *NeurIPS* 33 (2020), 15042–15053.

[33] Mert Gurbuzbalaban, Umut Simsekli, and Lingjiong Zhu. 2021. The heavy-tail phenomenon in SGD. In *ICML*. PMLR, 3964–3975.

[34] Kaiming He, Xiangyu Zhang, Shaoqing Ren, and Jian Sun. 2016. Deep residual learning for image recognition. In *CVPR*. 770–778.

[35] Matthew Jagielski, Jonathan Ullman, and Alina Oprea. 2020. Auditing differentially private machine learning: How private is private sgd? *Advances in Neural Information Processing Systems* 33 (2020), 22205–22216.

[36] Christopher Jung, Katrina Ligett, Seth Neel, Aaron Roth, Saeed Sharifi-Malvajerdi, and Moshe Shenfeld. 2020. A New Analysis of Differential Privacy's Generalization Guarantees. In *11th Innovations in Theoretical Computer Science Conference (ITCS 2020)*. Schloss Dagstuhl–Leibniz-Zentrum für Informatik, 31–1.

[37] Peter Kairouz, Sewoong Oh, and Pramod Viswanath. 2015. The composition theorem for differential privacy. In *ICML*. PMLR, 1376–1385.

[38] Gautam Kamath, Xingtu Liu, and Huanyu Zhang. 2022. Improved rates for differentially private stochastic convex optimization with heavy-tailed data. In *ICML*. PMLR, 10633–10660.

[39] Ron Kohavi and Barry Becker. 1996. Adult (Census Income) Data Set. https://archive.ics.uci.edu/ml/datasets/adult. UCI Machine Learning Repository.

[40] Anastasia Koloskova, Hadrien Hendrikx, and Sebastian U Stich. 2023. Revisiting Gradient Clipping: Stochastic bias and tight convergence guarantees. In *ICML*. PMLR, 17343–17363.

[41] Alex Krizhevsky. 2009. Learning Multiple Layers of Features from Tiny Images. (2009), 32–33.

[42] Frederik Kunstner, Alan Milligan, Robin Yadav, Mark Schmidt, and Alberto Bietti. 2024. Heavy-tailed class imbalance and why adam outperforms gradient descent on language models. *NeurIPS* 37 (2024), 30106–30148.

[43] Yann LeCun, Léon Bottou, Yoshua Bengio, and Patrick Haffner. 1998. Gradient-based learning applied to document recognition. *Proc. IEEE* 86, 11 (1998), 2278–2324.

[44] Chris Junchi Li. 2018. A note on concentration inequality for vector-valued martingales with weak exponential-type tails. *arXiv preprint arXiv:1809.02495* (2018).

[45] Shaojie Li and Yong Liu. 2022. High probability guarantees for nonconvex stochastic gradient descent with heavy tails. In *ICML*. PMLR, 12931–12963.

[46] Shaojie Li and Yong Liu. 2023. High Probability Analysis for Non-Convex Stochastic Optimization with Clipping. In *ECAI*. IOS Press.

[47] Xiaoyu Li and Francesco Orabona. 2020. A high probability analysis of adaptive sgd with momentum. *arXiv preprint arXiv:2007.14294* (2020).

[48] Xuechen Li, Florian Tramer, Percy Liang, and Tatsunori Hashimoto. 2022. Large Language Models Can Be Strong Differentially Private Learners. In *ICLR*.

[49] Junxu Liu, Jian Lou, Li Xiong, Jinfei Liu, and Xiaofeng Meng. 2021. Projected federated averaging with heterogeneous differential privacy. *Proceedings of the VLDB Endowment* 15, 4 (2021), 828–840.

[50] Yuhan Liu, Sheng Wang, Yixuan Liu, Feifei Li, and Hong Chen. 2024. Unleash the Power of Ellipsis: Accuracy-Enhanced Sparse Vector Technique with Exponential Noise. *Proceedings of the VLDB Endowment* 18, 2 (2024), 187–199.

[51] Andrew Lowy and Meisam Razaviyayn. 2023. Private stochastic optimization with large worst-case lipschitz parameter: Optimal rates for (non-smooth) convex losses and extension to non-convex losses. In *ALT*. PMLR, 986–1054.

[52] Liam Madden, Emiliano Dall'Anese, and Stephen Becker. 2024. High probability convergence bounds for non-convex stochastic gradient descent with sub-weibull noise. *Journal of Machine Learning Research* 25, 241 (2024), 1–36.

[53] Frank D McSherry. 2009. Privacy integrated queries: an extensible platform for privacy-preserving data analysis. In *SIGMOD*. 19–30.

[54] Ilya Mironov. 2017. Rényi differential privacy. In *CSF*. IEEE, 263–275.

[55] Paulo Moro, Paulo Cortez, and Paulo Rita. 2014. Bank Marketing Data Set. https://archive.ics.uci.edu/dataset/222/bank+marketing. UCI Machine Learning Repository.

[56] Meenatchi Sundaram Muthu Selva Annamalai and Emiliano De Cristofaro. 2024. Nearly tight black-box auditing of differentially private machine learning. *NeurIPS* 37 (2024), 131482–131502.

[57] K Papinesi. 2002. Bleu: A method for automatic evaluation of machine translation. In *ACL*. 311–318.

[58] Seulki Park, Jongin Lim, Younghan Jeon, and Jin Young Choi. 2021. Influence-balanced loss for imbalanced visual classification. In *ICCV*. 735–744.

[59] Haichao Sha, Ruixuan Liu, Yixuan Liu, and Hong Chen. 2023. PCDP-SGD: Improving the Convergence of Differentially Private SGD via Projection in Advance. *arXiv preprint arXiv:2312.03792* (2023).

[60] Umut Simsekli, Levent Sagun, and Mert Gurbuzbalaban. 2019. A tail-index analysis of stochastic gradient noise in deep neural networks. In *ICML*. PMLR, 5827–5837.

[61] Umut Simsekli, Lingjiong Zhu, Yee Whye Teh, and Mert Gurbuzbalaban. 2020. Fractional underdamped langevin dynamics: Retargeting sgd with momentum under heavy-tailed gradient noise. In *ICML*. PMLR, 8970–8980.

[62] Thomas Steinke, Milad Nasr, and Matthew Jagielski. 2023. Privacy auditing with one (1) training run. *NeurIPS* 36 (2023), 49268–49280.

[63] Dajun Sun, Wei Dong, and Ke Yi. 2023. Confidence Intervals for Private Query Processing. *Proceedings of the VLDB Endowment* 17, 3 (2023), 373–385.

[64] Florian Tramer and Dan Boneh. 2021. Differentially Private Learning Needs Better Features (or Much More Data). In *ICLR*.

[65] Roman Vershynin. 2018. *High-dimensional probability: An introduction with applications in data science*. Vol. 47. Cambridge university press.

[66] Mariia Vladimirova, Stéphane Girard, Hien Nguyen, and Julyan Arbel. 2020. Sub-Weibull distributions: Generalizing sub-Gaussian and sub-Exponential properties to heavier tailed distributions. *Stat* 9, 1 (2020), e318.

[67] Martin J Wainwright. 2019. *High-dimensional statistics: A non-asymptotic viewpoint*. Vol. 48. Cambridge university press.

[68] Di Wang, Hanshen Xiao, Srinivas Devadas, and Jinhui Xu. 2020. On differentially private stochastic convex optimization with heavy-tailed data. In *ICML*. PMLR, 10081–10091.

[69] Fei Wei, Ergute Bao, Xiaokui Xiao, Yin Yang, and Bolin Ding. 2024. AAA: an Adaptive Mechanism for Locally Differential Private Mean Estimation. *Proc. VLDB Endow.* 17, 8 (2024), 1843–1855.

[70] Jianxin Wei, Ergute Bao, Xiaokui Xiao, and Yin Yang. 2022. Dpis: An enhanced mechanism for differentially private sgd with importance sampling. In *CCS*. 2885–2899.

[71] Adina Williams, Nikita Nangia, and Samuel Bowman. 2018. A broad-coverage challenge corpus for sentence understanding through inference. In *Proceedings of the 2018 conference of the North American chapter of the association for computational linguistics: human language technologies, volume 1 (long papers)*. 1112–1122.

[72] William H. Wolberg, W. Nick Street, and Olvi L. Mangasarian. 1995. Breast Cancer Wisconsin (Diagnostic) Data Set. https://archive.ics.uci.edu/dataset/17/breast+cancer+wisconsin+diagnostic. UCI Machine Learning Repository.

[73] Tianyu Xia, Shuheng Shen, Su Yao, Xinyi Fu, Ke Xu, Xiaolong Xu, and Xing Fu. 2023. Differentially private learning with per-sample adaptive clipping. In *AAAI*, Vol. 37. 10444–10452.

[74] Han Xiao, Kashif Rasul, and Roland Vollgraf. 2017. Fashion-MNIST: a Novel Image Dataset for Benchmarking Machine Learning Algorithms. *CoRR* (2017).

[75] Hanshen Xiao, Zihang Xiang, Di Wang, and Srinivas Devadas. 2023. A theory to instruct differentially-private learning via clipping bias reduction. In *SP*. IEEE, 2170–2189.

[76] Saining Xie, Ross Girshick, Piotr Dollár, Zhuowen Tu, and Kaiming He. 2017. Aggregated residual transformations for deep neural networks. In *CVPR*. 1492–1500.

[77] Xiaodong Yang, Huishuai Zhang, Wei Chen, and Tie-Yan Liu. 2022. Normalized/clipped sgd with perturbation for differentially private non-convex optimization. *arXiv preprint arXiv:2206.13033* (2022).

[78] I-Cheng Yeh and Che-hui Lien. 2009. Default of Credit Card Clients Data Set. https://archive.ics.uci.edu/ml/datasets/default+of+credit+card+clients. UCI Machine Learning Repository.

[79] Jingzhao Zhang, Tianxing He, Suvrit Sra, and Ali Jadbabaie. 2020. Why gradient clipping accelerates training: A theoretical justification for adaptivity. *ICLR* (2020).

[80] Jingzhao Zhang, Sai Praneeth Karimireddy, Andreas Veit, Seungyeon Kim, Sashank Reddi, Sanjiv Kumar, and Suvrit Sra. 2020. Why are adaptive methods good for attention models? *NeurIPS* 33 (2020), 15383–15393.

[81] Tong Zhang. 2005. Data dependent concentration bounds for sequential prediction algorithms. In *COLT*. Springer, 173–187.

[82] Xinwei Zhang, Zhiqi Bu, Steven Wu, and Mingyi Hong. 2023. Differentially Private SGD Without Clipping Bias: An Error-Feedback Approach. In *ICLR*.

[83] Xinwei Zhang, Xiangyi Chen, Mingyi Hong, Zhiwei Steven Wu, and Jinfeng Yi. 2022. Understanding clipping for federated learning: Convergence and client-level differential privacy. In *ICML*.

[84] Yingxue Zhou, Steven Wu, and Arindam Banerjee. 2021. Bypassing the Ambient Dimension: Private SGD with Gradient Subspace Identification. In *ICLR*.

[85] Yuqing Zhu and Yu-Xiang Wang. 2020. Improving sparse vector technique with renyi differential privacy. *NeurIPS* 33 (2020), 20249–20258.

Appendix

A Theoretical Foundations and Notations

A.1 Summary of Theoretical Results

Table 6: Summary of state-of-the-art optimization results, where c is the clipping threshold, θ is the heavy-tail index, T is the number of iterations, and δ is a small probability. 'Gradient Symmetry' means the gradient variability $\mathcal{G}_t$ satisfies $\mathbb{P}(\mathcal{G}_t) = \mathbb{P}(-\mathcal{G}_t)$. $G_{\min}$ is the minimum Lipschitz constant, $0 < p < 1$ is the tail proportion and $f_c(\theta) := \max\left(\mathbb{O}\left(\log^{\theta}(1/\delta), \log^{\theta}(\sqrt{T})\right)\right)$.

Method	Upper Bound	Loss Function	Gradient Assumption	Clipping Guidance
NSGD [77]	$\mathbb{O}\left(\varphi^{1/2}\right)$	Non-convex	Light-tailed Gradient Variability	Normalized $c = 1$
Auto-S [11]	$\mathbb{O}\left(\varphi\right)$	Non-convex	Light-tailed Gradient Variability; Gradient Symmetry	Normalized $c = 1$
Clipped DPSGD [19]	$\mathbb{O}\left(\varphi^{1-\theta}\right)$	Convex	Heavy-tailed Lipschitz	$c \leq G_{\min}$
Clipped DPSGD [19]	$\mathbb{O}\left(\delta^{-\frac{2\theta}{2-\theta}}\varphi^{1-\frac{\theta}{2-\theta}}\right)$	Non-convex	Heavy-tailed Lipschitz	$c = \mathbb{O}\left((\delta^2\varphi)^{-\frac{\theta}{2-\theta}}\right)$
Our Clipped DPSGD (Thm 3.1)	$\mathbb{O}\left(\log^{\max(1,\theta)}(T/\delta)\log^{2\theta}(\sqrt{T})\varphi^{1/2}\right)$	Non-convex	Heavy-tailed Gradient Variability	$c = f_c(\theta)$
Our DC-DPSGD (Thm 4.2 Cor 4.3)	$p * \mathbb{O}\left(\log^{\max(1,\theta)}(T/\delta)\log^{2\theta}(\sqrt{T})\varphi^{\frac{1}{2}}\right)$ $+(1-p) * \mathbb{O}\left(\log(T/\delta)\log(\sqrt{T})\varphi^{\frac{1}{2}}\right)$	Non-convex	Heavy-tailed Gradient Variability	Tail: $c_1 = f_c(\theta)$ Body: $c_2 = f_c(\frac{1}{2})$

A.2 Summary of notations

B Preliminaries

A random variable X called a sub-Weibull random variable with tail parameter θ and scale factor K, which is denoted by $X \sim subW(\theta, K)$. We next introduce the equivalent properties and theoretical tools of sub-Weibull distributions.

B.1 Properties

Definition B.1 (Sub-Weibull Equivalent Properties [66]). *Let X be a random variable and $\theta \geq 0$, and there exists some constant K_1, K_2, K_3, K_4 depending on θ. Then the following characterizations are equivalent:*

(1) The tails of X satisfy

$$\exists K_1 > 0 \text{ such that } \mathbb{P}(|X| > t) \leq 2\exp(-(t/K_1)^{\frac{1}{\theta}}), \forall t > 0.$$

(2) The moments of X satisfy

$$\exists K_2 > 0 \text{ such that } \|X\|_p \leq K_2 p^{\theta}, \forall k \geq 1.$$

(3) The moment generating function (MGF) of $|X|^{\frac{1}{\theta}}$ satisfies

$$\exists K_3 > 0 \text{ such that } \mathbb{E}[\exp((\lambda|X|)^{\frac{1}{\theta}})] \leq \exp((\lambda K_3)^{\frac{1}{\theta}}), \forall \lambda \in (0, 1/K_3).$$

(4) The MGF of $|X|^{\frac{1}{\theta}}$ is bounded at some point,

$$\exists K_4 > 0 \text{ such that } \mathbb{E}[\exp((|X|/K_4)^{\frac{1}{\theta}})] \leq 2.$$

Table 7: Summary of notations

Definition of Notations	
$\mathbf{w}$	the model parameter
d	the dimension of model parameters
z	the training sample
n	the training data size
B	the mini-batch size
ℓ	the loss function
$S\ S'$	the neighboring datasets
ε_{gp}	the privacy budget for differential privacy
ε_{tr}	the privacy budget for preserving traces
σ_{gp}	the noise multiplier for differential privacy
σ_{tr}	the noise multiplier for preserving traces
$V_{t,k}$	top-k dimensional the random projection vector
K	the variance-related positive constant
$\nabla L(\mathbf{w}_t)$	the true average gradient for training data
T	the total iterations of training
η_t	the learning rate in t iteration
c	the clipping threshold
c_1	the large clipping threshold for heavy tail
c_2	the small clipping threshold for light body
θ	the heavy-tail index
p	the proportion of heavy tail
$\lambda_{t,i}^{\text{tr}}$	the empirical trace of the sample
$\hat{\lambda}_{t,i}^{\text{tr}}$	the population trace of the sample
$\widetilde{\lambda}_{t,i}^{\text{tr}}$	the perturbed trace of the sample
S^{tail}	the set of gradients in the heavy-tail region
S^{body}	the set of gradients in the light-body region
$\mathcal{C}_{gt}$	the gradient variability

B.2 Theoretical Tools

Based on the properties of sub-Weibull variables, we have the following high probability bounds and concentration inequalities for heavier tails as theoretical tools. Besides, We define l_p norm as $\|\|\|_p$, for any $p \geq 1$.

Lemma B.1. *Let a variable $X \sim subW(\theta, K)$, for any $\delta \in (0,1)$, then with probability $(1-\delta)$ we have*

$$|X| \leq K \log^{\theta}(2/\delta). \tag{1}$$

Proof. Let $K_1 = K$ in Definition B.1, and take $t = K\log^{\theta}(2/\delta)$, then the inequality holds with probability $1-\delta$. □

Lemma B.2 ([52, 66]). *Let $X_1, ..., X_n$ are $subW(\theta, K_i)$ random variables with scale parameters $K_1, ...K_n$. $\forall x \geq 0$, we have*

$$\mathbb{P}(|\sum_{i=1}^{n} X_i| \geq x) \leq 2 \cdot \exp(-(\frac{x}{g(\theta)\sum_{i=1}^{n} K_i})^{\frac{1}{\theta}}), \tag{2}$$

where $g(\theta) = (4e)^{\theta}$ for $\theta \leq 1$ and $g(\theta) = 2(2e\theta)^{\theta}$ for $\theta \geq 1$.

Lemma B.3 (Sub-Weibull Freedman Inequality [52]). *Let $(\Omega, \mathcal{F}, (\mathcal{F}_i), \mathbb{P})$ be a filtered probability space. Let (ξ_i) and (K_i) be adapted to $(\mathcal{F}_i)$. Let $n \in \mathbb{N}$, then $\forall i \in [n]$, assume $K_{i-1} \geq 0$, $\mathbb{E}[\xi_i|\mathcal{F}_{i-1}] = 0$, and $\mathbb{E}[\exp((|\xi_i|/K_{i-1})^{\frac{1}{\theta}})|\mathcal{F}_{i-1}] \leq 2$ where $\theta \geq 1/2$. If $\theta > 1/2$, assume there exists (m_i) such that $K_{i-1} \leq m_i$.*

if $\theta = 1/2$, let $a = 2$, then $\forall x, \beta \geq 0$, $\alpha > 0$, and $\lambda \in [0, \frac{1}{2\alpha}]$,

$$\mathbb{P}\left(\bigcup_{k\in[n]} \left\{\sum_{i=1}^{k} \xi_i \geq x \text{ and } \sum_{i=1}^{k} aK_{i-1}^2 \leq \alpha \sum_{i=1}^{k} \xi_i + \beta\right\}\right) \leq \exp(-\lambda x + 2\lambda^2\beta), \tag{3}$$

and $\forall x, \beta, \lambda \geq 0$,

$$\mathbb{P}\left(\bigcup_{k\in[n]}\left\{\sum_{i=1}^{k}\xi_i \geq x \text{ and } \sum_{i=1}^{k} aK_{i-1}^2 \leq \beta\right\}\right) \leq \exp(-\lambda x + \frac{\lambda^2}{2}\beta). \tag{4}$$

If $\theta \in (\frac{1}{2}, 1]$, *let* $a = (4\theta)^{2\theta}e^2$ *and* $b = (4\theta)^{\theta}e$. $\forall x, \beta \geq 0$, *and* $\alpha \geq b\max_{i\in[n]} m_i$, *and* $\lambda \in [0, \frac{1}{2\alpha}]$,

$$\mathbb{P}\left(\bigcup_{k\in[n]}\left\{\sum_{i=1}^{k}\xi_i \geq x \text{ and } \sum_{i=1}^{k} aK_{i-1}^2 \leq \alpha\sum_{i=1}^{k}\xi_i + \beta\right\}\right) \leq \exp(-\lambda x + 2\lambda^2\beta), \tag{5}$$

and $\forall x, \beta \geq 0$, *and* $\lambda \in [0, \frac{1}{b\max_{i\in[n]} m_i}]$,

$$\mathbb{P}\left(\bigcup_{k\in[n]}\left\{\sum_{i=1}^{k}\xi_i \geq x \text{ and } \sum_{i=1}^{k} aK_{i-1}^2 \leq \beta\right\}\right) \leq \exp(-\lambda x + \frac{\lambda^2}{2}\beta). \tag{6}$$

If $\theta > 1$, *let* $\delta \in (0,1)$. *Let* $a = (2^{2\theta+1}+2)\Gamma(2\theta+1) + 2^{3\theta}\Gamma(3\theta+1)/3$ *and* $b = 2\log n/\delta^{\theta-1}$, *where* $\Gamma(x) = \int_0^\infty t^{x-1}e^{-t}dt$. $\forall x, \beta \geq 0$, $\alpha \geq b\max_{i\in[n]} m_i$, *and* $\lambda \in [0, \frac{1}{2\alpha}]$,

$$\mathbb{P}\left(\bigcup_{k\in[n]}\left\{\sum_{i=1}^{k}\xi_i \geq x \text{ and } \sum_{i=1}^{k} aK_{i-1}^2 \leq \alpha\sum_{i=1}^{k}\xi_i + \beta\right\}\right) \leq \exp(-\lambda x + 2\lambda^2\beta) + 2\delta, \tag{7}$$

and $\forall x, \beta \geq 0$, *and* $\lambda \in [0, \frac{1}{b\max_{i\in[n]} m_i}]$,

$$\mathbb{P}\left(\bigcup_{k\in[n]}\left\{\sum_{i=1}^{k}\xi_i \geq x \text{ and } \sum_{i=1}^{k} aK_{i-1}^2 \leq \beta\right\}\right) \leq \exp(-\lambda x + \frac{\lambda^2}{2}\beta) + 2\delta. \tag{8}$$

Lemma B.4 ([81]). *Let* $z_1, ..., z_n$ *be a sequence of randoms variables such that* z_k *may depend the previous variables* $z_1, ..., z_{k-1}$ *for all* $k = 1, ..., n$. *Consider a sequence of functionals* $\xi_k(z_1, ..., z_k)$, $k = 1, ..., n$. *Let* $\sigma_n^2 = \sum_{k=1}^n \mathbb{E}_{z_k}[(\xi_k - \mathbb{E}_{z_k}[\xi_k])^2]$ *be the conditional variance. Assume* $|\xi_k - \mathbb{E}_{z_k}[\xi_k]| \leq b$ *for each* k. *Let* $\rho \in (0,1]$ *and* $\delta \in (0,1)$. *With probability at least* $1-\delta$ *we have*

$$\sum_{k=1}^{n}\xi_k - \sum_{k=1}^{n}\mathbb{E}_{z_k}[\xi_k] \leq \frac{\rho\sigma_n^2}{b} + \frac{b\log\frac{1}{\delta}}{\rho}. \tag{9}$$

Lemma B.5 ([17]). *For any vector* $\mathbf{g} \in \mathbb{R}^d$, $\langle \mathbf{g}/\|\mathbf{g}\|_2, \nabla L_S(\mathbf{w})\rangle \geq \frac{\|\nabla L_S(\mathbf{w})\|_2}{3} - \frac{8\|\mathbf{g}-L_S(\mathbf{w})\|_2}{3}$.

Lemma B.6 ([52]). *If* $X \sim subW(\theta, K)$, *then* $\mathbb{E}[|X^p|] \leq 2\Gamma(p\theta+1)K^p$ $\forall p > 0$. *In particular,* $\mathbb{E}[X^2] \leq 2\Gamma(2\theta+1)K^2$.

Lemma B.7 ([5]). *Suppose* $X_1, ..., X_m \overset{d}{=} X$ *are independent and identically distributed random variables whose right tails are captured by an increasing and continuous function* $I : \mathbb{R} \to \mathbb{R}^{\geq 0}$ *with the property* $I(x) = \mathbb{O}(x)$ *as* $x \to \infty$. *Let* $X^L = X\mathbb{I}(X \leq L)$, $S_m = \sum_{i=1}^m X_i$ *and* $Z^L := X^L - \mathbb{E}[X]$. *Define* $x_{\max} := \sup\{x \geq 0 : x \leq \eta v(mx, \eta)\frac{I(mx)}{mx}\}$, *then*

$$\mathbb{P}(S_m - \mathbb{E}[S_m] > mx) \leq \begin{cases} \exp(-c_x\eta I(mx)) + m\exp(-I(mx)), & \text{if } x \geq x_{\max}, \\ \exp(-\dfrac{mx^2}{2v(mx_{\max},\eta)}) + m\exp(-\dfrac{mx_{\max}^2(\eta)}{\eta v(mx_{\max},\eta)}), & \text{if } 0 \leq x \leq x_{\max}, \end{cases} \tag{10}$$

where $c_x = 1 - \frac{\eta v(mx,\eta)I(mx)}{2mx^2}$ *and* $v(L,\eta) = \mathbb{E}\big[(Z^L)^2\mathbb{I}(Z^L \leq 0) + (Z^L)^2\exp(\eta\frac{I(L)}{L}Z^L)\mathbb{I}(Z^L > 0)\big], \forall \beta \in (0,1]$.

Lemma B.8 ([5]). *Consider the same settings as the ones in Lemma B.7. Assume* $\mathbb{E}[X_i] = 0$, *then* $\forall t \geq 0$ *we have*

$$\mathbb{P}(S_m > mt) \leq \exp(-\frac{mt^2}{2v(mt,\eta)}) + \exp(-\eta\max\{c_t, \frac{1}{2}\}I(mt)) + m\exp(-I(mt)). \tag{11}$$

Lemma B.9 (**Ahlswede-Winter Inequality**). *Let Y be a random, symmetric, positive semi-definite dd matrix such that $\|\mathbb{E}[Y]\|_2 \leq 1$. Suppose $\|Y\|_2 \leq R$ for some fixed scalar $R \geq 1$. Let $Y_1, ..., Y_m$ be independent copies of Y (i.e., independently sampled matrix with the same distribution as Y). For any $\mu \in (0, 1)$, we have*

$$\mathbb{P}(\|\frac{1}{m}\sum_{i=1}^{m} Y_i - \mathbb{E}[Y_i]\|_2 > \mu) \leq 2d \cdot \exp(-m\mu^2/4R). \tag{12}$$

Lemma B.10 ([28, 44]). *Let $\theta \in (0, \infty)$ be given. Assume that $(\mathbf{X}_i, i = 1, \cdots, N)$ is a sequence of $\mathbb{R}^d$-valued martingale differences with respect to filtration $\mathcal{F}_i$, i.e. $\mathbb{E}[\mathbf{X}_i|\mathcal{F}_{i-1}] = 0$, and it satisfies the following weak exponential-type tail condition: for some $\theta > 0$ and all $i = 1, \cdots, N$ we have for some scalar $0 < K_i$,*

$$\mathbb{E}\left[\exp\left(\left\|\frac{\mathbf{X}_i}{K_i}\right\|^{\frac{1}{\theta}}\right)\right] \leq 2.$$

Assume that $K_i < \infty$ for each $i = 1, \cdots, N$. Then for an arbitrary $N \geq 1$ and $t > 0$,

$$\mathbb{P}\left(\max_{n \leq N}\left\|\sum_{i=1}^{n} \mathbf{X}_i\right\| \geq t\right) \leq 4\left[3 + (3\theta)^{2\theta}\frac{128\sum_{i=1}^{N} K_i^2}{t^2}\right]\exp\left\{-\left(\frac{t^2}{64\sum_{i=1}^{N} K_i^2}\right)^{\frac{1}{2\theta+1}}\right\}. \tag{13}$$

Lemma B.11 (restated from Theorem 3.5 in [36]). *Suppose M is (ε, δ)-differentially private and (α, β)-accurate with respect to samples. Then for any analyst $\mathcal{A}$ that chooses a sequence of queries adaptively, we have*

$$\mathbb{P}_{\substack{Data\sim\mathcal{D} \\ (\hat{f}_{\mathcal{J}}, \mathcal{J})\sim\text{Interaction}(\mathcal{A}, M|Data)}}\left[\max_{i\in\mathcal{J}}\left|\hat{f}_i - \mathbb{E}_{Data'\sim\mathcal{D}}\left[f_i(Data')\right]\right| \geq \alpha + (e^{\varepsilon} - 1) + v_1 + 2v_2\right] \leq \frac{\beta}{v_1} + \frac{\delta}{v_2}. \tag{14}$$

C Convergence of Heavy-Tailed Clipped DPSGD

Theorem C.1 (**Convergence of Clipped DPSGD under Heavy-tailed Sub-Weibull Gradient Variability Assumption**). *Under Assumptions 2.1 and 2.2, let* $\mathbf{w}_t$ *be the iterative parameter produced by clipped DPSGD of Algorithm 1 with* $T = \mathbb{O}(\frac{n\varepsilon}{\sqrt{d\log(1/\delta)}})$, $T \geq 1$, *and* $\eta_t = \frac{1}{\sqrt{T}}$. *Define* $\hat{\sigma}_{\text{gp}}^2 := m_2\frac{Tdc^2B^2\log(1/\delta)}{n^2\varepsilon^2}$. *If* $\theta = \frac{1}{2}$ *and* $K \leq \hat{\sigma}_{\text{gp}}$, *then* $c = \max\left(4K\log^{\theta}(\sqrt{T}), \frac{19K\log^{\frac{1}{2}}(1/\delta)}{12}\right)$. *If* $\theta = \frac{1}{2}$ *and* $K \geq \hat{\sigma}_{\text{gp}}$, *then* $c = \max\left(4K\log^{\theta}(\sqrt{T}), 39K\log^{\frac{1}{2}}(2/\delta)\right)$. *If* $\theta > \frac{1}{2}$, *then* $c = \max\left(4K\log^{\theta}(\sqrt{T}), 20K\log^{\theta}(2/\delta)\right)$. *For any* $\delta \in (0,1)$, *with probability* $1-\delta$, *we have*

$$\frac{1}{T}\sum_{t=1}^{T}\min\left\{\|\nabla L_S(\mathbf{w}_t)\|_2, \|\nabla L_S(\mathbf{w}_t)\|_2^2\right\} \leq \mathbb{O}\left(\frac{d^{\frac{1}{4}}\log^{\frac{1}{4}}(T/\delta)\hat{\log}(T/\delta)\log^{2\theta}(\sqrt{T})}{(n\varepsilon)^{\frac{1}{2}}}\right),$$

where $\hat{\log}(T/\delta) := \log^{\max(1,\theta)}(T/\delta)$.

Proof. We consider two cases: $\|\nabla L_S(\mathbf{w}_t)\|_2 \leq c/2$ and $\|\nabla L_S(\mathbf{w}_t)\|_2 \geq c/2$. To simplify notation, we omit the subscript of privacy parameters throughout, such as ε_{gp}.

Firstly, we first consider the case $\|\nabla L_S(\mathbf{w}_t)\|_2 \leq c/2$.

$$\begin{aligned}
&L_S(\mathbf{w}_{t+1}) - L_S(\mathbf{w}_t) \leq \langle \mathbf{w}_{t+1} - \mathbf{w}_t, \nabla L_S(\mathbf{w}_t)\rangle + \frac{1}{2}\beta\|\mathbf{w}_{t+1} - \mathbf{w}_t\|_2^2 \qquad (15)\\
&\leq -\eta_t\langle \overline{\mathbf{g}}_t + \zeta_t, \nabla L_S(\mathbf{w}_t)\rangle + \frac{1}{2}\beta\eta_t^2\|\overline{\mathbf{g}}_t + \zeta_t\|_2^2\\
&= -\eta_t\langle \overline{\mathbf{g}}_t - \mathbb{E}_t[\overline{\mathbf{g}}_t] + \mathbb{E}_t[\overline{\mathbf{g}}_t] - \nabla L_S(\mathbf{w}_t), \nabla L_S(\mathbf{w}_t)\rangle - \eta_t\langle \zeta_t, \nabla L_S(\mathbf{w}_t)\rangle\\
&- \eta_t\|\nabla L_S(\mathbf{w}_t)\|_2^2 + \frac{1}{2}\beta\eta_t^2\|\overline{\mathbf{g}}_t\|_2^2 + \frac{1}{2}\beta\eta_t^2\|\zeta_t\|_2^2 + \beta\eta_t^2\langle \overline{\mathbf{g}}_t, \zeta_t\rangle\\
&= -\eta_t\langle \overline{\mathbf{g}}_t - \mathbb{E}_t[\overline{\mathbf{g}}_t], \nabla L_S(\mathbf{w}_t)\rangle - \eta_t\langle \mathbb{E}_t[\overline{\mathbf{g}}_t] - \nabla L_S(\mathbf{w}_t), \nabla L_S(\mathbf{w}_t)\rangle - \eta_t\langle \zeta_t, \nabla L_S(\mathbf{w}_t)\rangle\\
&- \eta_t\|\nabla L_S(\mathbf{w}_t)\|_2^2 + \frac{1}{2}\beta\eta_t^2\|\overline{\mathbf{g}}_t\|_2^2 + \frac{1}{2}\beta\eta_t^2\|\zeta_t\|_2^2 + \beta\eta_t^2\langle \overline{\mathbf{g}}_t, \zeta_t\rangle
\end{aligned}$$

Considering all T iterations, we get

$$\begin{aligned}
&\sum_{t=1}^{T}\eta_t\|\nabla L_S(\mathbf{w}_t)\|_2^2 \leq L_S(\mathbf{w}_1) - L_S(\mathbf{w}_S) + \sum_{t=1}^{T}\frac{1}{2}\beta\eta_t^2c^2 + \underbrace{\sum_{t=1}^{T}\frac{1}{2}\beta\eta_t^2\|\zeta_t\|_2^2}_{\text{Eq.1}} + \underbrace{\sum_{t=1}^{T}\beta\eta_t^2\langle \overline{\mathbf{g}}_t, \zeta_t\rangle}_{\text{Eq.2}}\\
&\underbrace{-\sum_{t=1}^{T}\eta_t\langle \zeta_t, \nabla L_S(\mathbf{w}_t)\rangle}_{\text{Eq.3}} \underbrace{-\sum_{t=1}^{T}\eta_t\langle \overline{\mathbf{g}}_t - \mathbb{E}_t[\overline{\mathbf{g}}_t], \nabla L_S(\mathbf{w}_t)\rangle}_{\text{Eq.4}} \underbrace{-\sum_{t=1}^{T}\eta_t\langle \mathbb{E}_t[\overline{\mathbf{g}}_t] - \nabla L_S(\mathbf{w}_t), \nabla L_S(\mathbf{w}_t)\rangle}_{\text{Eq.5}} \qquad (16)
\end{aligned}$$

For Eq.1, Eq.2 and Eq.3, since $\zeta_t \sim \mathbb{N}(0, c\sigma_{\text{gp}}\mathbb{I}_d)$, according to sub-Gaussian properties and Lemma B.2, with probability at least $1-\delta$, we have

$$\begin{aligned}
\sum_{t=1}^{T}\frac{1}{2}\beta\eta_t^2\|\zeta_t\|_2^2 &\leq 2\beta K^2e\log(2/\delta)\sum_{t=1}^{T}\eta_t^2\\
&\leq 2\beta m_2ed\frac{Tc^2B^2\log^2(2/\delta)}{n^2\varepsilon^2}\sum_{t=1}^{T}\eta_t^2. \qquad (17)
\end{aligned}$$

Also, with probability at least $1-\delta$, we get

$$\begin{aligned}
\sum_{t=1}^{T}\beta\eta_t^2\langle \overline{\mathbf{g}}_t, \zeta_t\rangle &\leq \sum_{t=1}^{T}\beta\eta_t^2\|\overline{\mathbf{g}}_t\|_2\|\zeta_t\|_2\\
&\leq \sum_{t=1}^{T}2\beta cK\sqrt{e}\log^{\frac{1}{2}}(2/\delta)\eta_t^2\\
&\leq 2\beta\sqrt{em_2Td}\frac{c^2B\log(2/\delta)}{n\varepsilon}\sum_{t=1}^{T}\eta_t^2. \qquad (18)
\end{aligned}$$

Due to $\nabla L_S(\mathbf{w}_t) \le c/2$, for the term $-\sum_{t=1}^{T} \eta_t \langle \zeta_t, \nabla L_S(\mathbf{w}_t) \rangle$, with probability at least $1-\delta$, we have

$$\begin{aligned} -\sum_{t=1}^{T} \eta_t \langle \zeta_t, \nabla L_S(\mathbf{w}_t) \rangle &\le \sum_{t=1}^{T} \eta_t \|\zeta_t\|_2 \|\nabla L_S(\mathbf{w}_t)\|_2 \\ &\le \sum_{t=1}^{T} 2cK\sqrt{e} \log^{\frac{1}{2}}(2/\delta)\eta_t \\ &\le 2\sqrt{em_2 Td} \frac{c^2 B \log(2/\delta)}{n\varepsilon} \sum_{t=1}^{T} \eta_t. \end{aligned} \tag{19}$$

Since $\mathbb{E}_t[-\eta_t \langle \overline{\mathbf{g}}_t - \mathbb{E}_t[\overline{\mathbf{g}}_t], \nabla L_S(\mathbf{w}_t) \rangle] = 0$, the sequence $(-\eta_t \langle \overline{\mathbf{g}}_t - \mathbb{E}_t[\overline{\mathbf{g}}_t], \nabla L_S(\mathbf{w}_t) \rangle, t \in \mathbb{N})$ is a martingale difference sequence. Applying Lemma B.4, we define $\xi_t = -\eta_t \langle \overline{\mathbf{g}}_t - \mathbb{E}_t[\overline{\mathbf{g}}_t], \nabla L_S(\mathbf{w}_t) \rangle$ and have

$$|\xi_t| \le \eta_t (\|\overline{\mathbf{g}}_t\|_2 + \|\mathbb{E}_t[\overline{\mathbf{g}}_t]\|_2) \|\nabla L_S(\mathbf{w}_t)\|_2 \le \eta_t c^2. \tag{20}$$

Applying $\mathbb{E}_t[(\xi_t - \mathbb{E}_t\xi_t)^2] \le \mathbb{E}_t[\xi_t^2]$, we have

$$\begin{aligned} \sum_{t=1}^{T} \mathbb{E}_t[(\xi_t - \mathbb{E}_t\xi_t)^2] &\le \sum_{t=1}^{T} \eta_t^2 \mathbb{E}_t[\|\overline{\mathbf{g}}_t - \mathbb{E}_t[\overline{\mathbf{g}}_t]\|_2^2 \|\nabla L_S(\mathbf{w}_t)\|_2^2] \\ &\le 4c^2 \sum_{t=1}^{T} \eta_t^2 \|\nabla L_S(\mathbf{w}_t)\|_2^2. \end{aligned} \tag{21}$$

Then, with probability $1-\delta$, we obtain

$$\sum_{t=1}^{T} \xi_t \le \frac{\rho 4c^2 \sum_{t=1}^{T} \eta_t^2 \|\nabla L_S(\mathbf{w}_t)\|_2^2}{\eta_t c^2} + \frac{\eta_t c^2 \log(1/\delta)}{\rho}. \tag{22}$$

Next, to bound term Eq.5, we have

$$\sum_{t=1}^{T} \eta_t \langle \mathbb{E}_t[\overline{\mathbf{g}}_t] - \nabla L_S(\mathbf{w}_t), \nabla L_S(\mathbf{w}_t) \rangle \le \frac{1}{2} \sum_{t=1}^{T} \eta_t \|\mathbb{E}_t[\overline{\mathbf{g}}_t] - \nabla L_S(\mathbf{w}_t)\|_2^2 + \frac{1}{2} \sum_{t=1}^{T} \eta_t \|\nabla L_S(\mathbf{w}_t)\|_2^2.$$

Setting $a_t = \mathbb{I}_{\|\mathbf{g}_t\|_2 > c}$ and $b_t = \mathbb{I}_{\|\mathbf{g}_t - \nabla L_S(\mathbf{w}_t)\|_2 > \frac{c}{2}}$, for term $\|\mathbb{E}_t[\overline{\mathbf{g}}_t] - \nabla L_S(\mathbf{w}_t)\|_2$, we have

$$\begin{aligned} \|\mathbb{E}_t[\overline{\mathbf{g}}_t] - \nabla L_S(\mathbf{w}_t)\|_2 &= \|\mathbb{E}_t[(\overline{\mathbf{g}}_t - \mathbf{g}_t)a_t]\|_2 \\ &= \|\mathbb{E}_t[(\mathbf{g}_t(\frac{c}{\|\mathbf{g}_t\|_2} - 1)a_t]\|_2 \\ &\le \mathbb{E}_t[\|(\mathbf{g}_t(\frac{c}{\|\mathbf{g}_t\|_2} - 1)a_t\|_2] \\ &\le \mathbb{E}_t[|\|\mathbf{g}_t\|_2 - c|a_t] \\ &\le \mathbb{E}_t[|\|\mathbf{g}_t\|_2 - \|\nabla L_S(\mathbf{w}_t)\|_2|a_t] \\ &\le \mathbb{E}_t[|\|\mathbf{g}_t - \nabla L_S(\mathbf{w}_t)\|_2|a_t] \\ &\le \mathbb{E}_t[|\|\mathbf{g}_t - \nabla L_S(\mathbf{w}_t)\|_2|b_t] \\ &\le \sqrt{\mathbb{E}_t[\|\mathbf{g}_t - \nabla L_S(\mathbf{w}_t)\|_2^2]\mathbb{E}_t b_t^2}. \end{aligned} \tag{23}$$

Applying Lemma B.6, we get $\mathbb{E}_t[\|\mathbf{g}_t - \nabla L_S(\mathbf{w}_t)\|_2^2] \le 2K^2\Gamma(2\theta+1)$. Then, for term $\mathbb{E}_t b_t^2$, with sub-Weibull properties and probability $1-\delta$ we have

$$\mathbb{E}_t b_t^2 = \mathbb{P}(\|\mathbf{g}_t - \nabla L_S(\mathbf{w}_t)\|_2 > \frac{c}{2}) \le 2\exp(-(\frac{c}{4K})^{\frac{1}{\theta}}) \tag{24}$$

So, we get formula (22) as

$$\sqrt{\mathbb{E}_t[\|\mathbf{g}_t - \nabla L_S(\mathbf{w}_t)\|_2^2]\mathbb{E}_t b_t^2} \le 2\sqrt{K^2\Gamma(2\theta+1)\exp(-(\frac{c}{4K})^{\frac{1}{\theta}})}. \tag{25}$$

Thus, for Eq.5, with probability $1 - T\delta$ we finally obtain

$$\sum_{t=1}^{T} \eta_t \langle \mathbb{E}_t[\overline{\mathbf{g}}_t] - \nabla L_S(\mathbf{w}_t), \nabla L_S(\mathbf{w}_t) \rangle \\ \leq 2K^2\Gamma(2\theta+1) \sum_{t=1}^{T} \eta_t \exp(-(\frac{c}{4K})^{\frac{1}{\theta}}) + \frac{1}{2}\sum_{t=1}^{T} \eta_t \|\nabla L_S(\mathbf{w}_t)\|_2^2. \tag{26}$$

Combining Eq.1-5 with the inequality (10), with probability $1 - 4\delta - T\delta$, we have

$$\sum_{t=1}^{T} \eta_t \|\nabla L_S(\mathbf{w}_t)\|_2^2 \leq L_S(\mathbf{w}_1) - L_S(\mathbf{w}_S) + \sum_{t=1}^{T} \frac{1}{2}\beta\eta_t^2 c^2 + 2\beta m_2 e d \frac{T c^2 B^2 \log^2(2/\delta)}{n^2\varepsilon^2} \sum_{t=1}^{T} \eta_t^2 \\ + 2\beta\sqrt{em_2 T d}\frac{c^2 B \log(2/\delta)}{n\varepsilon} \sum_{t=1}^{T} \eta_t^2 + 2\sqrt{em_2 T d}\frac{c^2 B \log(2/\delta)}{n\varepsilon} \sum_{t=1}^{T} \eta_t + \frac{\eta_t c^2 \log(1/\delta)}{\rho} \\ + \frac{4\rho c^2 \sum_{t=1}^{T} \eta_t^2 \|\nabla L_S(\mathbf{w}_t)\|_2^2}{\eta_t c^2} + 2K^2\Gamma(2\theta+1)\exp(-(\frac{c}{4K})^{\frac{1}{\theta}}) \sum_{t=1}^{T} \eta_t + \frac{1}{2}\sum_{t=1}^{T} \eta_t \|\nabla L_S(\mathbf{w}_t)\|_2^2. \tag{27}$$

Setting $\rho = \frac{1}{16}$, $T = \mathbb{O}(\frac{n\varepsilon}{\sqrt{d\log(1/\delta)}})$ and $\eta_t = \frac{1}{\sqrt{T}}$, we have

$$\frac{1}{4}\sum_{t=1}^{T} \eta_t \|\nabla L_S(\mathbf{w}_t)\|_2^2 \leq L_S(\mathbf{w}_1) - L_S(\mathbf{w}_S) + \frac{1}{2}\beta c^2 + 2\beta m_2 e \frac{d^{\frac{1}{2}} c^2 B^2 \log^{\frac{3}{2}}(2/\delta)}{n\varepsilon} \\ + 2\beta\sqrt{em_2}\frac{d^{\frac{1}{4}} c^2 B \log^{\frac{1}{2}}(2/\delta)}{\sqrt{n\varepsilon}} + 2\sqrt{em_2} c^2 B \log^{\frac{1}{2}}(2/\delta) + \frac{16 d^{\frac{1}{4}} c^2 \log^{\frac{5}{4}}(1/\delta)}{\sqrt{n\varepsilon}} \\ \underbrace{+ 2K^2\Gamma(2\theta+1)\exp(-(\frac{c}{4K})^{\frac{1}{\theta}})\sqrt{T}}_{\text{Eq.6}}. \tag{28}$$

Then, we pay attention to term Eq.6. If $c \to 0$, then $\exp(-(\frac{c}{4K})^{\frac{1}{\theta}}) \to 1$ and $\sqrt{T}$ will dominate term Eq.6. We know that in classical clipped DPSGD, a small c is regarded as the clipping threshold guide, which will cause the variance term Eq.6 to dominate the entire bound. For this, we will provide guidance on the clipping values of DPSGD under the heavy-tailed assumption.

Let $\exp(-(\frac{c}{4K})^{\frac{1}{\theta}}) \leq \frac{1}{\sqrt{T}}$, then we have $c \geq 4K\log^{\theta}(\sqrt{T})$. So, we obtain

$$\sum_{t=1}^{T} \eta_t \|\nabla L_S(\mathbf{w}_t)\|_2^2 \leq 4(L_S(\mathbf{w}_1) - L_S(\mathbf{w}_S)) + 2\beta c^2 + 8\beta m_2 e \frac{d^{\frac{1}{2}} c^2 B^2 \log^{\frac{3}{2}}(2/\delta)}{n\varepsilon} \\ + 8\beta\sqrt{em_2}\frac{d^{\frac{1}{4}} c^2 B \log^{\frac{1}{2}}(2/\delta)}{\sqrt{n\varepsilon}} + 8\sqrt{em_2} c^2 B \log^{\frac{1}{2}}(2/\delta) + \frac{64 d^{\frac{1}{4}} c^2 \log^{\frac{5}{4}}(1/\delta)}{\sqrt{n\varepsilon}} + 8K^2\Gamma(2\theta+1). \tag{29}$$

Multiplying $\frac{1}{\sqrt{T}}$ on both sides, we get

$$\frac{1}{\sqrt{T}}\sum_{t=1}^{T} \eta_t \|\nabla L_S(\mathbf{w}_t)\|_2^2 \leq \frac{1}{\sqrt{T}}\Bigg(4(L_S(\mathbf{w}_1) - L_S(\mathbf{w}_S)) + 2\beta c^2 + 8\beta m_2 e \frac{d^{\frac{1}{2}} c^2 B^2 \log^{\frac{3}{2}}(2/\delta)}{n\varepsilon} \\ + 8\beta\sqrt{em_2}\frac{d^{\frac{1}{4}} c^2 B \log^{\frac{1}{2}}(2/\delta)}{\sqrt{n\varepsilon}} + 8\sqrt{em_2} c^2 B \log^{\frac{1}{2}}(2/\delta) + \frac{64 d^{\frac{1}{4}} c^2 \log^{\frac{5}{4}}(1/\delta)}{\sqrt{n\varepsilon}} + 8K^2\Gamma(2\theta+1)\Bigg). \tag{30}$$

Taking $c = 4K\log^{\theta}(\sqrt{T})$, due to $T \geq 1$, we achieve

$$\begin{aligned}\frac{1}{\sqrt{T}}\sum_{t=1}^{T}\eta_t\|\nabla L_S(\mathbf{w}_t)\|_2^2 \leq\ & \frac{4(L_S(\mathbf{w}_1)-L_S(\mathbf{w}_S))}{\sqrt{T}} + \frac{8K^2\Gamma(2\theta+1)}{\sqrt{T}} \\ &+ \frac{16K^2\log^{2\theta}(\sqrt{T})\log(2/\delta)}{\sqrt{T}}\left(2\beta + 8\beta m_2 e\frac{d^{\frac{1}{2}}B^2\log^{\frac{1}{2}}(2/\delta)}{n\varepsilon}\right. \\ &\left.+8\beta\sqrt{em_2}\frac{d^{\frac{1}{4}}B\log^{-\frac{1}{2}}(2/\delta)}{\sqrt{n\varepsilon}} + 8\sqrt{em_2}B\log^{-\frac{1}{2}}(2/\delta) + \frac{64d^{\frac{1}{4}}\log^{\frac{1}{4}}(1/\delta)}{\sqrt{n\varepsilon}}\right) \\ \leq\ & \mathbb{O}\left(\frac{\log^{2\theta}(\sqrt{T})\log(1/\delta)}{\sqrt{T}}\cdot\frac{d^{\frac{1}{4}}\log^{\frac{1}{4}}(1/\delta)}{\sqrt{n\varepsilon}}\right) \\ \leq\ & \mathbb{O}\left(\frac{\log^{2\theta}(\sqrt{T})\log(1/\delta)d^{\frac{1}{4}}\log^{\frac{1}{4}}(1/\delta)}{\sqrt{n\varepsilon}}\right). \end{aligned} \tag{31}$$

Due to $\frac{1}{T}\sum_{t=1}^{T}\|\nabla L_S(\mathbf{w}_t)\|_2^2 \leq \frac{1}{\sqrt{T}}\sum_{t=1}^{T}\eta_t\|\nabla L_S(\mathbf{w}_t)\|_2^2$, we have

$$\frac{1}{T}\sum_{t=1}^{T}\|\nabla L_S(\mathbf{w}_t)\|_2^2 \leq \mathbb{O}\left(\frac{d^{\frac{1}{4}}\log^{2\theta}(\sqrt{T})\log^{\frac{5}{4}}(1/\delta)}{(n\varepsilon)^{\frac{1}{2}}}\right), \tag{32}$$

with probability $1 - T\delta - 4\delta$.

By substitution, with probability $1-\delta$, we get

$$\frac{1}{T}\sum_{t=1}^{T}\|\nabla L_S(\mathbf{w}_t)\|_2^2 \leq \mathbb{O}\left(\frac{d^{\frac{1}{4}}\log^{2\theta}(\sqrt{T})\log^{\frac{5}{4}}(T/\delta)}{(n\varepsilon)^{\frac{1}{2}}}\right). \tag{33}$$

Secondly, we consider the case $\|\nabla L_S(\mathbf{w}_t)\|_2 \geq c/2$.

$$\begin{aligned} L_S(\mathbf{w}_{t+1}) - L_S(\mathbf{w}_t) &\leq \langle \mathbf{w}_{t+1}-\mathbf{w}_t, \nabla L_S(\mathbf{w}_t)\rangle + \frac{1}{2}\beta\|\mathbf{w}_{t+1}-\mathbf{w}_t\|_2^2 \\ &\leq \underbrace{-\eta_t\langle \overline{\mathbf{g}}_t + \zeta_t, \nabla L_S(\mathbf{w}_t)\rangle}_{\text{Eq.7}} + \underbrace{\frac{1}{2}\beta\eta_t^2\|\overline{\mathbf{g}}_t+\zeta_t\|_2^2}_{\text{Eq.8}} \end{aligned} \tag{34}$$

We have discussed term Eq.8 in the above case, so we focus on Eq.7 here. Setting $s_t^+ = \mathbb{I}_{\|\mathbf{g}_t\|_2 \geq c}$ and $s_t^- = \mathbb{I}_{\|\mathbf{g}_t\|_2 \leq c}$.

$$\begin{aligned} &-\eta_t\langle \overline{\mathbf{g}}_t + \zeta_t, \nabla L_S(\mathbf{w}_t)\rangle \\ &= -\eta_t\langle \frac{c\mathbf{g}_t}{\|\mathbf{g}_t\|_2}s_t^+ + \mathbf{g}_t s_t^-, \nabla L_S(\mathbf{w}_t)\rangle - \eta_t\langle \zeta_t, \nabla L_S(\mathbf{w}_t)\rangle. \end{aligned} \tag{35}$$

Applying Lemma B.5 to term $-\eta_t\langle \frac{c\mathbf{g}_t}{\|\mathbf{g}_t\|_2}s_t^+, \nabla L_S(\mathbf{w}_t)\rangle$, we have

$$\begin{aligned} -\eta_t\langle \frac{c\mathbf{g}_t}{\|\mathbf{g}_t\|_2}s_t^+, \nabla L_S(\mathbf{w}_t)\rangle &\leq -\frac{c\eta_t s_t^+\|\nabla L_S(\mathbf{w}_t)\|_2}{3} + \frac{8c\eta_t\|\mathbf{g}_t - \nabla L_S(\mathbf{w}_t)\|_2}{3} \\ &\leq -\frac{c\eta_t(1-s_t^-)\|\nabla L_S(\mathbf{w}_t)\|_2}{3} + \frac{8c\eta_t\|\mathbf{g}_t - \nabla L_S(\mathbf{w}_t)\|_2}{3}. \end{aligned} \tag{36}$$

For term $-\eta_t\langle \mathbf{g}_t s_t^-, \nabla L_S(\mathbf{w}_t)\rangle$, we obtain

$$\begin{aligned} -\eta_t\langle \mathbf{g}_t s_t^-, \nabla L_S(\mathbf{w}_t)\rangle &= -\eta_t s_t^-(\langle \mathbf{g}_t - \nabla L_S(\mathbf{w}_t), \nabla L_S(\mathbf{w}_t)\rangle + \|\nabla L_S(\mathbf{w}_t)\|_2^2) \\ &\leq -\eta_t s_t^-(-\|\mathbf{g}_t - \nabla L_S(\mathbf{w}_t)\|_2\|\nabla L_S(\mathbf{w}_t)\|_2 + \|\nabla L_S(\mathbf{w}_t)\|_2^2) \\ &\leq \eta_t\|\mathbf{g}_t - \nabla L_S(\mathbf{w}_t)\|_2\|\nabla L_S(\mathbf{w}_t)\|_2 - \frac{c}{2}\eta_t s_t^-\|\nabla L_S(\mathbf{w}_t)\|_2 \\ &\leq \eta_t\|\mathbf{g}_t - \nabla L_S(\mathbf{w}_t)\|_2\|\nabla L_S(\mathbf{w}_t)\|_2 - \frac{c}{3}\eta_t s_t^-\|\nabla L_S(\mathbf{w}_t)\|_2. \end{aligned} \tag{37}$$

According to Lemma B.1, with probability at least $1-\delta$, we have

$$\|\mathbf{g}_t - \nabla L_S(\mathbf{w}_t)\|_2 \leq K\log^{\theta}(2/\delta), \tag{38}$$

then we get

$$-\eta_t\langle \mathbf{g}_t s_t^-, \nabla L_S(\mathbf{w}_t)\rangle \leq K\log^{\theta}(2/\delta)\|\nabla L_S(\mathbf{w}_t)\|_2 - \frac{c}{3}\eta_t s_t^-\|\nabla L_S(\mathbf{w}_t)\|_2, \tag{39}$$

and

$$-\eta_t\langle\frac{c\mathbf{g}_t}{\|\mathbf{g}_t\|_2}s_t^+,\nabla L_S(\mathbf{w}_t)\rangle\leq-\frac{c\eta_t(1-s_t^-)\|\nabla L_S(\mathbf{w}_t)\|_2}{3}+\frac{8c\eta_tK\log^\theta(2/\delta)}{3}. \tag{40}$$

Using Lemma B.2 to term $-\sum_{t=1}^T\eta_t\langle\zeta_t,\nabla L_S(\mathbf{w}_t)\rangle$, with probability at least $1-\delta$, we have

$$-\sum_{t=1}^T\eta_t\langle\zeta_t,\nabla L_S(\mathbf{w}_t)\rangle\leq 4\sqrt{em_2Td}\frac{cB\log(2/\delta)}{n\varepsilon}\sum_{t=1}^T\eta_t\|\nabla L_S(\mathbf{w}_t)\|_2. \tag{41}$$

So, combining formula (38), formula (39) and formula (40) with term Eq.7, with probability at least $1-2\delta-T\delta$, we obtain

$$\begin{aligned}
&-\sum_{t=1}^T\eta_t\langle\overline{\mathbf{g}}_t+\zeta_t,\nabla L_S(\mathbf{w}_t)\rangle\leq-\sum_{t=1}^T\frac{c\eta_t}{3}\|\nabla L_S(\mathbf{w}_t)\|_2+\sum_{t=1}^T\frac{8c\eta_tK\log^\theta(2/\delta)}{3}\\
&+K\log^\theta(2/\delta)\sum_{t=1}^T\eta_t\|\nabla L_S(\mathbf{w}_t)\|_2+4\sqrt{em_2Td}\frac{cB\log(2/\delta)}{n\varepsilon}\sum_{t=1}^T\eta_t\|\nabla L_S(\mathbf{w}_t)\|_2\\
&\leq-\sum_{t=1}^T\frac{c\eta_t}{3}\|\nabla L_S(\mathbf{w}_t)\|_2+(\frac{19}{3}K\log^\theta(2/\delta)+4\sqrt{em_2Td}\frac{cB\log(2/\delta)}{n\varepsilon})\sum_{t=1}^T\eta_t\|\nabla L_S(\mathbf{w}_t)\|_2.
\end{aligned} \tag{42}$$

Next, considering all T iterations and term Eq.8 with $\hat{\sigma}_{\text{gp}}^2:=dc^2\sigma_{\text{gp}}^2=m_2\frac{Tdc^2B^2\log(1/\delta)}{n^2\varepsilon^2}$ and probability $1-4\delta-T\delta$, we have

$$\begin{aligned}
&(\frac{c}{3}-\frac{19}{3}K\log^\theta(2/\delta)-4\sqrt{e}\hat{\sigma}_{\text{gp}}\log^{\frac{1}{2}}(1/\delta))\sum_{t=1}^T\eta_t\|\nabla L_S(\mathbf{w}_t)\|_2\leq L_S(\mathbf{w}_1)-L_S(\mathbf{w}_S)\\
&+(2\beta m_2ed\frac{Tc^2B^2\log^2(2/\delta)}{n^2\varepsilon^2}+2\beta\sqrt{em_2Td}\frac{c^2B\log(2/\delta)}{n\varepsilon}+\frac{1}{2}\beta c^2)\sum_{t=1}^T\eta_t^2.
\end{aligned} \tag{43}$$

If $\theta=\frac{1}{2}$ and $K\geq\hat{\sigma}_{\text{gp}}$, let $\frac{c}{3}\geq\frac{39}{3}K\log^{\frac{1}{2}}(2/\delta)$, i.e. $c\geq 39K\log^{\frac{1}{2}}(2/\delta)$, taking $c=39K\log^{\frac{1}{2}}(2/\delta)$, $T=\mathbb{O}(\frac{n\varepsilon}{\sqrt{d\log(1/\delta)}})$ and $\eta_t=\frac{1}{\sqrt{T}}$, we have

$$\begin{aligned}
\sum_{t=1}^T\eta_t\|\nabla L_S(\mathbf{w}_t)\|_2&\leq\frac{3}{K\log^{\frac{1}{2}}(2/\delta)}(L_S(\mathbf{w}_1)-L_S(\mathbf{w}_S))\\
&+\frac{3\sum_{t=1}^T\eta_t^2}{K\log^{\frac{1}{2}}(2/\delta)}\left(2\beta m_2ed\frac{Tc^2B^2\log^2(2/\delta)}{n^2\varepsilon^2}+2\beta\sqrt{em_2Td}\frac{c^2B\log(2/\delta)}{n\varepsilon}+\frac{1}{2}\beta c^2\right)\\
&\leq\frac{L_S(\mathbf{w}_1)-L_S(\mathbf{w}_S)+2\beta e\hat{\sigma}_{\text{gp}}^2\log(2/\delta)+2\beta c\sqrt{e}\hat{\sigma}_{\text{gp}}\log^{\frac{1}{2}}(2/\delta)+\frac{39^2}{2}\beta K^2\log(2/\delta)}{\frac{1}{3}K\log^{\frac{1}{2}}(2/\delta)}\\
&\leq\frac{3(L_S(\mathbf{w}_1)-L_S(\mathbf{w}_S))}{K\log^{\frac{1}{2}}(2/\delta)}+6\beta eK\log^{\frac{1}{2}}(2/\delta)+6\beta\sqrt{e}\log^{\frac{1}{2}}(2/\delta)+3\beta\frac{(39)^2}{2}K\log^{\frac{1}{2}}(2/\delta).
\end{aligned} \tag{44}$$

Thus, with probability $1-4\delta-T\delta$, we have

$$\frac{1}{T}\sum_{t=1}^T\|\nabla L_S(\mathbf{w}_t)\|_2\leq\frac{1}{\sqrt{T}}\sum_{t=1}^T\eta_t\|\nabla L_S(\mathbf{w}_t)\|_2\leq\mathbb{O}(\frac{\log^{\frac{1}{2}}(1/\delta)}{\sqrt{T}})=\mathbb{O}(\frac{\log^{\frac{1}{2}}(1/\delta)d^{\frac{1}{4}}\log^{\frac{1}{4}}(1/\delta)}{\sqrt{n\varepsilon}}),$$

implying that with probability $1-\delta$, we have

$$\frac{1}{T}\sum_{t=1}^T\|\nabla L_S(\mathbf{w}_t)\|_2\leq\mathbb{O}(\frac{d^{\frac{1}{4}}\log^{\frac{3}{4}}(T/\delta)}{\sqrt{n\varepsilon}}). \tag{45}$$

If $\theta = \frac{1}{2}$ and $K \le \hat{\sigma}_{\text{gp}}$, that is, $c \ge \frac{19\log^{\frac{1}{2}}(1/\delta)K}{12}$, thus there exists $T = \mathbb{O}(\frac{n\varepsilon}{\sqrt{d\log(1/\delta)}})$, $T \ge 1$ and $\eta_t = \frac{1}{\sqrt{T}}$ that we obtain

$$\begin{aligned}
\sum_{t=1}^{T}\eta_t\|\nabla L_S(\mathbf{w}_t)\|_2 &\le \frac{1}{\sqrt{e}\hat{\sigma}_{\text{gp}}\log^{\frac{1}{2}}(1/\delta)}(L_S(\mathbf{w}_1) - L_S(\mathbf{w}_S)) \\
&+ \frac{\sum_{t=1}^{T}\eta_t^2}{\sqrt{e}\hat{\sigma}_{\text{gp}}\log^{\frac{1}{2}}(1/\delta)}\left(2\beta m_2 ed\frac{Tc^2B^2\log^2(2/\delta)}{n^2\varepsilon^2} + 2\beta\sqrt{em_2Td}\frac{c^2B\log(2/\delta)}{n\varepsilon} + \frac{1}{2}\beta c^2\right) \\
&\le \frac{1}{\sqrt{e}\hat{\sigma}_{\text{gp}}\log^{\frac{1}{2}}(1/\delta)}(L_S(\mathbf{w}_1) - L_S(\mathbf{w}_S)) \\
&+ \frac{\sum_{t=1}^{T}\eta_t^2}{\sqrt{e}\hat{\sigma}_{\text{gp}}\log^{\frac{1}{2}}(1/\delta)}\left(2\beta e\hat{\sigma}_{\text{gp}}^2\log(2/\delta) + 2\beta\sqrt{e}\hat{\sigma}_{\text{gp}}\log^{\frac{1}{2}}(2/\delta) + \frac{27^2}{2}\beta e\hat{\sigma}_{\text{gp}}^2\log(2/\delta)\right) \\
&\le \frac{L_S(\mathbf{w}_1) - L_S(\mathbf{w}_S)}{K\log^{\frac{1}{2}}(2/\delta)} + 2\beta eK\log^{\frac{1}{2}}(2/\delta) + 2\beta\sqrt{e}\log^{\frac{1}{2}}(2/\delta) + \beta\frac{(27)^2}{2}K\log^{\frac{1}{2}}(2/\delta). \qquad (46)
\end{aligned}$$

Therefore, with probability $1 - 4\delta - T\delta$, we have

$$\frac{1}{T}\sum_{t=1}^{T}\|\nabla L_S(\mathbf{w}_t)\|_2 \le \mathbb{O}(\frac{\log^{\frac{1}{2}}(1/\delta)d^{\frac{1}{4}}\log^{\frac{1}{4}}(1/\delta)}{\sqrt{n\varepsilon}}),$$

then, with probability $1 - \delta$, we have

$$\frac{1}{T}\sum_{t=1}^{T}\|\nabla L_S(\mathbf{w}_t)\|_2 \le \mathbb{O}(\frac{d^{\frac{1}{4}}\log^{\frac{3}{4}}(T/\delta)}{\sqrt{n\varepsilon}}). \qquad (47)$$

If $\theta > \frac{1}{2}$, then term $\log^{\theta}(2/\delta)$ dominates the left-hand inequality, i.e. $\frac{19}{3}K\log^{\theta}(2/\delta) \ge 4\sqrt{e}\hat{\sigma}_{\text{gp}}\log^{\frac{1}{2}}(1/\delta)$. Let $\frac{c}{3} \ge \frac{20}{3}K\log^{\theta}(2/\delta)$, $T = \mathbb{O}(\frac{n\varepsilon}{\sqrt{d\log(1/\delta)}})$ and $\eta_t = \frac{1}{\sqrt{T}}$, we obtain

$$\begin{aligned}
\sum_{t=1}^{T}\eta_t\|\nabla L_S(\mathbf{w}_t)\|_2 &\le \frac{3}{K\log^{\theta}(2/\delta)}(L_S(\mathbf{w}_1) - L_S(\mathbf{w}_S)) \\
&+ \frac{3\sum_{t=1}^{T}\eta_t^2}{K\log^{\theta}(2/\delta)}\left(2\beta m_2 ed\frac{Tc^2B^2\log^2(2/\delta)}{n^2\varepsilon^2} + 2\beta\sqrt{em_2Td}\frac{c^2B\log(2/\delta)}{n\varepsilon} + \frac{1}{2}\beta c^2\right) \\
&\le \frac{3(L_S(\mathbf{w}_1) - L_S(\mathbf{w}_S))}{K\log^{\theta}(2/\delta)} + \frac{19^2}{24}\beta K\log^{\theta}(2/\delta) + 190\beta K\log^{\theta}(2/\delta) + 3\beta(20)^2K\log^{\theta}(2/\delta). \qquad (48)
\end{aligned}$$

Consequently, with probability $1 - \delta$, we have

$$\frac{1}{T}\sum_{t=1}^{T}\|\nabla L_S(\mathbf{w}_t)\|_2 \le \mathbb{O}(\frac{\log^{\theta}(T/\delta)d^{\frac{1}{4}}\log^{\frac{1}{4}}(T/\delta)}{\sqrt{n\varepsilon}}). \qquad (49)$$

Integrating the above results, when $\nabla L_S(\mathbf{w}_t) \ge c/2$ we have

$$\frac{1}{T}\sum_{t=1}^{T}\|\nabla L_S(\mathbf{w}_t)\|_2 \le \mathbb{O}(\frac{d^{\frac{1}{4}}\log^{\theta+\frac{1}{4}}(T/\delta)}{\sqrt{n\varepsilon}}), \qquad (50)$$

with probability $1 - \delta$ and $\theta \ge \frac{1}{2}$.

To sum up, covering the two cases, we ultimately come to the conclusion with probability $1 - \delta$, $T = \mathbb{O}(\frac{n\varepsilon}{\sqrt{d\log(1/\delta)}})$, $T \ge 1$, and $\eta_t = \frac{1}{\sqrt{T}}$

$$\begin{aligned}
\frac{1}{T}\sum_{t=1}^{T}\min\left\{\|\nabla L_S(\mathbf{w}_t)\|_2, \|\nabla L_S(\mathbf{w}_t)\|_2^2\right\} &\le \mathbb{O}(\frac{d^{\frac{1}{4}}\log^{\theta+\frac{1}{4}}(T/\delta)}{(n\varepsilon)^{\frac{1}{2}}}) + \mathbb{O}(\frac{d^{\frac{1}{4}}\log^{2\theta}(\sqrt{T})\log^{\frac{5}{4}}(T/\delta)}{(n\varepsilon)^{\frac{1}{2}}}) \\
&\le \mathbb{O}(\frac{d^{\frac{1}{4}}\log^{\frac{5}{4}}(T/\delta)\left(\log^{\theta-1}(T/\delta) + \log^{2\theta}(\sqrt{T})\right)}{(n\varepsilon)^{\frac{1}{2}}}) \\
&\le \mathbb{O}(\frac{d^{\frac{1}{4}}\log^{\frac{1}{4}}(T/\delta)\hat{\log}(T/\delta)\log^{2\theta}(\sqrt{T})}{(n\varepsilon)^{\frac{1}{2}}}), \qquad (51)
\end{aligned}$$

where $\hat{\log}(T/\delta) = \log^{\max(1,\theta)}(T/\delta)$. If $\theta = \frac{1}{2}$ and $K \leq \hat{\sigma}_{\text{gp}}$, then $c = \max\left(4K\log^{\frac{1}{2}}(\sqrt{T}), \frac{19K\log^{\frac{1}{2}}(1/\delta)}{12}\right)$. If $\theta = \frac{1}{2}$ and $K \geq \hat{\sigma}_{\text{gp}}$, then $c = \max\left(4K\log^{\frac{1}{2}}(\sqrt{T}), 39K\log^{\frac{1}{2}}(2/\delta)\right)$. If $\theta > \frac{1}{2}$, then $c = \max\left(4K\log^{\theta}(\sqrt{T}), 20K\log^{\theta}(2/\delta)\right)$. □

The proof of Theorem 3.1 is completed.

D Utility Bound for Heavy-Tail Selection

Theorem D.1 (**Utility Bound for Heavy-Tail Identification**). *Under the empirical projection subspace $M = V_{t,k}V_{t,k}^\top \in \mathbb{R}^{d\times d}$ and $\lambda_{t,i}^{\mathrm{tr}} = \mathrm{tr}(V_{t,k}^\top \hat{\mathbf{g}}_t(z_i)\hat{\mathbf{g}}_t^\top(z_i)V_{t,k})$, for the error $\mathcal{E}_{\mathrm{trace}}$ of the SVT-based heavy-tail selection, with probability $1-\delta_{\mathrm{tr}}$, we have*

$$\mathcal{E}_{\mathrm{trace}} \le \mathbb{O}\left(\frac{\log(d/\delta_{\mathrm{tr}})\sqrt{\log(1/\delta_{\mathrm{tr}})\log(n^*/\delta_{\mathrm{tr}})}}{k\varepsilon_{\mathrm{tr}}}\right).$$

Proof. Assume that the empirical projection subspace $M = V_{t,k}V_{t,k}^\top \in \mathbb{R}^{d\times d}$ with $V_{t,k}^\top V_{t,k} = \mathbb{I}_k$ approximates the population projection subspace $\hat{M} = \hat{V}_{t,k}\hat{V}_{t,k}^\top = \mathbb{E}_{V_{t,k}\sim\mathcal{P}}[V_{t,k}V_{t,k}^\top]$, $\lambda_{t,i}^{\mathrm{tr}} = \mathrm{tr}(V_{t,k}^\top \hat{\mathbf{g}}_t(z_i)\hat{\mathbf{g}}_t^\top(z_i)V_{t,k})$ and $\hat{\lambda}_{t,i}^{\mathrm{tr}} = \mathrm{tr}(\hat{V}_{t,k}^\top \hat{\mathbf{g}}_t(z_i)\hat{\mathbf{g}}_t^\top(z_i)\hat{V}_{t,k})$. For all i and each query $f_i(S)$ on the dataset S, if the total perturbation induced by the noisy threshold and the query noise is bounded by α_{svt}, i.e.,

$$|\mathcal{T} - \widetilde{\mathcal{T}}| + \max_{i\in[n^*]}|\nu_i| \le \alpha_{\mathrm{svt}}, \tag{52}$$

then the Sparse Vector Technique is $(\alpha_{\mathrm{svt}}, \delta_{\mathrm{svt}})$-accurate [36, 85] in the following sense:

$$\hat{\lambda}_{t,i}^{\mathrm{tr}} = \top \;\Rightarrow\; f_i(S) \ge \mathcal{T} - |\mathcal{T} - \widetilde{\mathcal{T}}| - |\nu_i| \ge \mathcal{T} - \alpha_{\mathrm{svt}}, \tag{53}$$

and

$$\hat{\lambda}_{t,i}^{\mathrm{tr}} = \bot \;\Rightarrow\; f_i(S) \le \mathcal{T} + |\mathcal{T} - \widetilde{\mathcal{T}}| + |\nu_i| \le \mathcal{T} + \alpha_{\mathrm{svt}}. \tag{54}$$

We will also have that for any $i < n^*$,

$$f_i(S) < \mathcal{T} - \alpha_{\mathrm{svt}} < \mathcal{T} - |\nu_i| - |\,\widetilde{\mathcal{T}} - \mathcal{T}|, \tag{55}$$

and hence

$$f_i(S) + \nu_i \le \widetilde{\mathcal{T}}, \tag{56}$$

which implies that $\hat{\lambda}_{t,i}^{\mathrm{tr}} = \bot$. Therefore, the algorithm does not halt before n^* queries are answered.

However, $\hat{\lambda}_{t,i}^{\mathrm{tr}}$ corresponds to the population trace that achieves the desired selection accuracy. In practice, however, we can only compute an empirical trace by constructing a random projection subspace. Therefore, it is necessary to bound the discrepancy $|\lambda_{t,i}^{\mathrm{tr}} - \hat{\lambda}_{t,i}^{\mathrm{tr}}|$ between the empirical trace $\lambda_{t,i}^{\mathrm{tr}}$ and the population trace $\hat{\lambda}_{t,i}^{\mathrm{tr}}$ in order to quantify the projection skewing error.

Consequently, the utility bound $\mathcal{E}_{\mathrm{trace}}$ for SVT-based heavy-tail selection can be decomposed into two additive terms: the projection skewing error arising from subspace approximation, and the error introduced by the SVT mechanism. That is,

$$\mathcal{E}_{\mathrm{trace}} = \underbrace{|\lambda_{t,i}^{\mathrm{tr}} - \hat{\lambda}_{t,i}^{\mathrm{tr}}|}_{\text{projection skewing}} + \underbrace{\max_{i\in[n^*]}|\nu_i| + |\mathcal{T} - \widetilde{\mathcal{T}}|}_{\text{SVT error}} \tag{57}$$

Firstly, we study the projection skewing error $|\lambda_{t,i}^{\mathrm{tr}} - \hat{\lambda}_{t,i}^{\mathrm{tr}}|$. For simplicity, we abbreviate $\hat{\mathbf{g}}_t(z_i)$ as $\hat{\mathbf{g}}_t$. Due to the Fact.1, $V_{t,k}^\top V_{t,k} = \mathbb{I}$ and $\hat{V}_{t,k}^\top \hat{V}_{t,k} = \mathbb{I}$, we omit subscripts of expectation and have

$$\begin{aligned}
|\lambda_{t,i}^{\mathrm{tr}} - \hat{\lambda}_{t,i}^{\mathrm{tr}}| &:= |\mathrm{tr}(V_{t,k}^\top \hat{\mathbf{g}}_t\hat{\mathbf{g}}_t^\top V_{t,k}) - \mathrm{tr}(\hat{V}_{t,k}^\top \hat{\mathbf{g}}_t\hat{\mathbf{g}}_t^\top \hat{V}_{t,k})| \\
&= |\|V_{t,k}^\top \hat{\mathbf{g}}_t\|_2^2 - \|\hat{V}_{t,k}^\top \hat{\mathbf{g}}_t\|_2^2| \\
&= |\|V_{t,k}V_{t,k}^\top \hat{\mathbf{g}}_t\|_2^2 - \|\hat{V}_{t,k}\hat{V}_{t,k}^\top \hat{\mathbf{g}}_t\|_2^2| \\
&\le \|V_{t,k}V_{t,k}^\top \hat{\mathbf{g}}_t - \hat{V}_{t,k}\hat{V}_{t,k}^\top \hat{\mathbf{g}}_t\|_2^2 \\
&\le \|V_{t,k}V_{t,k}^\top - \hat{V}_{t,k}\hat{V}_{t,k}^\top\|_2^2 \|\hat{\mathbf{g}}_t\|_2^2.
\end{aligned} \tag{58}$$

To bound $\mathbb{E}\|V_{t,k}V_{t,k}^\top - \hat{V}_{t,k}\hat{V}_{t,k}^\top\|_2^2$, we need to bound the gap between the sum of the random positive semidefinite matrix $M := V_{t,k}V_{t,k}^\top = \frac{1}{k}\sum_{i=1}^k v_{t,i}v_{t,i}^\top$ and the expectation $\hat{M} := \hat{V}_{t,k}\hat{V}_{t,k}^\top = \mathbb{E}[V_{t,k}V_{t,k}^\top]$.

Due to $\|v_j\|_2 = 1$, we can easily get

$$\begin{aligned}\|M\|_2 &= \|\frac{1}{k}\sum_{i=1}^{k} v_{t,i}v_{t,i}^\top\|_2 \le \frac{1}{k}\sum_{i=1}^{k}\|v_{t,i}v_{t,i}^\top\|_2 \\ &= \sup_{x:\|x\|_2=1}\frac{1}{k}\sum_{i=1}^{k} x^T v_{t,i}v_{t,i}^\top x \\ &= \sup_{x:\|x\|_2=1}\frac{1}{k}\sum_{i=1}^{k}\langle x, v_{t,i}\rangle \\ &\le \frac{1}{k}\sum_{i=1}^{k}\|x\|_2\|v_{t,i}\|_2 \\ &= 1. \end{aligned} \tag{59}$$

Thus, $\|M\|_2 \le 1$ and $\|\mathbb{E}M\|_2 = \|M \cdot \mathbb{P}(M)\|_2 \le 1$ because of $\mathbb{P}(M) \le 1$.

Then, according to Ahlswede-Winter Inequality with $R = 1$ and $m = k$, we have for any $\mu \in (0, 1)$

$$\mathbb{P}(\|M - \hat{M}\|_2 > \mu) \le 2d \cdot \exp(\frac{-k\mu^2}{4}), \tag{60}$$

where d is dimension of gradients. The inequality shows that the bounded spectral norm of random matrix $\|M\|_2$ concentrates around its expectation with high probability $1 - 2d \cdot \exp(-k\mu^2/4)$.

Since $\|M\|_2 \in [0, 1]$ and $\|\mathbb{E}M\|_2 \in [0, 1]$, $\|M - \hat{M}\|_2$ is always bounded by 1. Therefore, for $\mu \ge 1$, $\|M - \hat{M}\|_2 > u$ holds with probability 0. So that for any $\mu > 0$, we have

$$\mathbb{P}(\|M - \hat{M}\|_2 > 2\sqrt{\frac{\log 2d}{k}}\mu) \le \exp(-\mu^2). \tag{61}$$

Based on the inequality above, with probability $1 - \delta_m$, we have

$$\|M - \hat{M}\|_2 \le 2\frac{\log^{\frac{1}{2}}(2d/\delta_m)}{\sqrt{k}}. \tag{62}$$

Next, considering that we have implicitly normalized the term $\|\hat{\mathbf{g}}_t\|_2$ by the threshold 1, the upper bound of $\|\hat{\mathbf{g}}_t\|_2^2$ can be bounded by $\|\hat{\mathbf{g}}_t\|_2 \le 1$. As a result, we obtain

$$\begin{aligned}|\lambda_{t,i}^{\text{tr}} - \hat{\lambda}_{t,i}^{\text{tr}}| &\le \|V_{t,k}V_{t,k}^\top - \hat{V}_{t,k}\hat{V}_{t,k}^\top\|_2^2\|\hat{\mathbf{g}}_t\|_2^2 \\ &\le \|V_{t,k}V_{t,k}^\top - \hat{V}_{t,k}\hat{V}_{t,k}^\top\|_2^2 \\ &\le \|M - \hat{M}\|_2^2 \\ &\le \frac{4\log(2d/\delta_m)}{k}, \end{aligned} \tag{63}$$

with probability $1 - \delta_m$.

Secondly, we study the error induced by the SVT mechanism according to Lemma B.11. We consider an SVT-based trace identification problem with a sequence of queries $\{f_i(S)\}_{i=1}^k$, where each query has L_2-sensitivity $\Delta = \frac{1}{k}$ due to the normalization $\|\hat{\mathbf{g}}_t(z)\|_2 \le 1$ and the orthogonal projection $V_{t,k}V_{t,k}^\top = \frac{1}{k}\sum_{i=1}^{k} v_{t,i}v_{t,i}^\top$, which bounds each trace query in $[0, 1/k]$. Then, the Gaussian-SVT mechanism perturbs both the threshold and the query answers:

$$\hat{\mathcal{T}} = \mathcal{T} + \rho, \quad \rho \sim \mathbb{N}(0, \Delta\sigma_1^2\mathbb{I}), \tag{64}$$

$$\tilde{f_i}(S) = f_i(S) + \nu_i, \quad \nu_i \sim \mathbb{N}(0, \Delta\sigma_2^2\mathbb{I}), \tag{65}$$

and compares

$$\tilde{f_i}(S) \ge \hat{\mathcal{T}}. \tag{66}$$

For a Gaussian random variable $Z \sim \mathbb{N}(0, \sigma^2)$, we have

$$\mathbb{P}(|Z| \ge t) \le 2\exp\left(-\frac{t^2}{2\sigma^2}\right). \tag{67}$$

The error of the SVT decision comes from two sources:

(1) the noisy threshold error $|\mathcal{T} - \hat{\mathcal{T}}| = |\rho|$,

(2) the noisy query error $\max_{i\le n^*}|v_i|$.

We aim to control both terms simultaneously. We require

$$\mathbb{P}\left(|\mathcal{T}-\hat{\mathcal{T}}|\ge\frac{\alpha_{\text{svt}}}{2}\right)\le\frac{\delta_{\text{svt}}}{2}. \tag{68}$$

Using the Gaussian tail bound, this holds if $2\exp\left(-\frac{(\alpha_{\text{svt}}/2)^2}{2\sigma^2}\right)\le\frac{\delta_{\text{svt}}}{2}$, which implies

$$\alpha_{\text{svt}}\gtrsim\sigma\sqrt{2\log(1/\delta_{\text{svt}})}. \tag{69}$$

Similarly, we require

$$\mathbb{P}\left(\max_{i\le n^*}|v_i|\ge\frac{\alpha_{\text{svt}}}{2}\right)\le\frac{\delta_{\text{svt}}}{2}. \tag{70}$$

By the union bound,

$$\mathbb{P}\left(\max_{i\le n^*}|v_i|\ge\frac{\alpha_{\text{svt}}}{2}\right)\le n^*\cdot 2\exp\left(-\frac{(\alpha_{\text{svt}}/2)^2}{2\sigma^2}\right). \tag{71}$$

Thus, it suffices that

$$n^*\cdot 2\exp\left(-\frac{\alpha_{\text{svt}}^2}{8\sigma^2}\right)\le\frac{\delta_{\text{svt}}}{2}, \tag{72}$$

which yields

$$\alpha_{\text{svt}}\gtrsim\sigma\sqrt{2\log(n^*/\delta_{\text{svt}})}. \tag{73}$$

Combining the two bounds, the dominant term is $\alpha_{\text{svt}}=\mathbb{O}\left(\sigma\sqrt{2\log(n^*/\delta_{\text{svt}})}\right)$.

Hence, due to $\sigma_1=\frac{\sqrt{2\log(1.25/\delta_1)}}{\varepsilon_1}$ and $\sigma_2=\frac{\sqrt{2\log(1.25n^*/\delta_2)}}{\varepsilon_2/n^*}$, Gaussian-SVT is $(\alpha_{\text{svt}},\delta_{\text{svt}})$-sample accurate with $\sigma=\Delta\cdot\max(\sigma_1,\sigma_2)$ [26]and

$$\alpha_{\text{svt}}=\mathbb{O}\left(\frac{\sigma\sqrt{2\log(n^*/\delta_{\text{svt}})}}{k}\right). \tag{74}$$

As suggested in [50, 85], we allocate the privacy budget according to

$$\varepsilon_2=w\varepsilon_1,\qquad w=(2n^*)^{2/3}.$$

Since the total privacy budget satisfies $\varepsilon_{\text{tr}}=\varepsilon_1+\varepsilon_2$, this yields

$$\varepsilon_2=\frac{(2n^*)^{2/3}}{(2n^*)^{2/3}+1}\,\varepsilon_{\text{tr}}.$$

When n^* is sufficiently large, we have $\varepsilon_2\approx\varepsilon_{\text{tr}}$. Consequently, we have

$$\alpha_{\text{svt}}=\mathbb{O}\left(\frac{\sqrt{4\log(1.25/\delta)\log(n^*/\delta_{\text{svt}})}}{k\varepsilon_{\text{tr}}}\right) \tag{75}$$

for uniformity.

To align the threshold with the query sensitivity, we obtain $\mathcal{T}=\frac{\sqrt{4\log(1.25/\delta)\log(n^*/\delta_{\text{svt}})}}{n^*k\varepsilon_{\text{tr}}}$.

The above derivation establishes the $(\alpha_{\text{svt}},\delta_{\text{svt}})$-sample accuracy of Gaussian-SVT.

In conclusion, for the per-sample trace, there is a high probability $1-\delta_{\text{tr}}$, where $\delta_{\text{tr}}=\delta_m+\delta_{\text{svt}}+\delta$ that is

$$C_{\text{trace}}\le\mathbb{O}\left(\frac{4\log(2d/\delta_{\text{tr}})}{k}\right)+\mathbb{O}\left(\frac{\sqrt{4\log(1.25/\delta)\log(n^*/\delta_{\text{tr}})}}{k\varepsilon_{\text{tr}}}\right) \tag{76}$$

$$\le\mathbb{O}\left(\frac{\log(d/\delta_{\text{tr}})\sqrt{\log(1/\delta_{\text{tr}})\log(n^*/\delta_{\text{tr}})}}{k\varepsilon_{\text{tr}}}\right). \tag{77}$$

that we can accurately identify heavy-tailed samples within a finite error dependent on the privacy budget and projection subspace dimension with the factor $\mathbb{O}(\frac{1}{k\varepsilon_{\text{tr}}})$.

□

The proof of Theorem 4.1 is completed.

E Convergence of Discriminative Clipping

In DC-DPSGD, the convergence bounds for the two regions correspond to c_1 and c_2, respectively. First, we optimize the theoretical tools by transforming the concentration inequalities for the sum of sub-Weibull random variables X into two-region versions distinguished by the tail probability $\mathbb{P}(|X| > x)$, namely sub-Gaussian tail decay rate $\exp(-x^2)$ and heavy-tailed decay rate $\exp(-x^{1/\theta})$, $\theta > \frac{1}{2}$. Then, we analyze the high probability bounds for the gradient variability of clipped DPSGD in each region. In the heavy-tail region, we make the inequality $\mathbb{P}(\|\mathbf{g}_t - \nabla L_S(\mathbf{w}_t)\|_2 > c_1) \leq 2\exp(-c_1^{1/\theta})$ hold and derive the dependence of factor $\log^{\theta}(1/\delta)$ for c_1. In the light-body region, we have $\mathbb{P}(\|\mathbf{g}_t - \nabla L_S(\mathbf{w}_t)\|_2 > c_2) \leq 2\exp(-c_2^2)$, resulting in the factor $\log^{1/2}(1/\delta)$ of c_2. Next, we investigate the high probability error on the unbounded clipped DPSGD privacy noise using Gaussian distribution properties. Finally, we integrate the results regarding gradient variability and privacy noise to determine the optimal clipping thresholds for both regions and achieve faster convergence rates for the optimization performance. To simplify the notation, we emphasize the **heavy-tail region** to refer to the impact of $\mathbf{g}_t^{\text{tail}}(z_i)$ on the convergence of the model parameters $\mathbf{w}_t$, and the **light-body region** to refer to the impact of $\mathbf{g}_t^{\text{body}}(z_i)$ on the $\mathbf{w}_t$, *i.e.*, splitting $\mathbf{w}_{t+1} = \mathbf{w}_t - \eta_t \cdot \text{DC-DPSGD}\left(\mathbf{g}_t^{\text{tail}}(z_i) + \mathbf{g}_t^{\text{body}}(z_i)\right)$ into two regions, each subject to bound separately. In the proof, we take it as a default that the clipping threshold c corresponds to c_1 for the heavy-tail region and to c_2 for the light-body region.

Theorem E.1 (**Convergence of Discriminative Clipping**). *Under Assumptions 2.1, 2.2 and 2.3, Let $\mathbf{w}_t$ be the iterative parameter produced by discriminative clipping of Algorithm 2 with with $T = \mathbb{O}(\frac{n\varepsilon}{\sqrt{d\log(1/\delta)}})$, $T \geq 1$ and $\eta_t = \frac{1}{\sqrt{T}}$. Define $\hat{\log}(T/\delta) = \log^{\max(1,\theta)}(T/\delta)$, $\hat{\sigma}_{\text{gp}}^2 = m_2\frac{Tc^2dB^2\log(1/\delta)}{n^2\varepsilon^2}$, $a = 2$ if $\theta = 1/2$, $a = (4\theta)^{2\theta}e^2$ if $\theta \in (1/2, 1]$ and $a = (2^{2\theta+1}+2)\Gamma(2\theta+1) + \frac{2^{3\theta}\Gamma(3\theta+1)}{3}$ if $\theta > 1$, for any $\delta \in (0,1)$, with probability $1-\delta$, then we have:*

*(i). **In the heavy-tail region** ($c = c_1$):*

$$\frac{1}{T}\sum_{t=1}^{T}\min\left\{\|\nabla L_S(\mathbf{w}_t)\|_2, \|\nabla L_S(\mathbf{w}_t)\|_2^2\right\} \leq \mathbb{O}\left(\frac{d^{\frac{1}{4}}\log^{\frac{1}{4}}(T/\delta)\hat{\log}(T/\delta)\log^{2\theta}(\sqrt{T})}{(n\varepsilon)^{\frac{1}{2}}}\right).$$

(1) *If $\theta = \frac{1}{2}$ and $K \leq \hat{\sigma}_{\text{gp}}$, then $c_1 = \max\left(4K\log^{\frac{1}{2}}(\sqrt{T}), \frac{16aK\log^{\frac{1}{2}}(1/\delta)}{12}\right)$.* (2) *If $\theta = \frac{1}{2}$ and $K \geq \hat{\sigma}_{\text{gp}}$, then $c_1 = \max\left(4K\log^{\frac{1}{2}}(\sqrt{T}), 33\sqrt{2a}K\log^{\frac{1}{2}}(2/\delta)\right)$.*
(3) *If $\theta > \frac{1}{2}$, then $c_1 = \max\left(4^{\theta}2K\log^{\theta}(\sqrt{T}), 17K\log^{\theta}(2/\delta)\right)$.*

*(ii). **In the light-body region** ($c = c_2$):*

$$\frac{1}{T}\sum_{t=1}^{T}\min\left\{\|\nabla L_S(\mathbf{w}_t)\|_2, \|\nabla L_S(\mathbf{w}_t)\|_2^2\right\} \leq \mathbb{O}\left(\frac{d^{\frac{1}{4}}\log^{\frac{5}{4}}(T/\delta)\log(\sqrt{T})}{(n\varepsilon)^{\frac{1}{2}}}\right).$$

(1) *If $K \leq \hat{\sigma}_{\text{gp}}$, then $c_2 = \max\left(2\sqrt{2a}K\log^{\frac{1}{2}}(\sqrt{T}), 27\sqrt{e}\hat{\sigma}_{\text{gp}}\log^{\frac{1}{2}}(1/\delta)\right)$.* (2) *If $K \geq \hat{\sigma}_{\text{gp}}$, then $c_2 = \max\left(2\sqrt{2a}K\log^{\frac{1}{2}}(\sqrt{T}), 33\sqrt{2a}K\log^{\frac{1}{2}}(2/\delta)\right)$.*

Proof. We review two cases in Discriminative Clipping DPSGD: $\|\nabla L_S(\mathbf{w}_t)\|_2 \leq c/2$ and $\|\nabla L_S(\mathbf{w}_t)\|_2 \geq c/2$. To simplify notation, we write ε_{gp} as ε, omitting the subscript throughout.

Firstly, in the case $\|\nabla L_S(\mathbf{w}_t)\|_2 \leq c/2$:

$$\begin{aligned}
&L_S(\mathbf{w}_{t+1}) - L_S(\mathbf{w}_t) \leq \langle \mathbf{w}_{t+1} - \mathbf{w}_t, \nabla L_S(\mathbf{w}_t)\rangle + \frac{1}{2}\beta\|\mathbf{w}_{t+1} - \mathbf{w}_t\|_2^2 \\
&\leq -\eta_t\langle \overline{\mathbf{g}}_t - \mathbb{E}_t[\overline{\mathbf{g}}_t], \nabla L_S(\mathbf{w}_t)\rangle - \eta_t\langle \mathbb{E}_t[\overline{\mathbf{g}}_t] - \nabla L_S(\mathbf{w}_t), \nabla L_S(\mathbf{w}_t)\rangle - \eta_t\langle \zeta_t, \nabla L_S(\mathbf{w}_t)\rangle \\
&- \eta_t\|\nabla L_S(\mathbf{w}_t)\|_2^2 + \frac{1}{2}\beta\eta_t^2\|\overline{\mathbf{g}}_t\|_2^2 + \frac{1}{2}\beta\eta_t^2\|\zeta_t\|_2^2 + \beta\eta_t^2\langle \overline{\mathbf{g}}_t, \zeta_t\rangle
\end{aligned}$$

Applying the properties of Gaussian tails and Lemma B.2 to ζ_t, Lemma B.4 to term $\sum_{t=1}^{T}\eta_t\langle \overline{\mathbf{g}}_t - \mathbb{E}_t[\overline{\mathbf{g}}_t], \nabla L_S(\mathbf{w}_t)\rangle$, with probability $1-4\delta$, we have

$$\begin{aligned}
&\sum_{t=1}^{T}\eta_t\|\nabla L_S(\mathbf{w}_t)\|_2^2 \leq L_S(\mathbf{w}_1) - L_S(\mathbf{w}_S) + \sum_{t=1}^{T}\frac{1}{2}\beta\eta_t^2c^2 + 2\beta m_2 ed\frac{Tc^2B^2\log^2(2/\delta)}{n^2\varepsilon^2}\sum_{t=1}^{T}\eta_t^2 \\
&+ 2\beta\sqrt{em_2Td}\frac{c^2B\log(2/\delta)}{n\varepsilon}\sum_{t=1}^{T}\eta_t^2 + 2\sqrt{em_2Td}\frac{c^2B\log(2/\delta)}{n\varepsilon}\sum_{t=1}^{T}\eta_t + \frac{\eta_t c^2\log(1/\delta)}{\rho} \\
&+ \frac{4\rho c^2\sum_{t=1}^{T}\eta_t^2\|\nabla L_S(\mathbf{w}_t)\|_2^2}{\eta_t c^2} - \underbrace{\sum_{t=1}^{T}\eta_t\langle \mathbb{E}_t[\overline{\mathbf{g}}_t] - \nabla L_S(\mathbf{w}_t), \nabla L_S(\mathbf{w}_t)\rangle}_{\text{Eq.9}}.
\end{aligned} \tag{78}$$

We will consider a truncated version of term Eq.9 in the following. Similarly,

$$\sum_{t=1}^{T}\eta_t\langle\mathbb{E}_t[\overline{\mathbf{g}}_t]-\nabla L_S(\mathbf{w}_t),\nabla L_S(\mathbf{w}_t)\rangle\le\frac{1}{2}\sum_{t=1}^{T}\eta_t\|\mathbb{E}_t[\overline{\mathbf{g}}_t]-\nabla L_S(\mathbf{w}_t)\|_2^2+\frac{1}{2}\sum_{t=1}^{T}\eta_t\|\nabla L_S(\mathbf{w}_t)\|_2^2.$$

For term $\|\mathbb{E}_t[\overline{\mathbf{g}}_t]-\nabla L_S(\mathbf{w}_t)\|_2$, we also define $a_t=\mathbb{I}_{\|\mathbf{g}_t\|_2>c}$ and $b_t=\mathbb{I}_{\|\mathbf{g}_t-\nabla L_S(\mathbf{w}_t)\|_2>\frac{c}{2}}$, and have

$$\begin{aligned}\|\mathbb{E}_t[\overline{\mathbf{g}}_t]-\nabla L_S(\mathbf{w}_t)\|_2&=\|\mathbb{E}_t[(\overline{\mathbf{g}}_t-\mathbf{g}_t)a_t]\|_2\\&\le\mathbb{E}_t[\|(\mathbf{g}_t(\frac{c-\|\mathbf{g}_t\|_2}{\|\mathbf{g}_t\|_2})a_t\|_2]\\&\le\mathbb{E}_t[|\|\mathbf{g}_t\|_2-\|\nabla L_S(\mathbf{w}_t)\|_2|a_t]\\&\le\mathbb{E}_t[|\|\mathbf{g}_t-\nabla L_S(\mathbf{w}_t)\|_2|b_t]\\&\le\sqrt{\mathbb{E}_t[\|\mathbf{g}_t-\nabla L_S(\mathbf{w}_t)\|_2^2]\mathbb{E}_t b_t^2}.\end{aligned}\tag{79}$$

Due to $\mathbb{E}[\mathbf{g}_t-\nabla L_S(\mathbf{w}_t)]=0$, applying Lemma B.7 and B.8 with

$$\begin{aligned}&m=1\\&\sup_{\eta\in(0,1]}\{v(L,\eta)\}=aK^2\\&x_{\max}=\frac{\eta I(x)}{x}aK^2\\&c_t\in[\frac{1}{2},1]\\&\eta=\frac{1}{2}.\end{aligned}$$

In the light-body region, i.e. $x\ge x_{\max}$, we have

$$\begin{aligned}\mathbb{P}(\|\mathbf{g}_t-\nabla L_S(\mathbf{w}_t)\|_2>x)&\le\exp(-c_t\eta I(x))+\exp(-I(x))\\&\le\exp(-\frac{1}{4}I(x))+\exp(-I(x))\\&\le 2\exp(-\frac{1}{4}I(x)).\end{aligned}\tag{80}$$

Then, in the heavy-tail region, i.e. $0\le x\le x_{\max}$, the inequality

$$\begin{aligned}\mathbb{P}(\|\mathbf{g}_t-\nabla L_S(\mathbf{w}_t)\|_2>x)&\le\exp(-\frac{x^2}{2v(x_{\max},\eta)})+m\exp(-\frac{x_{\max}^2(\eta)}{\eta v(x_{\max},\eta)})\\&\le 2\exp(-\frac{x^2}{2v(x_{\max},\eta)})\\&\le 2\exp(-\frac{x^2}{2aK^2})\end{aligned}\tag{81}$$

holds.

Therefore, when $0\le x\le x_{\max}$, we have the follow-up truncated conclusions:
If $\theta=\frac{1}{2}$, $\forall\alpha>0$ and $a=2$, we have the following inequality with probability at least $1-\delta$

$$\|\mathbf{g}_t-\nabla L_S(\mathbf{w}_t)\|_2\le 2K\log^{\frac{1}{2}}(2/\delta).$$

If $\theta\in(\frac{1}{2},1]$, let $a=(4\theta)^{2\theta}e^2$, we have the following inequality with probability at least $1-\delta$

$$\|\mathbf{g}_t-\nabla L_S(\mathbf{w}_t)\|_2\le\sqrt{2}e(4\theta)^{\theta}K\log^{\frac{1}{2}}(2/\delta).$$

If $\theta>1$, let $a=(2^{2\theta+1}+2)\Gamma(2\theta+1)+\frac{2^{3\theta}\Gamma(3\theta+1)}{3}$, we have the following inequality with probability at least $1-\delta$

$$\|\mathbf{g}_t-\nabla L_S(\mathbf{w}_t)\|_2\le\sqrt{2(2^{2\theta+1}+2)\Gamma(2\theta+1)+\frac{2^{3\theta}\Gamma(3\theta+1)}{3}}K\log^{\frac{1}{2}}(2/\delta).$$

When $x\ge x_{\max}$, let $I(x)=(x/K)^{\frac{1}{\theta}}$, $\forall\theta\in(\frac{1}{2},1]$, with probability at least $1-\delta$, then we have

$$\|\mathbf{g}_t-\nabla L_S(\mathbf{w}_t)\|_2\le 4^{\theta}K\log^{\theta}(2/\delta).$$

Apply the truncated corollary above, when $0 \le x \le x_{\max}$, we have

$$\mathbb{E}_t[\|\mathbf{g}_t - \nabla L_S(\mathbf{w}_t)\|_2] \le \sqrt{2a}K \tag{82}$$

and with probability $1-\delta$,

$$\mathbb{E}_t b_t^2 = \mathbb{P}(\|\mathbf{g}_t - \nabla L_S(\mathbf{w}_t)\|_2 > \frac{c}{2}) \le 2\exp(-(\frac{c}{2\sqrt{2a}K})^2) \tag{83}$$

where $a = 2$ if $\theta = 1/2$, $a = (4\theta)^{2\theta}e^2$ if $\theta \in (1/2, 1]$ and $a = (2^{2\theta+1}+2)\Gamma(2\theta+1) + \frac{2^{3\theta}\Gamma(3\theta+1)}{3}$ if $\theta > 1$.

When $x \ge x_{\max}$, the inequalities

$$\mathbb{E}_t[\|\mathbf{g}_t - \nabla L_S(\mathbf{w}_t)\|_2] \le 4^{\theta}K \tag{84}$$

and

$$\mathbb{E}_t b_t^2 = \mathbb{P}(\|\mathbf{g}_t - \nabla L_S(\mathbf{w}_t)\|_2 > \frac{c}{2}) \le 2\exp(-\frac{1}{4}(\frac{c}{2K})^{\frac{1}{\theta}}) \tag{85}$$

hold with probability $1-\delta$, where $\theta \ge \frac{1}{2}$.

Thus, with probability $1 - T\delta$, we get

$$\sum_{t=1}^{T}\eta_t\langle\mathbb{E}_t[\overline{\mathbf{g}}_t] - \nabla L_S(\mathbf{w}_t), \nabla L_S(\mathbf{w}_t)\rangle \le 2aK^2\sum_{t=1}^{T}\eta_t\exp(-(\frac{c}{2\sqrt{2a}K})^2) + \frac{1}{2}\sum_{t=1}^{T}\eta_t\|\nabla L_S(\mathbf{w}_t)\|_2^2, \tag{86}$$

when $0 \le x \le x_{\max}$.

With probability $1 - T\delta$, we obtain

$$\sum_{t=1}^{T}\eta_t\langle\mathbb{E}_t[\overline{\mathbf{g}}_t] - \nabla L_S(\mathbf{w}_t), \nabla L_S(\mathbf{w}_t)\rangle \le 4^{2\theta}K^2\sum_{t=1}^{T}\eta_t\exp(-\frac{1}{4}(\frac{c}{2K})^{\frac{1}{\theta}}) + \frac{1}{2}\sum_{t=1}^{T}\eta_t\|\nabla L_S(\mathbf{w}_t)\|_2^2, \tag{87}$$

when $x \ge x_{\max}$.

By setting $\rho = \frac{1}{16}$, $T = \mathbb{O}(\frac{n\varepsilon}{\sqrt{d\log(1/\delta)}})$ and $\eta_t = \frac{1}{\sqrt{T}}$, with probability $1 - 4\delta - T\delta$, we have

$$\begin{aligned}\frac{1}{4}\sum_{t=1}^{T}\eta_t\|\nabla L_S(\mathbf{w}_t)\|_2^2 \le{}& L_S(\mathbf{w}_1) - L_S(\mathbf{w}_S) + \frac{1}{2}\beta c^2 + 2\beta m_2 e\frac{d^{\frac{1}{2}}c^2B^2\log^{\frac{3}{2}}(2/\delta)}{n\varepsilon}\\ &+ 2\beta\sqrt{em_2}\frac{d^{\frac{1}{4}}c^2B\log^{\frac{1}{2}}(2/\delta)}{\sqrt{n\varepsilon}} + 2\sqrt{em_2}c^2B\log^{\frac{1}{2}}(2/\delta) + \frac{16d^{\frac{1}{4}}c^2\log^{\frac{5}{4}}(1/\delta)}{\sqrt{n\varepsilon}}\\ &+ \text{Eq.10}\begin{cases}2aK^2\sum_{t=1}^{T}\eta_t\exp(-(\frac{c}{2\sqrt{2a}K})^2), & \text{if } 0 \le x \le x_{\max},\\ 4^{2\theta}K^2\sum_{t=1}^{T}\eta_t\exp(-\frac{1}{4}(\frac{c}{2K})^{\frac{1}{\theta}}), & \text{if } x \ge x_{\max}.\end{cases}\end{aligned} \tag{88}$$

Let the term Eq.10 $\le \frac{1}{\sqrt{T}}$, and we have $c \ge 2\sqrt{2a}K\log^{\frac{1}{2}}(\sqrt{T})$ if $0 \le x \le x_{\max}$ and $c \ge 4^{\theta}2K\log^{\theta}(\sqrt{T})$ if $x \ge x_{\max}$.

In the light-body region that $0 \le x \le x_{\max}$, by taking $c_2 = c = 2\sqrt{2a}K\log^{\frac{1}{2}}(\sqrt{T})$ we achieve

$$\begin{aligned}\frac{1}{\sqrt{T}}\sum_{t=1}^{T}\eta_t\|\nabla L_S(\mathbf{w}_t)\|_2^2 \le{}& \frac{4(L_S(\mathbf{w}_1) - L_S(\mathbf{w}_S))}{\sqrt{T}} + \frac{2aK^2}{\sqrt{T}}\\ &+ \frac{8aK^2\log(\sqrt{T})\log(2/\delta)}{\sqrt{T}}\Bigg(2\beta + 8\beta m_2 eB^2(\frac{d^{\frac{1}{4}}\log^{\frac{1}{4}}(2/\delta)}{\sqrt{n\varepsilon}})^2\\ &+8\beta\sqrt{em_2}\frac{d^{\frac{1}{4}}B\log^{-\frac{1}{2}}(2/\delta)}{\sqrt{n\varepsilon}} + 8\sqrt{em_2}B\log^{-\frac{1}{2}}(2/\delta) + \frac{64d^{\frac{1}{4}}\log^{\frac{1}{4}}(1/\delta)}{\sqrt{n\varepsilon}}\Bigg)\\ \le{}& \mathbb{O}(\frac{\log(\sqrt{T})\log(1/\delta)}{\sqrt{T}}\cdot\frac{d^{\frac{1}{4}}\log^{\frac{1}{4}}(1/\delta)}{\sqrt{n\varepsilon}})\\ \le{}& \mathbb{O}(\frac{\log(\sqrt{T})d^{\frac{1}{4}}\log^{\frac{5}{4}}(1/\delta)}{\sqrt{n\varepsilon}}).\end{aligned} \tag{89}$$

In the heavy-tail region that $x \geq x_{\max}$, by taking $c_1 = c = 4^\theta 2K \log^\theta(\sqrt{T})$ we achieve

$$\begin{aligned}\frac{1}{\sqrt{T}}\sum_{t=1}^{T}\eta_t\|\nabla L_S(\mathbf{w}_t)\|_2^2 \leq\ & \frac{4(L_S(\mathbf{w}_1)-L_S(\mathbf{w}_S))}{\sqrt{T}}+\frac{2aK^2}{\sqrt{T}}\\ &+\frac{4^{2\theta+1}\log^{2\theta}(\sqrt{T})\log(2/\delta)}{\sqrt{T}}\left(2\beta+8\beta m_2 eB^2(\frac{d^{\frac{1}{4}}\log^{\frac{1}{4}}(2/\delta)}{\sqrt{n\varepsilon}})^2\right.\\ &\left.+8\beta\sqrt{em_2}\frac{d^{\frac{1}{4}}B\log^{-\frac{1}{2}}(2/\delta)}{\sqrt{n\varepsilon}}+8\sqrt{em_2}B\log^{-\frac{1}{2}}(2/\delta)+\frac{64d^{\frac{1}{4}}\log^{\frac{1}{4}}(1/\delta)}{\sqrt{n\varepsilon}}\right)\\ \leq\ & \mathbb{O}(\frac{\log^{2\theta}(\sqrt{T})\log(1/\delta)}{\sqrt{T}}\cdot\frac{d^{\frac{1}{4}}\log^{\frac{1}{4}}(1/\delta)}{\sqrt{n\varepsilon}})\\ \leq\ & \mathbb{O}(\frac{\log^{2\theta}(\sqrt{T})d^{\frac{1}{4}}\log^{\frac{5}{4}}(1/\delta)}{\sqrt{n\varepsilon}}).\end{aligned} \tag{90}$$

Secondly, we pay extra attention to the bound in the case $\|\nabla L_S(\mathbf{w}_t)\|_2 \geq c/2$.

$$\begin{aligned}L_S(\mathbf{w}_{t+1})-L_S(\mathbf{w}_t) &\leq \langle \mathbf{w}_{t+1}-\mathbf{w}_t, \nabla L_S(\mathbf{w}_t)\rangle+\frac{1}{2}\beta\|\mathbf{w}_{t+1}-\mathbf{w}_t\|_2^2\\ &\leq \underbrace{-\eta_t\langle \overline{\mathbf{g}}_t+\zeta_t, \nabla L_S(\mathbf{w}_t)\rangle}_{\text{Eq.11}}+\frac{1}{2}\beta\eta_t^2\|\overline{\mathbf{g}}_t+\zeta_t\|_2^2.\end{aligned} \tag{91}$$

We revisit term Eq.11 in the case and also set $s_t^+ = \mathbb{I}_{\|\mathbf{g}_t\|_2\geq c}$ and $s_t^- = \mathbb{I}_{\|\mathbf{g}_t\|_2\leq c}$.

$$-\eta_t\langle \overline{\mathbf{g}}_t+\zeta_t, \nabla L_S(\mathbf{w}_t)\rangle = -\eta_t\langle \frac{c\mathbf{g}_t}{\|\mathbf{g}_t\|_2}s_t^+ + \mathbf{g}_t s_t^-, \nabla L_S(\mathbf{w}_t)\rangle - \eta_t\langle \zeta_t, \nabla L_S(\mathbf{w}_t)\rangle. \tag{92}$$

For term $-\sum_{t=1}^{T}\eta_t\langle \mathbf{g}_t s_t^-, \nabla L_S(\mathbf{w}_t)\rangle$, we obtain

$$\begin{aligned}-\sum_{t=1}^{T}\eta_t\langle \mathbf{g}_t s_t^-, \nabla L_S(\mathbf{w}_t)\rangle &= -\sum_{t=1}^{T}\eta_t s_t^-(\langle \mathbf{g}_t-\nabla L_S(\mathbf{w}_t), \nabla L_S(\mathbf{w}_t)\rangle+\|\nabla L_S(\mathbf{w}_t)\|_2^2)\\ &\leq -\sum_{t=1}^{T}\eta_t s_t^-\langle \mathbf{g}_t-\nabla L_S(\mathbf{w}_t), \nabla L_S(\mathbf{w}_t)\rangle-\sum_{t=1}^{T}\eta_t s_t^-\|\nabla L_S(\mathbf{w}_t)\|_2^2\\ &\leq -\sum_{t=1}^{T}\eta_t s_t^-\langle \mathbf{g}_t-\nabla L_S(\mathbf{w}_t), \nabla L_S(\mathbf{w}_t)\rangle-\frac{c}{2}\sum_{t=1}^{T}\eta_t s_t^-\|\nabla L_S(\mathbf{w}_t)\|_2^2\\ &\leq \underbrace{-\sum_{t=1}^{T}\eta_t s_t^-\langle \mathbf{g}_t-\nabla L_S(\mathbf{w}_t), \nabla L_S(\mathbf{w}_t)\rangle}_{\text{Eq.12}}-\frac{c}{3}\sum_{t=1}^{T}\eta_t s_t^-\|\nabla L_S(\mathbf{w}_t)\|_2^2.\end{aligned} \tag{93}$$

Let consider the term Eq.12. Since $\mathbb{E}_t[\eta_t s_t^-\langle \mathbf{g}_t-\nabla L_S(\mathbf{w}_t), \nabla L_S(\mathbf{w}_t)\rangle]=0$, the sequence $(-\eta_t s_t^-\langle \mathbf{g}_t-\nabla L_S(\mathbf{w}_t), \nabla L_S(\mathbf{w}_t)\rangle, t\in\mathbb{N})$ is a martingale difference sequence. In addition, the term $\mathbf{g}_t-\nabla L_S(\mathbf{w}_t)$ is a $subW(\theta,K)$ random variable, thus we apply sub-Weibull Freedman inequality with Lemma B.3 and concentration inequality with Lemma B.7 and B.8 to bound it.

In Lemma B.3, Define

$$v(L,\eta) := \mathbb{E}\big[(X^L-\mathbb{E}[X])^2\mathbb{I}(X^L\leq\mathbb{E}[X])\big]+\mathbb{E}\big[(X^L-\mathbb{E}[X])^2\exp\big(\eta(X^L-\mathbb{E}[X])\big)\mathbb{I}(X^L>\mathbb{E}[X])\big],$$

and make $\beta = kv(L,\eta)$, then we have $\sup_{\eta\in(0,1]}\{kv(L,\eta)\} = a\sum_{i=1}^{k}K_i^2$ based on Lemma B.7 and B.8 in [5] and obtain

$$\begin{aligned}\mathbb{P}\left(\bigcup_{k\in\mathbb{N}}\left\{\sum_{i=1}^{k}\xi_i\geq kx \text{ and } \sum_{i=1}^{k}aK_{i-1}^2\leq\beta\right\}\right) &\leq \exp(-\lambda kx+\frac{\lambda^2}{2}\beta)\\ &= \exp(-\lambda kx+kv(L,\eta)\frac{\lambda^2}{2}).\end{aligned} \tag{94}$$

Subsequently, we define the inflection point $x_{\max} := \frac{\eta I(kx)}{kx}a\sum_{i=1}^{k}K_i^2$ and have

(1) In the light-body region where $x \geq x_{\max}$, we choose $L = kx$ and $\lambda = \frac{\eta I(kx)}{kx}$, that is $\frac{x}{v(kx,\eta)} \geq \frac{x_{\max}}{v(kx,\eta)} = \frac{\eta I(kx)}{kx}$. Then the inequality achieves

$$\begin{aligned}\mathbb{P}\left(\bigcup_{k\in\mathbb{N}}\left\{\sum_{i=1}^{k}\xi_i \geq kx \text{ and } \sum_{i=1}^{k} aK_{i-1}^2 \leq \beta\right\}\right) &\leq \exp(-\eta I(kx) + v(L,\eta)\frac{\eta^2 I^2(kx)}{2kx^2}) \\ &\leq \exp(-\eta I(kx)(1 - v(L,\eta)\frac{\eta I(kx)}{2kx^2})) \\ &\leq \exp(-\eta c_x I(kx)) \\ &\leq \exp(-\frac{1}{2}\eta I(kx)),\end{aligned} \tag{95}$$

where $c_x = 1 - \frac{\eta v(kx,\eta) I(kx)}{2kx^2}$ and the last inequality holds due to $c_x \geq \frac{1}{2}$.

(2) In the heavy-tail region where $x \leq x_{\max}$, we choose $L = kx_{\max}$ and $\lambda = \frac{x}{v(L,\eta)} \leq \frac{x_{\max}}{v(L,\eta)} = \frac{\eta I(L)}{L}$. Then, we get

$$\begin{aligned}\mathbb{P}\left(\bigcup_{k\in\mathbb{N}}\left\{\sum_{i=1}^{k}\xi_i \geq kx \text{ and } \sum_{i=1}^{k} aK_{i-1}^2 \leq \beta\right\}\right) &\leq \exp(-\frac{kx^2}{v(L,\eta)} + \frac{kx^2}{2v(L,\eta)}) \\ &\leq \exp(-\frac{kx^2}{2v(L,\eta)}).\end{aligned} \tag{96}$$

Implementing the above inferences and propositions with

$$\begin{aligned}&\xi_t = \eta_t \langle \mathbf{g}_t - \nabla L_S(\mathbf{w}_t), \nabla L_S(\mathbf{w}_t)\rangle \\ &\Lambda := -\sum_{i=1}^{T} \eta_t s_t^- \langle \mathbf{g}_t - \nabla L_S(\mathbf{w}_t), \nabla L_S(\mathbf{w}_t)\rangle \\ &K_{t-1} = \eta_t K \|\nabla L_S(\mathbf{w}_t)\|_2 \\ &m_t = \eta_t KG \\ &k = T \\ &\eta = 1/2\end{aligned}$$

If $\theta = \frac{1}{2}$, $\forall \alpha > 0$ and $a = 2$, when $x \leq x_{\max}$ we have the following inequality with probability at least $1 - \delta$

$$\begin{aligned}-\sum_{t=1}^{T} \eta_t s_t^- \langle \mathbf{g}_t - \nabla L_S(\mathbf{w}_t), \nabla L_S(\mathbf{w}_t)\rangle &\leq \sqrt{2Tv(L,\eta)}\log^{\frac{1}{2}}(1/\delta) \\ &\leq \sqrt{2a\sum_{t=1}^{T} K_t^2}\log^{\frac{1}{2}}(1/\delta) \\ &\leq 2\sqrt{\sum_{t=1}^{T}\eta_t^2 K^2 \|\nabla L_S(\mathbf{w}_t)\|_2^2}\log^{\frac{1}{2}}(1/\delta) \\ &\leq 2KG\sqrt{\sum_{t=1}^{T}\eta_t^2}\log^{\frac{1}{2}}(1/\delta),\end{aligned} \tag{97}$$

when $x \geq x_{\max}$, with $I(Tx) = (Tx/\sum_{i=1}^{T} K_i)^2$, we have

$$\begin{aligned}-\sum_{t=1}^{T} \eta_t s_t^- \langle \mathbf{g}_t - \nabla L_S(\mathbf{w}_t), \nabla L_S(\mathbf{w}_t)\rangle &\leq 4^{\frac{1}{2}}\frac{1}{T}\sum_{t=1}^{T} K_t \log^{\frac{1}{2}}(1/\delta) \\ &\leq 2\frac{KG}{T}\sum_{t=1}^{T}\eta_t \log^{\frac{1}{2}}(1/\delta).\end{aligned} \tag{98}$$

If $\theta \in (\frac{1}{2}, 1]$, let $a = (4\theta)^{2\theta}e^2$, when $x \le x_{\max}$ we have the following inequality with probability at least $1-\delta$

$$-\sum_{t=1}^{T}\eta_t s_t^- \langle \mathbf{g}_t - \nabla L_S(\mathbf{w}_t), \nabla L_S(\mathbf{w}_t)\rangle \le \sqrt{2a\sum_{t=1}^{T}K_t^2}\log^{\frac{1}{2}}(1/\delta)$$
$$\le \sqrt{2}(4\theta)^{\theta}eKG\sqrt{\sum_{t=1}^{T}\eta_t^2}\log^{\frac{1}{2}}(1/\delta), \tag{99}$$

when $x \ge x_{\max}$, let $I(Tx) = (Tx/\sum_{i=1}^{T}K_i)^{\frac{1}{\theta}},\ \forall\theta \in (\frac{1}{2}, 1]$, then we have

$$-\sum_{t=1}^{T}\eta_t s_t^- \langle \mathbf{g}_t - \nabla L_S(\mathbf{w}_t), \nabla L_S(\mathbf{w}_t)\rangle \le \frac{4^{\theta}}{T}\sum_{t=1}^{T}K_t\log^{\frac{1}{2}}(1/\delta)$$
$$\le \frac{4^{\theta}KG}{T}\sum_{t=1}^{T}\eta_t\log^{\theta}(1/\delta). \tag{100}$$

If $\theta > 1$, let $a = (2^{2\theta+1}+2)\Gamma(2\theta+1) + \frac{2^{3\theta}\Gamma(3\theta+1)}{3}$, when $x \le x_{\max}$ we have the following inequality with probability at least $1-3\delta$

$$-\sum_{t=1}^{T}\eta_t s_t^- \langle \mathbf{g}_t - \nabla L_S(\mathbf{w}_t), \nabla L_S(\mathbf{w}_t)\rangle \le \sqrt{2a\sum_{t=1}^{T}K_t^2}\log^{\frac{1}{2}}(1/\delta)$$
$$\le \sqrt{2(2^{2\theta+1}+2)\Gamma(2\theta+1) + \frac{2^{3\theta}\Gamma(3\theta+1)}{3}}KG\sqrt{\sum_{t=1}^{T}\eta_t^2}\log^{\frac{1}{2}}(1/\delta), \tag{101}$$

when $x \ge x_{\max}$, let $I(Tx) = (Tx/\sum_{i=1}^{T}K_i)^{\frac{1}{\theta}},\ \forall\theta > 1$, then we have

$$-\sum_{t=1}^{T}\eta_t s_t^- \langle \mathbf{g}_t - \nabla L_S(\mathbf{w}_t), \nabla L_S(\mathbf{w}_t)\rangle \le \frac{4^{\theta}}{T}\sum_{t=1}^{T}K_t\log^{\frac{1}{2}}(1/\delta)$$
$$\le \frac{4^{\theta}KG}{T}\sum_{t=1}^{T}\eta_t\log^{\theta}(1/\delta). \tag{102}$$

To continue the proof, employing Lemma B.5 in term $-\eta_t\langle\frac{c\mathbf{g}_t}{\|\mathbf{g}_t\|_2}s_t^+, \nabla L_S(\mathbf{w}_t)\rangle$ and covering all T iterations, we have

$$-\sum_{t=1}^{T}\eta_t\langle\frac{c\mathbf{g}_t}{\|\mathbf{g}_t\|_2}s_t^+, \nabla L_S(\mathbf{w}_t)\rangle \le -\frac{c\sum_{t=1}^{T}\eta_t s_t^+\|\nabla L_S(\mathbf{w}_t)\|_2}{3} + \frac{8c\sum_{t=1}^{T}\eta_t\|\mathbf{g}_t - \nabla L_S(\mathbf{w}_t)\|_2}{3}$$
$$\le -\frac{c\sum_{t=1}^{T}\eta_t(1-s_t^-)\|\nabla L_S(\mathbf{w}_t)\|_2}{3}$$
$$+\frac{16\sum_{t=1}^{T}\eta_t\|\mathbf{g}_t - \nabla L_S(\mathbf{w}_t)\|_2\|\nabla L_S(\mathbf{w}_t)\|_2}{3}. \tag{103}$$

With the truncated corollaries above, we have

(1) If $0 \le x \le x_{\max}$, with probability at least $1-3\delta$

$$-\sum_{t=1}^{T}\eta_t\langle\frac{c\mathbf{g}_t}{\|\mathbf{g}_t\|_2}s_t^+, \nabla L_S(\mathbf{w}_t)\rangle \le -\frac{c\sum_{t=1}^{T}\eta_t(1-s_t^-)\|\nabla L_S(\mathbf{w}_t)\|_2}{3}$$
$$+\frac{16\sum_{t=1}^{T}\eta_t\|\nabla L_S(\mathbf{w}_t)\|_2}{3}\begin{cases} 2K\log^{\frac{1}{2}}(2/\delta), & \text{if } \theta = \frac{1}{2},\\ \sqrt{2}e(4\theta)^{\theta}K\log^{\frac{1}{2}}(2/\delta), & \text{if } \theta \in (\frac{1}{2}, 1],\\ \sqrt{2(2^{2\theta+1}+2)\Gamma(2\theta+1) + \frac{2^{3\theta}\Gamma(3\theta+1)}{3}}K\log^{\frac{1}{2}}(2/\delta) & \text{if } \theta > 1. \end{cases} \tag{104}$$

(2) If $x \geq x_{\max}$ and $\theta \geq \frac{1}{2}$, with probability at least $1 - 3\delta$

$$-\sum_{t=1}^{T} \eta_t \langle \frac{c\mathbf{g}_t}{\|\mathbf{g}_t\|_2} s_t^+, \nabla L_S(\mathbf{w}_t) \rangle \leq -\frac{c\sum_{t=1}^{T} \eta_t (1 - s_t^-) \|\nabla L_S(\mathbf{w}_t)\|_2}{3} + \frac{16\sum_{t=1}^{T} \eta_t \|\nabla L_S(\mathbf{w}_t)\|_2}{3} 4^\theta K \log^\theta(2/\delta). \tag{105}$$

Then, according to Lemma B.1, combining the truncated results of $-\sum_{t=1}^{T} \eta_t \langle \mathbf{g}_t s_t^-, \nabla L_S(\mathbf{w}_t) \rangle$ and $-\sum_{t=1}^{T} \eta_t \langle \frac{c\mathbf{g}_t}{\|\mathbf{g}_t\|_2} s_t^+, \nabla L_S(\mathbf{w}_t) \rangle$, we have the inequality:

(1) If $0 \leq x \leq x_{\max}$, with probability at least $1 - 3\delta - T\delta$

$$\begin{aligned} -\sum_{t=1}^{T} \eta_t \langle \overline{\mathbf{g}}_t, \nabla L_S(\mathbf{w}_t) \rangle \leq & -\frac{c\sum_{t=1}^{T} \eta_t \|\nabla L_S(\mathbf{w}_t)\|_2}{3} \\ & + \begin{cases} 2KG\sqrt{\sum_{t=1}^{T} \eta_t^2} \log^{\frac{1}{2}}(1/\delta), & \text{if } \theta = \frac{1}{2}, \\ \sqrt{2}(4\theta)^\theta eKG\sqrt{\sum_{t=1}^{T} \eta_t^2} \log^{\frac{1}{2}}(1/\delta), & \text{if } \theta \in (\frac{1}{2}, 1], \\ \sqrt{2(2^{2\theta+1}+2)\Gamma(2\theta+1) + \frac{2^{3\theta}\Gamma(3\theta+1)}{3}} KG\sqrt{\sum_{t=1}^{T} \eta_t^2} \log^{\frac{1}{2}}(1/\delta) & \text{if } \theta > 1. \end{cases} \\ & + \frac{16\sum_{t=1}^{T} \eta_t \|\nabla L_S(\mathbf{w}_t)\|_2}{3} \begin{cases} 2K\log^{\frac{1}{2}}(2/\delta), & \text{if } \theta = \frac{1}{2}, \\ \sqrt{2}e(4\theta)^\theta K \log^{\frac{1}{2}}(2/\delta), & \text{if } \theta \in (\frac{1}{2}, 1], \\ \sqrt{2(2^{2\theta+1}+2)\Gamma(2\theta+1) + \frac{2^{3\theta}\Gamma(3\theta+1)}{3}} K\log^{\frac{1}{2}}(2/\delta) & \text{if } \theta > 1. \end{cases} \end{aligned} \tag{106}$$

(2) If $x \geq x_{\max}$ and $\theta \geq \frac{1}{2}$, with probability at least $1 - 3\delta - T\delta$

$$-\sum_{t=1}^{T} \eta_t \langle \overline{\mathbf{g}}_t, \nabla L_S(\mathbf{w}_t) \rangle \leq -\frac{c\sum_{t=1}^{T} \eta_t \|\nabla L_S(\mathbf{w}_t)\|_2}{3} + \frac{4^\theta KG}{T} \sum_{t=1}^{T} \eta_t \log^\theta(1/\delta) + \frac{16\sum_{t=1}^{T} \eta_t \|\nabla L_S(\mathbf{w}_t)\|_2}{3} 4^\theta K \log^\theta(2/\delta). \tag{107}$$

Therefore, we refer to formula (14) and formula (15), and apply Lemma B.2 due to $\zeta_t \sim \mathbb{N}(0, c\sigma_{\text{gp}}\mathbb{I}_d)$. Then, to simplify the notation, we define $\hat{\sigma}_{\text{gp}}^2 = dc^2\sigma_{\text{gp}}^2$. With $\hat{\sigma}_{\text{gp}}^2 = m_2 \frac{Tc^2dB^2\log(1/\delta)}{n^2\varepsilon^2}$ and probability $1 - 6\delta - T\delta$, if $0 \leq x \leq x_{\max}$, we have

$$\begin{aligned} & (\frac{c}{3} - \frac{16}{3}aK\log^{\frac{1}{2}}(2/\delta) - 4\sqrt{e}\hat{\sigma}_{\text{gp}}\log^{\frac{1}{2}}(1/\delta)) \sum_{t=1}^{T} \eta_t \|\nabla L_S(\mathbf{w}_t)\|_2 \leq L_S(\mathbf{w}_1) - L_S(\mathbf{w}_S) \\ & + (2\beta m_2 ed \frac{Tc^2B^2\log^2(2/\delta)}{n^2\varepsilon^2} + 2\beta\sqrt{em_2Td}\frac{c^2B\log(2/\delta)}{n\varepsilon} + \frac{1}{2}\beta c^2) \sum_{t=1}^{T} \eta_t^2 \\ & + \sqrt{2a}KG\sqrt{\sum_{t=1}^{T} \eta_t^2} \log^{\frac{1}{2}}(1/\delta), \end{aligned} \tag{108}$$

if $x \le x_{\max}$, we have

$$(\frac{c}{3} - \frac{16}{3}aK\log^{\theta}(2/\delta) - 4\sqrt{e}\hat{\sigma}_{\text{gp}}\log^{\frac{1}{2}}(1/\delta))\sum_{t=1}^{T}\eta_t\|\nabla L_S(\mathbf{w}_t)\|_2 \le L_S(\mathbf{w}_1) - L_S(\mathbf{w}_S)$$
$$+ (2\beta m_2 ed\frac{Tc^2B^2\log^2(2/\delta)}{n^2\varepsilon^2} + 2\beta\sqrt{em_2Td}\frac{c^2B\log(2/\delta)}{n\varepsilon} + \frac{1}{2}\beta c^2)\sum_{t=1}^{T}\eta_t^2$$
$$+ \sqrt{2a}KG\sqrt{\sum_{t=1}^{T}\eta_t^2}\log^{\theta}(1/\delta), \tag{109}$$

where $a = 2$ if $\theta = 1/2$, $a = (4\theta)^{2\theta}e^2$ if $\theta \in (1/2, 1]$ and $a = (2^{2\theta+1}+2)\Gamma(2\theta+1) + \frac{2^{3\theta}\Gamma(3\theta+1)}{3}$ if $\theta > 1$.

Afterwards,

(1) In case of light body, when $0 \le x \le x_{\max}$ and $\theta \ge \frac{1}{2}$:

If $K \ge \hat{\sigma}_{\text{gp}}$, let $\frac{c}{3} \ge \frac{33}{3}\sqrt{2a}K\log^{\frac{1}{2}}(2/\delta)$, $T = \mathbb{O}(\frac{n\varepsilon}{\sqrt{d\log(1/\delta)}})$ and $\eta_t = \frac{1}{\sqrt{T}}$, we obtain

$$\sum_{t=1}^{T}\eta_t\|\nabla L_S(\mathbf{w}_t)\|_2 \le \frac{3}{\sqrt{2a}K\log^{\frac{1}{2}}(2/\delta)}(L_S(\mathbf{w}_1) - L_S(\mathbf{w}_S)) + \frac{3\sqrt{2a}KG\sqrt{\sum_{t=1}^{T}\eta_t^2}\log^{\frac{1}{2}}(1/\delta)}{\sqrt{2a}K\log^{\frac{1}{2}}(2/\delta)}$$
$$+ \frac{3\sum_{t=1}^{T}\eta_t^2}{\sqrt{2a}K\log^{\frac{1}{2}}(2/\delta)}\left(2\beta m_2 ed\frac{Tc^2B^2\log^2(2/\delta)}{n^2\varepsilon^2} + 2\beta\sqrt{em_2Td}\frac{c^2B\log(2/\delta)}{n\varepsilon} + \frac{1}{2}\beta c^2\right)$$
$$\le \frac{3(L_S(\mathbf{w}_1) - L_S(\mathbf{w}_S))}{\sqrt{2a}K\log^{\frac{1}{2}}(2/\delta)} + \frac{3\sqrt{2a}KG\log^{\frac{1}{2}}(1/\delta)}{\sqrt{2a}K\log^{\frac{1}{2}}(2/\delta)}$$
$$+ \frac{6\beta ea^2K^2\log(2/\delta)}{\sqrt{2a}K\log^{\frac{1}{2}}(2/\delta)} + \frac{6\beta\sqrt{e}\sqrt{2a}K\log^{\frac{1}{2}}(2/\delta)}{\sqrt{2a}K\log^{\frac{1}{2}}(2/\delta)} + \frac{3\beta(33\sqrt{2a}K\log^{\frac{1}{2}}(2/\delta))^2}{2\sqrt{2a}K\log^{\frac{1}{2}}(2/\delta)}. \tag{110}$$

Therefore, with probability at least $1 - 6\delta - T\delta$, we have

$$\frac{1}{T}\sum_{t=1}^{T}\|\nabla L_S(\mathbf{w}_t)\|_2 \le \mathbb{O}(\frac{d^{\frac{1}{4}}\log^{\frac{3}{4}}(1/\delta)}{\sqrt{n\varepsilon}}),$$

then, with probability $1 - \delta$, we have

$$\frac{1}{T}\sum_{t=1}^{T}\|\nabla L_S(\mathbf{w}_t)\|_2 \le \mathbb{O}(\frac{d^{\frac{1}{4}}\log^{\frac{3}{4}}(T/\delta)}{\sqrt{n\varepsilon}}). \tag{111}$$

If $K \le \hat{\sigma}_{\text{gp}}$, let $\frac{c}{3} \ge 9\sqrt{e}\hat{\sigma}_{\text{gp}}\log^{\frac{1}{2}}(1/\delta)$, that is, $c \ge 27\sqrt{e}\hat{\sigma}_{\text{gp}}\log^{\frac{1}{2}}(1/\delta)$, thus there exists $T = \mathbb{O}(\frac{n\varepsilon}{\sqrt{d\log(1/\delta)}})$, $T \ge 1$ and $\eta_t = \frac{1}{\sqrt{T}}$ that we obtain

$$\sum_{t=1}^{T}\eta_t\|\nabla L_S(\mathbf{w}_t)\|_2 \le \frac{1}{\sqrt{e}\hat{\sigma}_{\text{gp}}\log^{\frac{1}{2}}(1/\delta)}(L_S(\mathbf{w}_1) - L_S(\mathbf{w}_S)) + \frac{\sqrt{2a}KG\sqrt{\sum_{t=1}^{T}\eta_t^2}\log^{\frac{1}{2}}(1/\delta)}{\sqrt{e}\hat{\sigma}_{\text{gp}}\log^{\frac{1}{2}}(1/\delta)}$$
$$+ \frac{\sum_{t=1}^{T}\eta_t^2}{\sqrt{e}\hat{\sigma}_{\text{gp}}\log^{\frac{1}{2}}(1/\delta)}\left(2\beta m_2 ed\frac{Tc^2B^2\log^2(2/\delta)}{n^2\varepsilon^2} + 2\beta\sqrt{em_2Td}\frac{c^2B\log(2/\delta)}{n\varepsilon} + \frac{1}{2}\beta c^2\right)$$
$$\le \frac{L_S(\mathbf{w}_1) - L_S(\mathbf{w}_S)}{\sqrt{e}\hat{\sigma}_{\text{gp}}\log^{\frac{1}{2}}(2/\delta)} + \frac{\sqrt{2a}KG}{\sqrt{e}\hat{\sigma}_{\text{gp}}} + 2\beta eK\log^{\frac{1}{2}}(2/\delta) + 2\beta\sqrt{e}\log^{\frac{1}{2}}(2/\delta) + \beta\frac{(27)^2}{2}K\log^{\frac{1}{2}}(2/\delta). \tag{112}$$

Therefore, with probability $1 - 6\delta - T\delta$, we have

$$\frac{1}{T}\sum_{t=1}^{T}\|\nabla L_S(\mathbf{w}_t)\|_2 \le \mathbb{O}(\frac{d^{\frac{1}{4}}\log^{\frac{3}{4}}(1/\delta)}{\sqrt{n\varepsilon}}),$$

then, with probability $1 - \delta$, we have

$$\frac{1}{T}\sum_{t=1}^{T}\|\nabla L_S(\mathbf{w}_t)\|_2 \le \mathbb{O}(\frac{d^{\frac{1}{4}}\log^{\frac{3}{4}}(T/\delta)}{\sqrt{n\varepsilon}}). \tag{113}$$

(2) In case of heavy tail, when $x \geq x_{\max}$:
If $\theta = \frac{1}{2}$ and $K \geq \hat{\sigma}_{\text{gp}}$, let $\frac{c}{3} \geq \frac{33}{3}\sqrt{2a}K\log^{\frac{1}{2}}(2/\delta)$, $T = \mathbb{O}(\frac{n\varepsilon}{\sqrt{d\log(1/\delta)}})$ and $\eta_t = \frac{1}{\sqrt{T}}$, we obtain

$$\begin{aligned}\sum_{t=1}^{T}\eta_t\|\nabla L_S(\mathbf{w}_t)\|_2 &\leq \frac{3}{\sqrt{2a}K\log^{\frac{1}{2}}(2/\delta)}(L_S(\mathbf{w}_1)-L_S(\mathbf{w}_S)) + \frac{3\sqrt{2a}KG\sqrt{\sum_{t=1}^{T}\eta_t^2}\log^{\frac{1}{2}}(1/\delta)}{\sqrt{2a}K\log^{\frac{1}{2}}(2/\delta)}\\ &+ \frac{3\sum_{t=1}^{T}\eta_t^2}{\sqrt{2a}K\log^{\frac{1}{2}}(2/\delta)}\left(2\beta m_2 ed\frac{Tc^2B^2\log^2(2/\delta)}{n^2\varepsilon^2} + 2\beta\sqrt{em_2Td}\frac{c^2B\log(2/\delta)}{n\varepsilon} + \frac{1}{2}\beta c^2\right)\\ &\leq \frac{3(L_S(\mathbf{w}_1)-L_S(\mathbf{w}_S))}{\sqrt{2a}K\log^{\frac{1}{2}}(2/\delta)} + \frac{3\sqrt{2a}KG\log^{\frac{1}{2}}(1/\delta)}{\sqrt{2a}K\log^{\frac{1}{2}}(2/\delta)}\\ &+ \frac{6\beta ea^2K^2\log(2/\delta)}{\sqrt{2a}K\log^{\frac{1}{2}}(2/\delta)} + \frac{6\beta\sqrt{e}\sqrt{2a}K\log^{\frac{1}{2}}(2/\delta)}{\sqrt{2a}K\log^{\frac{1}{2}}(2/\delta)} + \frac{3\beta(33\sqrt{2a}K\log^{\frac{1}{2}}(2/\delta))^2}{2\sqrt{2a}K\log^{\frac{1}{2}}(2/\delta)}.\end{aligned} \tag{114}$$

Therefore, with probability at least $1-6\delta-T\delta$, we have

$$\frac{1}{T}\sum_{t=1}^{T}\|\nabla L_S(\mathbf{w}_t)\|_2 \leq \mathbb{O}(\frac{d^{\frac{1}{4}}\log^{\frac{3}{4}}(1/\delta)}{\sqrt{n\varepsilon}}),$$

then, with probability $1-\delta$, we have

$$\frac{1}{T}\sum_{t=1}^{T}\|\nabla L_S(\mathbf{w}_t)\|_2 \leq \mathbb{O}(\frac{d^{\frac{1}{4}}\log^{\frac{3}{4}}(T/\delta)}{\sqrt{n\varepsilon}}). \tag{115}$$

If $\theta = \frac{1}{2}$ and $K \leq \hat{\sigma}_{\text{gp}}$, that is, $c \geq \frac{16aK\log^{\frac{1}{2}}(1/\delta)}{12}$, thus there exists $T = \mathbb{O}(\frac{n\varepsilon}{\sqrt{d\log(1/\delta)}})$, $T \geq 1$ and $\eta_t = \frac{1}{\sqrt{T}}$ that we obtain

$$\begin{aligned}\sum_{t=1}^{T}\eta_t\|\nabla L_S(\mathbf{w}_t)\|_2 &\leq \frac{1}{\sqrt{e}\hat{\sigma}_{\text{gp}}\log^{\frac{1}{2}}(1/\delta)}(L_S(\mathbf{w}_1)-L_S(\mathbf{w}_S)) + \frac{\sqrt{2a}KG\sqrt{\sum_{t=1}^{T}\eta_t^2}\log^{\frac{1}{2}}(1/\delta)}{\sqrt{e}\hat{\sigma}_{\text{gp}}\log^{\frac{1}{2}}(1/\delta)}\\ &+ \frac{\sum_{t=1}^{T}\eta_t^2}{\sqrt{e}\hat{\sigma}_{\text{gp}}\log^{\frac{1}{2}}(1/\delta)}\left(2\beta m_2 ed\frac{Tc^2B^2\log^2(2/\delta)}{n^2\varepsilon^2} + 2\beta\sqrt{em_2Td}\frac{c^2B\log(2/\delta)}{n\varepsilon} + \frac{1}{2}\beta c^2\right)\\ &\leq \frac{L_S(\mathbf{w}_1)-L_S(\mathbf{w}_S)}{\sqrt{e}\hat{\sigma}_{\text{gp}}\log^{\frac{1}{2}}(2/\delta)} + \frac{\sqrt{2a}KG}{\sqrt{e}\hat{\sigma}_{\text{gp}}} + 2\beta eK\log^{\frac{1}{2}}(2/\delta) + 2\beta\sqrt{e}\log^{\frac{1}{2}}(2/\delta) + \beta\frac{(27)^2}{2}K\log^{\frac{1}{2}}(2/\delta).\end{aligned} \tag{116}$$

Therefore, with probability $1-6\delta-T\delta$, we have

$$\frac{1}{T}\sum_{t=1}^{T}\|\nabla L_S(\mathbf{w}_t)\|_2 \leq \mathbb{O}(\frac{d^{\frac{1}{4}}\log^{\frac{3}{4}}(1/\delta)}{\sqrt{n\varepsilon}}),$$

then, with probability $1-\delta$, we have

$$\frac{1}{T}\sum_{t=1}^{T}\|\nabla L_S(\mathbf{w}_t)\|_2 \leq \mathbb{O}(\frac{d^{\frac{1}{4}}\log^{\frac{3}{4}}(T/\delta)}{\sqrt{n\varepsilon}}). \tag{117}$$

If $\theta > \frac{1}{2}$, then term $\log^{\theta}(2/\delta)$ dominates the inequality. Let $\frac{c}{3} \geq \frac{17}{3}K\log^{\theta}(2/\delta)$, $T = \mathbb{O}(\frac{n\varepsilon}{\sqrt{d\log(1/\delta)}})$ and $\eta_t = \frac{1}{\sqrt{T}}$, we obtain

$$\begin{aligned}\sum_{t=1}^{T}\eta_t\|\nabla L_S(\mathbf{w}_t)\|_2 &\leq \frac{3}{\sqrt{2a}K\log^{\theta}(2/\delta)}(L_S(\mathbf{w}_1)-L_S(\mathbf{w}_S)) + \frac{3\sqrt{2a}KG\sqrt{\sum_{t=1}^{T}\eta_t^2}\log^{\theta}(1/\delta)}{\sqrt{2a}K\log^{\theta}(2/\delta)}\\ &+ \frac{3\sum_{t=1}^{T}\eta_t^2}{\sqrt{2a}K\log^{\theta}(2/\delta)}\left(2\beta m_2 ed\frac{Tc^2B^2\log^2(2/\delta)}{n^2\varepsilon^2} + 2\beta\sqrt{em_2Td}\frac{c^2B\log(2/\delta)}{n\varepsilon} + \frac{1}{2}\beta c^2\right)\\ &\leq \frac{3(L_S(\mathbf{w}_1)-L_S(\mathbf{w}_S))}{\sqrt{2a}K\log^{\theta}(2/\delta)} + 3G + \frac{16^2}{24}\beta K\log^{\theta}(2/\delta) + 136\beta K\log^{\theta}(2/\delta) + 3\beta(17)^2K\log^{\theta}(2/\delta).\end{aligned} \tag{118}$$

As a result, with probability $1-\delta$, we have

$$\frac{1}{T}\sum_{t=1}^{T}\|\nabla L_S(\mathbf{w}_t)\|_2 \leq \mathbb{O}(\frac{\log^{\theta}(T/\delta)d^{\frac{1}{4}}\log^{\frac{1}{4}}(T/\delta)}{\sqrt{n\varepsilon}}). \tag{119}$$

Consequently, integrate the above results on the condition that $\nabla L_S(\mathbf{w}_t) \geq c/2$.

For light body, we have

$$\frac{1}{T}\sum_{t=1}^{T}\|\nabla L_S(\mathbf{w}_t)\|_2 \leq \mathbb{O}(\frac{d^{\frac{1}{4}}\log^{\frac{3}{4}}(T/\delta)}{\sqrt{n\varepsilon}}), \tag{120}$$

For heavy tail, we have

$$\frac{1}{T}\sum_{t=1}^{T}\|\nabla L_S(\mathbf{w}_t)\|_2 \leq \mathbb{O}(\frac{d^{\frac{1}{4}}\log^{\theta+\frac{1}{4}}(T/\delta)}{\sqrt{n\varepsilon}}), \tag{121}$$

with probability $1-\delta$ and $\theta \geq \frac{1}{2}$.

In a word, covering the two cases, we ultimately come to the conclusion with probability $1-\delta$, $T = \mathbb{O}(\frac{n\varepsilon}{\sqrt{d\log(1/\delta)}})$, $T \geq 1$ and $\eta_t = \frac{1}{\sqrt{T}}$:

1. In the heavy-tail region:

$$\begin{aligned}\frac{1}{T}\sum_{t=1}^{T}\min\left\{\|\nabla L_S(\mathbf{w}_t)\|_2, \|\nabla L_S(\mathbf{w}_t)\|_2^2\right\} &\leq \mathbb{O}(\frac{d^{\frac{1}{4}}\log^{\theta+\frac{1}{4}}(T/\delta)}{(n\varepsilon)^{\frac{1}{2}}}) + \mathbb{O}(\frac{d^{\frac{1}{4}}\log^{2\theta}(\sqrt{T})\log^{\frac{5}{4}}(T/\delta)}{(n\varepsilon)^{\frac{1}{2}}}) \\ &\leq \mathbb{O}(\frac{d^{\frac{1}{4}}\log^{\frac{1}{4}}(T/\delta)\left(\log^{\theta}(T/\delta)+\log^{2\theta}(\sqrt{T})\log(T/\delta)\right)}{(n\varepsilon)^{\frac{1}{2}}}) \\ &\leq \mathbb{O}(\frac{d^{\frac{1}{4}}\log^{\frac{1}{4}}(T/\delta)\hat{\log}(T/\delta)\log^{2\theta}(\sqrt{T})}{(n\varepsilon)^{\frac{1}{2}}}),\end{aligned} \tag{122}$$

where $\hat{\log}(T/\delta) = \log^{\max(1,\theta)}(T/\delta)$. If $\theta = \frac{1}{2}$ and $K \leq \hat{\sigma}_{\text{gp}}$, then $c_1 = \max\left(4K\log^{\frac{1}{2}}(\sqrt{T}), \frac{16aK\log^{\frac{1}{2}}(1/\delta)}{12}\right)$. If $\theta = \frac{1}{2}$ and $K \geq \hat{\sigma}_{\text{gp}}$, then $c_1 = \max\left(4K\log^{\frac{1}{2}}(\sqrt{T}), 33\sqrt{2a}K\log^{\frac{1}{2}}(2/\delta)\right)$. If $\theta > \frac{1}{2}$, then $c_1 = \max\left(4^{\theta}2K\log^{\theta}(\sqrt{T}), 17K\log^{\theta}(2/\delta)\right)$.

2. In the light-body region:

$$\begin{aligned}\frac{1}{T}\sum_{t=1}^{T}\min\left\{\|\nabla L_S(\mathbf{w}_t)\|_2, \|\nabla L_S(\mathbf{w}_t)\|_2^2\right\} &\leq \mathbb{O}(\frac{d^{\frac{1}{4}}\log^{\frac{3}{4}}(T/\delta)}{(n\varepsilon)^{\frac{1}{2}}}) + \mathbb{O}(\frac{d^{\frac{1}{4}}\log(\sqrt{T})\log^{\frac{5}{4}}(T/\delta)}{(n\varepsilon)^{\frac{1}{2}}}) \\ &\leq \mathbb{O}(\frac{d^{\frac{1}{4}}\log^{\frac{1}{4}}(T/\delta)\left(\log^{\frac{1}{2}}(T/\delta)+\log(\sqrt{T})\log(T/\delta)\right)}{(n\varepsilon)^{\frac{1}{2}}}) \\ &\leq \mathbb{O}(\frac{d^{\frac{1}{4}}\log^{\frac{5}{4}}(T/\delta)\log(\sqrt{T})}{(n\varepsilon)^{\frac{1}{2}}}),\end{aligned} \tag{123}$$

where if $K \leq \hat{\sigma}_{\text{gp}}$, then $c_2 = \max\left(2\sqrt{2a}K\log^{\frac{1}{2}}(\sqrt{T}), 27\sqrt{e}\hat{\sigma}_{\text{gp}}\log^{\frac{1}{2}}(1/\delta)\right)$. If $K \geq \hat{\sigma}_{\text{gp}}$, then $c_2 = \max\left(2\sqrt{2a}K\log^{\frac{1}{2}}(\sqrt{T}), 33\sqrt{2a}K\log^{\frac{1}{2}}(2/\delta)\right)$. □

The proof of Theorem 4.2 is completed.

F Union Bound (Formal Version) for Discriminative Clipping DPSGD

Corollary F.1 (**Union Bound (Formal Version) for Discriminative Clipping DPSGD**). *Let $\mathbf{w}_t$ be the iterative parameter produced by DC-DPSGD. Under Assumptions 2.1, 2.2 and 2.3, combining Theorem 2 and Theorem 3, for any $\delta' \in (0,1)$, with probability $1-\delta'$, we have*

$$\frac{1}{T}\sum_{t=1}^{T}\min\left\{\|\nabla L_S(\mathbf{w}_t)\|_2, \|\nabla L_S(\mathbf{w}_t)\|_2^2\right\} \le p * \mathbb{O}\left(\frac{d^{\frac{1}{4}}\log^{\frac{1}{4}}(T/\delta')\hat{\log}(T/\delta')\log^{2\theta}(\sqrt{T})}{(n\varepsilon)^{\frac{1}{2}}}\right) + (1-p)*\mathbb{O}\left(\frac{d^{\frac{1}{4}}\log^{\frac{5}{4}}(T/\delta')\log(\sqrt{T})}{(n\varepsilon)^{\frac{1}{2}}}\right),$$

where $\delta' = \delta_{\text{tr}} + \delta$, $\hat{\log}(T/\delta') = \log^{\max(1,\theta)}(T/\delta')$ and p is the proportion of heavy-tailed samples.

Proof. We combine the heavy-tail identification error (Theorem 4.1) with the optimization bound of Discriminative Clipping DPSGD (Theorem 4.2) in this section to align with our algorithm outline. We have already discussed the error of traces in previous chapters and considered the condition of additional noise that satisfies DP, obtaining an upper bound on the error that depends on the factor $\mathbb{O}(\frac{\log d\sqrt{\log n^*}}{k\varepsilon_{\text{tr}}})$. This conclusion means that, the divergence between the empirical trace $\lambda_{t,i}^{\text{tr}}$ and the true trace $\hat{\lambda}_{t,i}^{\text{tr}}$ under the high probability guarantee of $1-\delta_{\text{tr}}$, we can accurately identify the trace of the per-sample gradient with minimal error, and classify gradients into the light body and heavy tail based on the metric.

Specifically, based on statistical characteristics, approximately 5% -10% of the data will fall into the tail part. Thus, we select the top p% samples in the trace ranking as the tailed samples, where $p \in [0.05, 0.1]$. Furthermore, based on the relationship between trace and variance, the pn-th of sorted trace $\lambda_t^{\text{tr},p}$ can be seen as the inflection point $x_{\max}$ of distribution defined in truncated theories B.7 and B.8, which corresponds to the empirical sample results with theoretical population variance and the approximation error has bounded in Theorem 4.1. Therefore, in discriminative clipping DPSGD, we can accurately partition the sample into the heavy-tailed convergence bound with a high probability of $(1-\delta_{\text{tr}})*p$, and exactly induce the sample to the bound of light bodies with a high probability of $(1-\delta_{\text{tr}})*(1-p)$, while there is a discrimination error with probability δ_{tr}. Accordingly, we have

$$\begin{aligned} C_{\text{m}}(c_1,c_2) &:= \frac{1}{T}\sum_{t=1}^{T}\min\left\{\|\nabla L_S(\mathbf{w}_t)\|_2, \|\nabla L_S(\mathbf{w}_t)\|_2^2\right\} \\ &= (1-\delta_{\text{tr}})*p*C_{\text{tail}}(c_1) + (1-\delta_{\text{tr}})*(1-p)*C_{\text{body}}(c_2) + \delta_{\text{tr}}*|C_{\text{tail}}(c_1) - C_{\text{body}}(c_2)|. \end{aligned} \tag{124}$$

where $C_{\text{tail}}(c_1)$ means the convergence bound of $\frac{1}{T}\sum_{t=1}^{T}\min\left\{\|\nabla L_S(\mathbf{w}_t)\|_2, \|\nabla L_S(\mathbf{w}_t)\|_2^2\right\}$ when $\lambda_{t,i}^{\text{tr}} \ge \lambda_t^{\text{tr},p}$, i.e. $\mathbb{O}(\frac{d^{\frac{1}{4}}\log^{\frac{1}{4}}(T/\delta)\hat{\log}(1/\delta)\log^{2\theta}(\sqrt{T})}{(n\varepsilon)^{\frac{1}{2}}})$, $C_{\text{body}}(c_2)$ denotes the bound of $\frac{1}{T}\sum_{t=1}^{T}\min\left\{\|\nabla L_S(\mathbf{w}_t)\|_2, \|\nabla L_S(\mathbf{w}_t)\|_2^2\right\}$ when $0 \le \lambda_{t,i}^{\text{tr}} \le \lambda_t^{\text{tr},p}$ i.e. $\mathbb{O}(\frac{d^{\frac{1}{4}}\log^{\frac{5}{4}}(T/\delta)\log(\sqrt{T})}{(n\varepsilon)^{\frac{1}{2}}})$, with $c_1 = 4^{\theta}2K\log^{\theta}(\sqrt{T})$ and $c_2 = 2\sqrt{2a}K\log^{\frac{1}{2}}(\sqrt{T})$.

If $\theta = \frac{1}{2}$, then $C_{\text{tail}}(c_1) = C_{\text{body}}(c_2)$ and $\delta_{\text{tr}} \to 0$, thus we have

$$C_{\text{m}}(c_1,c_2) = C_{\text{tail}}(c_1) = \mathbb{O}\left(\frac{d^{\frac{1}{4}}\log^{\frac{5}{4}}(T/\delta)\log(\sqrt{T})}{(n\varepsilon)^{\frac{1}{2}}}\right). \tag{125}$$

If $\theta > \frac{1}{2}$, then $C_{\text{tail}}(c_1) \ge C_{\text{body}}(c_2)$, and we need to proof that $C_{\text{tail}}(c_1) \ge C_{\text{m}}(c_1,c_2)$, i.e.

$$\begin{aligned} C_{\text{tail}}(c_1) &\ge C_{\text{m}}(c_1,c_2) \\ &\ge (1-\delta_{\text{tr}})*p*C_{\text{tail}}(c_1) + (1-\delta_{\text{tr}})*(1-p)*C_{\text{body}}(c_2) + \delta_{\text{tr}}*|C_{\text{tail}}(c_1) - C_{\text{body}}(c_2)|. \end{aligned}$$

By transposition, we have

$$(1-\delta_{\text{tr}})(1-p)*C_{\text{tail}}(c_1) + \delta_{\text{tr}}*C_{\text{body}}(c_2) \ge (1-\delta_{\text{tr}})*(1-p)*C_{\text{body}}(c_2).$$

Then, we have

$$C_{\text{tail}}(c_1) \ge C_{\text{body}}(c_2) - \frac{\delta_{\text{tr}}}{(1-\delta_{\text{tr}})*(1-p)}C_{\text{body}}(c_2), \tag{126}$$

due to $\frac{\delta_{\text{tr}}}{(1-\delta_{\text{tr}})*(1-p)} \ge 0$, it is proved that $C_{\text{tail}}(c_1) \ge C_{\text{m}}(c_1,c_2)$.

From another perspective, for $C_{\text{m}}(c_1,c_2)$, with probability $1-\delta_{\text{tr}}$, we have

$$C_{\text{m}}(c_1,c_2) = p*C_{\text{tail}}(c_1) + *(1-p)*C_{\text{body}}(c_2). \tag{127}$$

Overall, for the formula (124), we define $\delta' = \delta_{\text{tr}} + \delta$. Then, with probability $1 - \delta'$, we have

$$\frac{1}{T}\sum_{t=1}^{T}\min\left\{\|\nabla L_S(\mathbf{w}_t)\|_2, \|\nabla L_S(\mathbf{w}_t)\|_2^2\right\} \leq p * \mathbb{O}\left(\frac{d^{\frac{1}{4}}\log^{\frac{1}{4}}(T/\delta')\hat{\log}(T/\delta')\log^{2\theta}(\sqrt{T})}{(n\varepsilon)^{\frac{1}{2}}}\right) + (1-p) * \mathbb{O}\left(\frac{d^{\frac{1}{4}}\log^{\frac{5}{4}}(T/\delta')\log(\sqrt{T})}{(n\varepsilon)^{\frac{1}{2}}}\right), \tag{128}$$

where $\hat{\log}(T/\delta') = \log^{\max(1,\theta)}(T/\delta')$.

□

Thus, if $p \leq \frac{1}{\mathbb{O}(\log^{\max(0,\theta-1)}(T/\delta')\log^{2\theta-1}(\sqrt{T}))+1}$ and $p \leq 1$, we have

$$\frac{1}{T}\sum_{t=1}^{T}\min\left\{\|\nabla L_S(\mathbf{w}_t)\|_2, \|\nabla L_S(\mathbf{w}_t)\|_2^2\right\} \leq \mathbb{O}\left(\frac{d^{\frac{1}{4}}\log^{\frac{5}{4}}(T/\delta')\log(\sqrt{T})}{(n\varepsilon)^{\frac{1}{2}}}\right).$$

The proof of Corollary 4.3 is completed.

G Privacy Guarantee

G.1 Privacy Analysis of Sampling Mechanism

Theorem G.1 (Noise scaling under partitioned sampling). *Under the same privacy budget ε, the partitioned mechanism requires a noise multiplier that requires*

$$\sigma_{\text{gp}} \approx \sqrt{\frac{pq_1^2 + (1-p)q_2^2}{\bar{q}^2}}\sigma_{\text{Pois}}. \tag{129}$$

Equality holds if and only if $q_1 = q_2 = \bar{q}$.

Proof. Denote by $\varepsilon_{\text{Pois}}(\alpha, q, \sigma)$ the Rényi Differential Privacy (RDP) cost of a Poisson-subsampled Gaussian mechanism with sampling rate q and noise scale σ at order $\alpha > 1$.

(1) RDP upper bound for partitioned sampling. Consider a partitioned mechanism where the dataset is divided into a *tail subset* (sampling rate q_1) and a *body subset* (sampling rate q_2), with mixing probability p for the tail subset. The total RDP of this mixed mechanism is upper bounded by

$$\varepsilon_{\text{gp}}(\alpha, \sigma) = \frac{1}{\alpha - 1}\log\left(p\, e^{(\alpha-1)\varepsilon_{\text{Pois}}(\alpha, q_1, \sigma)} + (1-p)\, e^{(\alpha-1)\varepsilon_{\text{Pois}}(\alpha, q_2, \sigma)}\right). \tag{130}$$

(2) Convexity in sampling rate. The function $\varepsilon_{\text{Pois}}(\alpha, q, \sigma)$ is monotonically increasing and convex in q. Let $\phi(q) = \exp((\alpha-1)\varepsilon_{\text{Pois}}(\alpha, q, \sigma))$. By Jensen's inequality,

$$p\,\phi(q_1) + (1-p)\,\phi(q_2) \geq \phi(pq_1 + (1-p)q_2) = \phi(\bar{q}), \tag{131}$$

where $\bar{q} = pq_1 + (1-p)q_2$ denotes the average sampling rate.

Substituting (131) into (130), we have

$$\varepsilon_{\text{gp}}(\alpha, \sigma) \geq \varepsilon_{\text{Pois}}(\alpha, \bar{q}, \sigma). \tag{132}$$

Hence, under the same noise scale σ, the per-step RDP of the partitioned mechanism is almost the same as that of Poisson sampling with the same average rate $\bar{q}$, which shares an approximately equivalent level of privacy amplification with uniform sampling without replacement.

Consequently, to achieve an identical target privacy loss ε, the required noise scale must satisfy

$$\sigma_{\text{gp}} \geq \sigma_{\text{Pois}}, \qquad \text{with equality iff } q_1 = q_2 = \bar{q}. \tag{133}$$

(3) Closed-form ratio under small sampling rate approximation. For small sampling rate $q \ll 1$, the RDP of the Poisson-subsampled Gaussian mechanism can be approximated by

$$\varepsilon_{\text{Pois}}(\alpha, q, \sigma) \approx \frac{\alpha}{2\sigma^2}q^2. \tag{134}$$

Substituting into (130), we obtain

$$\varepsilon_{\text{gp}}(\alpha, \sigma) \approx \frac{\alpha}{2\sigma^2}\left(pq_1^2 + (1-p)q_2^2\right), \quad \varepsilon_{\text{Pois}}(\alpha, \sigma) \approx \frac{\alpha}{2\sigma^2}\bar{q}^2. \tag{135}$$

Equating their privacy losses $\varepsilon_{\text{gp}}(\alpha, \sigma_{\text{gp}}) = \varepsilon_{\text{Pois}}(\alpha, \sigma_{\text{Pois}})$, we have

$$\sigma_{\text{gp}} \approx \sigma_{\text{Pois}}\sqrt{\frac{pq_1^2 + (1-p)q_2^2}{\bar{q}^2}} \geq \sigma_{\text{Pois}}. \tag{136}$$

The inequality follows from Jensen's inequality, $pq_1^2 + (1-p)q_2^2 \geq (pq_1 + (1-p)q_2)^2 = \bar{q}^2$.

(4) Conclusion. Therefore, to maintain the same privacy level ε, the partitioned mechanism must employ a noise scale at least as large as that of Poisson sampling:

$$\sigma_{\text{gp}} \approx \sigma_{\text{Pois}}\sqrt{\frac{pq_1^2 + (1-p)q_2^2}{\bar{q}^2}}.$$

□

G.2 Privacy Guarantee of DC-DPSGD

Next, we provide the complete privacy guarantee proof of Theorem 4.5 for our differential private mechanism M': Subsample∘PrivateSelection (PS)∘ GradientPerturbation (GP). The specific proof process is as follows, and our proof comprehensively encompasses mechanism M':

- **PrivateSelection**: We prove that PrivateSelection is $(\varepsilon_{\text{tr}}, \delta_{\text{tr}})$-DP.
- **PrivateSelection∘GradientPerturbation**: We prove that based on the results of PrivateSelection, with two different clipping threshold, the unified composition of PrivateSelection and GradientPerturbation is $(\varepsilon_{\text{tr}} + \varepsilon_{\text{gp}}, \delta)$-DP, where $\delta = \delta_{\text{tr}} + \delta_{\text{gp}}$.
- **Subsample∘PrivateSelection∘GradientPerturbation**: We prove that, under the premise of subsampling, the privacy amplification effect remains valid for our composition mechanism.

Proof. **(1) *Firstly***, we prove the Gaussian-SVT technique is $(\varepsilon_{\text{tr}}, \delta_{\text{tr}})$-differentially private. In the first step, we analyze the situation where the output is $\alpha \in \{\perp, \top\}^n$, a length-$n$ vector, indicating that all n queries are tested to be below the threshold.

$$\mathbb{P}[\mathcal{A}(S) = \perp^n] = \int_{-\infty}^{\infty} \mathbb{P}[\rho = z]\ \mathcal{F}_S(z)\, dz, \tag{137}$$

where

$$\mathcal{F}_S(z) \coloneqq \mathbb{P}[\mathcal{A}(S) = \perp^n |\ \rho = z] = \prod_{i=1}^{n} \mathbb{P}[f_i(S) + \nu_i < \mathcal{T}_i + z]. \tag{138}$$

Through a series of transformations and derivations, together with the sensitivity definition, we obtain that

$$\mathbb{P}[f_i(S) + \nu_i < \mathcal{T}_i + z] = \mathbb{P}[\nu_i < \mathcal{T}_i - f_i(S) + z] \le \mathbb{P}[\nu_i < \mathcal{T}_i + \Delta - f_i(S') + z] = \mathbb{P}[f_i(S') + \nu_i < \mathcal{T}_i + (z + \Delta)]. \tag{139}$$

Let $\rho \sim \mathbb{N}(0, \Delta^2\sigma_1^2\mathbb{I})$ with $\sigma_1 = \frac{\sqrt{2\log(1.25/\delta_1)}}{\varepsilon_1}$. By standard tail bounds of the Gaussian distribution, $\forall z$, it holds that

$$\mathbb{P}[\rho = z] \le e^{\varepsilon_1}\mathbb{P}[\rho = z + \Delta] + \delta.$$

Then, we have

$$\begin{aligned}
\mathbb{P}[\mathcal{A}(S) = \perp^n] &= \int_{-\infty}^{\infty} \mathbb{P}[\rho = z]\mathcal{F}_S(z)\, dz && (140)\\
&\le \int_{-\infty}^{\infty} (e^{\varepsilon_1}\mathbb{P}[\rho = z + \Delta] + \delta_1)\mathcal{F}_{S'}(z + \Delta)\, dz && (141)\\
&= e^{\varepsilon_1} \int_{-\infty}^{\infty} \mathbb{P}[\rho = z']\mathcal{F}_{S'}(z')\, dz' + \delta_1 \quad \text{Let } z' = z + \Delta && (142)\\
&= e^{\varepsilon_1}\mathbb{P}[\mathcal{A}(S') = \perp^n] + \delta_1. && (143)
\end{aligned}$$

In the second step, if the output includes both $\perp$ and $\top$, we analyze one branch at a time by conditioning on either the positive or the negative outcome, and bound the corresponding probability using the SVT technique. Formally, we define $\alpha \in \{\perp, \top\}^n$, $I_\top = \{i : \alpha_i = \top\}$ and $I_\perp = \{i : \alpha_i = \perp\}$. Then, we have

$$\mathbb{P}[\mathcal{A}(S) = \alpha] = \int_{-\infty}^{\infty} \mathbb{P}[\rho = z]\ \mathcal{F}_S(z)\, g_S(z)\, dz, \tag{144}$$

where

$$\mathcal{F}_S(z) = \prod_{i \in I_\perp} \mathbb{P}[f_i(S) + \nu_i < \mathcal{T}_i + z] \tag{145}$$

and

$$g_S(z) = \prod_{i \in I_\top} \mathbb{P}[f_i(S) + \nu_i \ge \mathcal{T}_i + z]\,. \tag{146}$$

Given

$$\mathbb{P}[\rho = z] \le e^{\varepsilon_1}\mathbb{P}[\rho = z + \Delta] \tag{147}$$

$$\tag{148}$$

and

$$\mathcal{F}_S(z) \le \mathcal{F}_{S'}(z + \Delta), \tag{149}$$

the above equation bounds the probability of all negative outcomes. We aim to prove

$$g_S(z) \le e^{\varepsilon_2} g_{S'}(z + \Delta) + \delta_2. \tag{150}$$

The equation, which corresponds to positive outcomes, follows from several observations. First, across the n^* parallel and disjoint domains, at most one positive outcome can occur. Second, for each disjoint domain, the sensitivity satisfies $|f_i(S) - f_i(S')| \le \Delta$. Third, the threshold evaluated on the neighboring dataset S' exceeds that on S by exactly Δ. Consequently, adding independent noise $\nu_i \sim \mathbb{N}(0, (2\Delta\sigma_2)^2\mathbb{I})$ with $\sigma_2 = \frac{\sqrt{2\log(1.25n^*/\delta_2)}}{\varepsilon_2}$ to each query yields the desired bound.

Specifically, let S and S' be neighboring datasets that differ in a single element x. Since the domains $\{S_j\}_{j=1}^{n^*}$ are pairwise disjoint, the differing element x belongs to at most one subdomain, denoted by S_{j^*}. Consequently, for all $j \ne j^*$, we have

$$S \cap S_j = S' \cap S_j. \tag{151}$$

Therefore, the outputs of the query mechanisms $M_j(S \cap S_j)$ and $M_j(S' \cap S_j)$ are identical for all $j \ne j^*$. Only the mechanism M_{j^*} is affected by the change from S to S'.

Thus, we need to prove

$$g_{S_{j^*}}(z) \le e^{\varepsilon_2} g_{S'_{j^*}}(z+\Delta) + \delta_2. \tag{152}$$

Then, with $I^*_\top = I_\top \cap \left(\mathcal{A}(S_{j^*}) \cup \mathcal{A}(S'_{j^*})\right)$, we have

$$\begin{aligned}
g_{S_{j^*}}(z) &= \prod_{i\in I^*_\top} \mathbb{P}\left[v_i \ge \mathcal{T}_i + z - f_i(S_{j^*})\right], && (153)\\
&\le \prod_{i\in I^*_\top} \mathbb{P}\left[v_i \ge \mathcal{T}_i + z - \Delta - f_i(S'_{j^*})\right], && (154)\\
&\le \prod_{i\in I^*_\top} e^{\varepsilon_2/n^*}\,\mathbb{P}\left[v_i \ge \mathcal{T}_i + z - \Delta - f_i(S'_{j^*}) + 2\Delta\right] + \sum_{i\in I^*_\top}\delta_i, \quad \text{due to Gaussian properties}, && (155)\\
&\le \prod_{i\in I^*_\top} e^{\varepsilon_2}\mathbb{P}\left[v_i \ge \mathcal{T}_i + z + \Delta - f_i(S'_{j^*})\right] + \delta_2, && (156)\\
&\le e^{\varepsilon_2} \prod_{i\in I^*_\top} \mathbb{P}\left[f_i(S'_{j^*}) + v_i \ge \mathcal{T}_i + z + \Delta\right] + \delta_2, \quad \text{due to } |I^*_\top| \le 1, && (157)\\
&= e^{\varepsilon_2} g_{S'_{j^*}}(z+\Delta) + \delta_2. && (158)
\end{aligned}$$

Since M_{j^*} satisfies (ε,δ)-differential privacy, for any measurable set O, it holds that

$$\mathbb{P}\left[M_{j^*}(S\cap S_{j^*}) \in O\right] \le e^{\varepsilon_2}\mathbb{P}\left[M_{j^*}(S'\cap S_{j^*}) \in O\right] + \delta_2. \tag{159}$$

As all other components of $M(S)$ remain unchanged, the joint query mechanism

$$M(S) \coloneqq \big(M_1(S\cap S_1), \dots M_{j^*}(S\cap S_{j^*}), \dots M_{n^*}(S\cap S_{n^*})\big), \tag{160}$$

i.e., $g_S(z) \le e^{\varepsilon_2} g_{S'}(z+\Delta) + \delta_2$ also satisfies (ε_2,δ_2)-differential privacy.

By integrating the results, we have

$$\mathbb{P}[\mathcal{A}(S)=\alpha] = e^{\varepsilon_1+\varepsilon_2}\mathbb{P}[\mathcal{A}(S')=\alpha] + \delta_{\text{tr}}, \quad \delta_{\text{tr}} = \delta_1+\delta_2. \tag{161}$$

Overall, the Gaussian-SVT technique is $(\varepsilon_{\text{tr}},\delta_{\text{tr}})$-differentially private with $\varepsilon_{\text{tr}} = \varepsilon_1+\varepsilon_2$.

Given the outcome $\mathcal{A}(S)=\alpha$, we partition the samples into a tail part and a body part according to the indicator α: samples with $\alpha_i = \top$ are assigned to the tail part and are grouped into mini-batches $\pi \subset S^{\text{tail}}$, while samples with $\alpha_i = \bot$ are assigned to the body part, corresponding to $\pi \subset S^{\text{body}}$. This partitioning is produced by a differentially private mechanism and therefore accounts for the possibility that a sample may change its tail or body membership when moving from S to the neighboring dataset S'. Moreover, all subsequent operations on S^{tail} and S^{body} constitute the post-processing property. □

(2) *Secondly*, we prove the unified composition of PrivateSelection∘GradientPerturbation is $(\varepsilon_{\text{tr}}+\varepsilon_{\text{gp}},\delta)$-DP. Based on the results of PrivateSelection, we employ two different clipping thresholds for GradientPerturbation.

Proof. We define the clipping threshold vector c for per-sample gradients via the PrivateSelection mechanism. Conditioned on the output of the PrivateSelection mechanism in Step 1 of Algorithm 2, the tail and body partitions $(S^{\text{tail}}, S^{\text{body}})$, where $S = (S^{\text{tail}} \cup S^{\text{body}})$, as well as the corresponding clipping thresholds (c_1, c_2) are fixed. The subsequent discriminative clipping and gradient perturbation in Step 2 operate solely on these fixed outputs and therefore constitute post-processing with respect to the private data.

$$\begin{aligned}
\mathbb{P}[M(S)=Y] &= \mathbb{P}[\mathcal{A}(S)=\alpha \text{ with } \alpha=\{\top,\bot\}^{|S|} \text{ AND GP}|S]\\
&= \int_{-\infty}^{\infty} \mathbb{P}[\mathcal{A}(S)=\alpha]\cdot\mathbb{P}[\text{GP with } (S^{\text{tail}}, S^{\text{body}})]dr\\
&= \int_{-\infty}^{\infty}\int_{-\infty}^{\infty} \mathbb{P}[\mathcal{A}(S)=\alpha]\cdot\mathbb{P}[\frac{1}{|B|}(\sum_{j}^{B\in S} g_j + c_j\zeta_j) = Y|c]drd\zeta\\
&= \int_{-\infty}^{\infty}\int_{-\infty}^{\infty} \mathbb{P}[\mathcal{A}(S)=\alpha]\cdot\mathbb{P}[f(S)=Y|c]\cdot\mathbb{P}[\zeta = c_j\zeta_j/|B|]drd\zeta = *,
\end{aligned} \tag{162}$$

where and $\zeta \sim \text{Gauss}(1/\varepsilon_{\text{gp}})$. For each mini-batch B, the L_2-sensitivity of the gradient update is bounded by c_1 if $B \subseteq S^{\text{tail}}$ and by c_2 otherwise. We here define $f(\cdot) = \text{GradientDescent}$ and $\Delta_f = c_1$ when training on S^{tail} else c_2. Then, with $1 - (\delta_{\text{tr}} + \delta_{\text{gp}})$, we have

$$
\begin{aligned}
* &= \int_{-\infty}^{\infty}\int_{-\infty}^{\infty} \exp(\varepsilon_{\text{tr}})\mathbb{P}[\mathcal{A}(S') = \alpha] \cdot \mathbb{P}[\frac{1}{B}(\sum_{j}^{B\in S'} g_j + c_j\zeta_j) = Y|c]drd\zeta \\
&= \int_{-\infty}^{\infty}\int_{-\infty}^{\infty} \exp(\varepsilon_{\text{tr}})\mathbb{P}[\mathcal{A}(S') = \alpha] \cdot \mathbb{P}[f(S') + c_j\zeta_j/B = Y + \Delta f|c]drd\zeta \\
&= \int_{-\infty}^{\infty}\int_{-\infty}^{\infty} \exp(\varepsilon_{\text{tr}})\mathbb{P}[\mathcal{A}(S') = \alpha] \cdot \mathbb{I}[f(S') = Y] \cdot \mathbb{P}[\zeta = c_j\zeta_j/B - \Delta f|c]drd\zeta \\
&\leq \int_{-\infty}^{\infty}\int_{-\infty}^{\infty} \exp(\varepsilon_{\text{tr}})\mathbb{P}[\mathcal{A}(S') = \alpha] \cdot \mathbb{I}[f(S') = Y] \cdot \exp(\varepsilon_{\text{gp}})\mathbb{P}[\zeta = c_j\zeta_j/B|c]drd\zeta \\
&\leq \exp(\varepsilon_{\text{tr}} + \varepsilon_{\text{gp}})\mathbb{P}[M(S') = Y],
\end{aligned} \tag{163}
$$

Thus, PrivateSelection∘GradientPerturbation is $(\varepsilon_{\text{tr}} + \varepsilon_{\text{gp}}, \delta)$-DP with $\delta = \delta_{\text{tr}} + \delta_{\text{gp}}$.

Applying the Gaussian mechanism to each update and composing it with the privacy guarantee of PrivateSelection, Algorithm 2 satisfies $(\varepsilon_{\text{tr}} + \varepsilon_{\text{gp}}, \delta_{\text{tr}} + \delta_{\text{gp}})$-differential privacy. □

(3) *Thirdly*, we provide the proof that privacy amplification with subsampling still holds with the mechanism M: PrivateSelection∘GradientPerturbation.

Proof. Let S and $S' = S \cup \{i\}$ be two adjacent datasets. In each iteration, the algorithm partitions the samples into a tail subset and a body subset with probability p and $1 - p$, respectively. Each subset is then subsampled independently with sampling rates q_1 and q_2, leading to an effective average sampling rate

$$\bar{q} = pq_1 + (1 - p)q_2. \tag{164}$$

Let M' denote the composed mechanism including the private sorting step and the discriminative clipping step, which together satisfy $(\varepsilon_{\text{tr}} + \varepsilon_{\text{gp}}, \delta)$-DP on the full dataset.

To show $(\bar{q}(e^{\varepsilon_{\text{tr}}+\varepsilon_{\text{gp}}} - 1), \bar{q}\delta)$-DP, we have to bound the ratio with $S' = S \cup i$:

$$\frac{\mathbb{P}[M'(S) = Y] - \bar{q}\delta}{\mathbb{P}[M'(S') = Y]} = \frac{\bar{q}\mathbb{P}[M(S_B) = Y \mid i \in B] + (1 - \bar{q})\mathbb{P}[M(S_B) = Y \mid i \notin B] - \bar{q}\delta}{\bar{q}\mathbb{P}[M(S'_B) = Y \mid i \in B] + (1 - \bar{q})\mathbb{P}[M(S'_B) = Y \mid i \notin B]} \tag{165}$$

To prove that M' satisfies $(\bar{q}(e^{\varepsilon_{\text{tr}}+\varepsilon_{\text{gp}}} - 1), \bar{q}\delta)$-DP, we follow the standard subsampling argument. Let $B \subseteq [n]$ denote the indices of the subsampled data S_B and the neighbor dataset S'_B. The probability that i is included in B equals $\bar{q}$, composed of two disjoint events: $(i \in \text{tail}) \wedge (i \in B)$ and $(i \in \text{body}) \wedge (i \in B)$.

For convenience, define the following quantities:

$$C_{\text{tail}} = \mathbb{P}[M(S_B) = Y \mid i \in B, \text{tail}], \tag{166}$$

$$C_{\text{body}} = \mathbb{P}[M(S_B) = Y \mid i \in B, \text{body}], \tag{167}$$

$$C' = \mathbb{P}[M(S'_B) = Y \mid i \in B], \tag{168}$$

$$E = \mathbb{P}[M(S_B) = Y \mid i \notin B] = \mathbb{P}[M(S'_B) = Y \mid i \notin B]. \tag{169}$$

Then the overall probabilities can be expressed as

$$\mathbb{P}[M'(S) = Y] = pq_1C_{\text{tail}} + (1 - p)q_2C_{\text{body}} + (1 - \bar{q})E, \tag{170}$$

$$\mathbb{P}[M'(S') = Y] = \bar{q}C' + (1 - \bar{q})E. \tag{171}$$

Since both tail and body mechanisms satisfy $(\varepsilon_{\text{tr}} + \varepsilon_{\text{gp}}, \delta)$-DP, we have

$$C_{\text{tail}} \leq e^{\varepsilon_{\text{tr}}+\varepsilon_{\text{gp}}} \min\{C', E\} + \delta, \qquad C_{\text{body}} \leq e^{\varepsilon_{\text{tr}}+\varepsilon_{\text{gp}}} \min\{C', E\} + \delta. \tag{172}$$

Substituting the above inequalities, we obtain

$$\mathbb{P}[M'(S) = Y] \leq \bar{q}\big(e^{\varepsilon_{\text{tr}}+\varepsilon_{\text{gp}}} \min\{C', E\} + \delta\big) + (1 - \bar{q})E. \tag{173}$$

Dividing both sides by $\mathbb{P}[M'(S') = Y] = \bar{q}C' + (1 - \bar{q})E$ and applying the same algebraic manipulation as in the standard subsampling lemma, we get

$$\frac{\mathbb{P}[M'(S) = Y] - \bar{q}\delta}{\mathbb{P}[M'(S') = Y]} \leq e^{\bar{q}(\varepsilon_{\text{tr}}+\varepsilon_{\text{gp}})}. \tag{174}$$

Hence, M' satisfies $(\bar{q}(e^{\varepsilon_{\text{tr}}+\varepsilon_{\text{gp}}} - 1),\ \bar{q}\delta)$-DP. □

To sum up, Theorem 4.5 is proven.

H Supplemental Experiments

H.1 Implementation Details

All experiments are conducted on a server with an Intel(R) Xeon(R) E5-2640 v4 CPU at 2.40GHz and a NVIDIA Tesla P40 GPU running on Ubuntu. By default, we uniformly set subspace dimension $k = 200$, $\varepsilon = \varepsilon_{\text{tr}} + \varepsilon_{\text{gp}}$ with $\varepsilon_{\text{tr}} = \varepsilon_{\text{gp}}$, $p = 0.1$, and sub-Weibull index $\theta = 2$ for all datasets. In particular, we use the LDAM [14] loss function for heavy-tailed tasks. Besides, we set $c_2 = 0.1$, $B = 128$, and $\eta = 0.1$ for MNIST and FMNIST. For CIFAR10, we set $c_2 = 0.1$, $B = 256$, and $\eta = 1$. For ImageNette, we set $c_2 = 0.15$, $\eta = 0.0001$ and $B = 1000$. For E2E, we adopt the DPAdam optimizer and use the same settings as [48], where $c_2 = 0.1$. By default, we set $c_1 = 10 * c_2$, and the heavy-tailed proportion p is 0.1. We implement pre-sample clipping by BackPACK [18]. Specially, we list the implementation details by categorizing the dataset below.

- **MNIST**: MNIST has ten classes, 60,000 training samples and 10,000 testing samples. We construct a two-layer CNN network and replace the BatchNorm of the convolutional layer with GroupNorm. We set 40 epochs, 128 batchsize, 0.1 small clipping threshold, 1 large clipping threshold, and 1 learning rate.
- **FMNIST**: FMNIST has ten classes, 60,000 training samples and 10,000 testing samples. we use the same two-layer CNN architecture, and the other hyperparameters are the same as MNIST.
- **CIFAR10**: CIFAR10 has 50,000 training samples and 10,000 testing. We set 50 epoch, 256 batchsize, 0.1 small clipping threshold and 1 large clipping threshold with model SimCLRv2 [64] pre-trained by unlabeled ImageNet. We refer the code for pre-trained SimCLRv2 to https://github.com/ftramer/Handcrafted-DP.
- **CIFAR10-HT**: CIFAR10-HT contains 32×32 pixel 12,406 training samples and 10,000 testing samples, and the proportion of 10 classes in training samples is as follows: [0:5000, 1:2997, 2:1796, 3:1077, 4:645, 5:387, 6:232, 7:139, 8:83, 9:50]. We train CIFAR10-HT on model ResNeXt-29 [76] pre-trained by CIFAR100 with the same parameters as CIFAR10. We can see pre-trained ResNeXt in https://github.com/ftramer/Handcrafted-DP and CIFAR10-HT with LDAM-DRW loss function in https://github.com/kaidic/LDAM-DRW.
- **ImageNette**: ImageNette is a 10-subclass set of ImageNet and contains 9469 training samples and 3925 testing samples. We train on model ResNet-9 [34] without pre-train and set 1000 batchsize, 0.15 small clipping threshold, 1.5 large clipping threshold and 0.0001 learning rate with 50 runs.
- **ImageNette-HT**: We construct the heavy-tailed version of ImageNette by the method in [14]. ImageNette-HT contains 2345 trainging samples and 3925 testing samples, which is difficult to train, and proportion of 10 classes in training data follows: [0:946, 1:567, 2:340, 3:204, 4:122, 5:73, 6:43, 7:26, 8:15, 9:9]. The other settings are the same as ImageNette. Our ResNet-9 refers to https://github.com/cbenitez81/Resnet9/ with 2.5M network parameters.
- **E2E**: We have conducted experiments on transform-based NLP tasks for the dataset E2E with BLEU metric and GPT-2 model, which generates natural language from tabular data in the catering industry. We adopt the DPAdam optimizer and use the same settings as [48], where small clipping threshold $c_2 = 0.1$ and large clipping threshold $c_1 = 10 * c_2$.
- **MNLI**: We conduct experiments on RoBERTa Model. We also adopt the DPAdam optimizer and use the same settings as [6, 48], where small clipping threshold $c_2 = 0.1$ and large clipping threshold $c_1 = 10 * c_2$.
- **Tabular Dataset**: We evaluate our method on six representative tabular datasets, including Product, Breast Cancer, Android Malware, Adult (Census Income), Bank Marketing, and Credit Card Default (Taiwan). The Product Classification and Clustering dataset contains 24,794 training samples and 6199 test samples with 7 textual attributes, where the 10-class classification task distinguishes products from different categories collected from 306 merchants on the PriceRunner platform. The Breast Cancer dataset contains 569 samples with 30 continuous attributes, where the binary classification task distinguishes malignant from benign tumors. The Android Malware dataset includes 4,464 samples extracted from Android applications, labeled as benign or malicious. The Adult (Census Income) dataset comprises 48,842 samples and aims to predict whether an individual belongs to the higher-income group. The Bank Marketing dataset contains 4,521 samples with 16 client and campaign-related features, where the task is to predict whether a customer will subscribe to a term deposit. Finally, the Credit Card Default (Taiwan) dataset includes 30,000 samples with 23 attributes and predicts whether a customer will default on credit card payments in the following month. All categorical features are one-hot encoded, and continuous features are normalized. Each dataset is randomly split into 80% training and 20% testing sets. We apply the DPSGD configuration with clipping threshold $c_2 = 0.1$, $c_1 = 1$, batch size 64, learning rate 0.1-0.5.

Moreover, we open our source code and simplified version for discriminative clipping on the following link: https://anonymous.4open.science/r/Discriminative_Clipping_DPSGD-1FE6.

H.2 Training Trajectory of DC-DPSGD

To provide intuitive evidence of the optimization performance during the training, we further demonstrate the trajectories of training accuracy using MNIST with $\varepsilon = 8$ in Figure 7, which clearly reveal the evolutionary pattern of model learning across epochs and highlight how different clipping strategies affect convergence behavior. These trajectories serve as an important diagnostic tool for understanding the stability and efficiency of private optimization, showing that DC-DPSGD achieves faster convergence, smoother training dynamics, and consistently higher accuracy compared to existing clipping mechanisms.

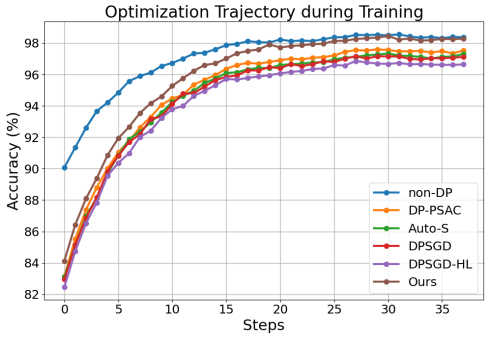

Figure 7: Optimization performance of DC-DPSGD.

H.3 Non-DP Effectiveness Experiment

We further conduct experiments in the non-DP setting, as reported in Tables 8, 9, and Table 10. The results show that our method still outperforms light-tailed baselines even without privacy constraints, since these methods typically rely on relatively small clipping thresholds, which introduce non-negligible clipping bias.

In the non-DP regime, our method performs slightly worse than vanilla SGD. This behavior is expected, as SGD effectively corresponds to using an infinite clipping threshold and therefore incurs no clipping loss. Notably, our method achieves performance comparable to DPSGD-HL in the non-DP setting. DPSGD-HL can be interpreted as employing a uniform clipping threshold that is close to (or even larger than) our upper threshold c_1, i.e. $c_{\text{DPSGD-HL}} \geq c_1$, which leads to a relatively small clipping loss and hence better utility when no privacy noise is added. However, this advantage does not carry over to the practical DP setting.

Importantly, the observations of DPSGD-HL also indicate that our stair-wise discriminative clipping strategy, with two thresholds c_1 and c_2, incurs a clipping loss that is nearly as small as that of DPSGD-HL using a single large threshold $c_{\text{DPSGD-HL}} \geq c_1$. This demonstrates the effectiveness of our method, providing evidence that using the larger threshold c_1 only for tail gradients, together with a smaller threshold c_2 for body gradients, is both adequate and well justified. At the same time, in the DP setting, our approach substantially reduces the amount of DP noise injected into the body gradients, as the noise scale is determined by the smaller threshold c_2, leading to improved trade-offs between privacy and utility.

Table 8: Test accuracy (%) comparison between DC-DPSGD and baselines on image datasets.

Algorithm	Privacy	MNIST	FMNIST	CIFAR10	ImageNette	CIFAR10-HT / ImageNette-HT
DPSGD	$\varepsilon = \infty, \delta = 1/n^{1.1}$ Non-DP	98.16±0.06	84.03±0.08	93.69±0.08	68.61±0.42	63.22±0.68 / 36.62±1.07
Auto-S		98.20±0.11	83.86±0.10	93.59±0.03	68.90±0.26	62.86±0.92 / 35.14 ±0.86
DP-PSAC		98.20±0.06	84.18±0.15	93.70±0.01	67.89±0.48	62.87±0.94 / 36.84±0.84
DPSGD-HL		98.54±0.06	85.25±0.05	94.28±0.08	70.86±0.84	67.11±0.56 / 39.09±0.73
Ours (DC-DPSGD)		98.44 ±0.10	84.92±0.18	94.21±0.06	70.32±0.48	66.57±1.22 / 38.78±1.04
SGD (Non-clipping)		**99.10±0.02**	**89.95±0.32**	**94.62±0.03**	**72.98±0.50**	**71.74±0.65/39.91±1.46**

Table 9: BLEU (%) and test accuracy (%) of DC-DPSGD on natural language dataset.

Algorithm	Privacy	E2E Full	E2E LoRA	MNLI Full
DPSGD	$\varepsilon = \infty$ $\delta = \frac{1}{n^{1.1}}$	69.463	69.692	80.72
Auto-S		69.463	69.682	80.50
DP-PSAC		69.473	69.692	80.50
DPSGD-HL		69.528	70.155	81.40
Ours		69.528	70.073	81.10
SGD		**69.682**	**70.189**	**81.90**

Table 10: Test accuracy (%) comparison between DC-DPSGD and baselines on tabular datasets.

Algorithm	Privacy	Product	Malware	Cancer	Adult	Bank	Credit
DPSGD	$\varepsilon = \infty$ $\delta = \frac{1}{n^{1.1}}$	95.45	99.55	96.49	85.55	89.94	81.95
Auto-S		95.47	99.33	96.49	85.54	89.72	81.95
DP-PSAC		95.50	99.55	95.61	85.62	89.72	82.08
DPSGD-HL		96.73	99.87	97.70	86.04	90.95	82.67
Ours		96.11	99.78	97.36	85.79	90.26	82.44
SGD		**97.50**	**99.87**	**98.80**	**90.07**	**91.80**	**85.05**

H.4 Ablation Experiments

We have included the remaining parameter ablation experiments in the appendix. For MNIST, FMNIST, ImageNette and ImageNette-HT, we evaluate the effects of four parameters on test accuracy in Table 11, Table 12, and Table 13, including the subspace-k, the allocation of privacy budget ε, the heavy tail index sub-Weibull-θ, and the heavy tail proportion p, with other parameters kept at default. The experimental results

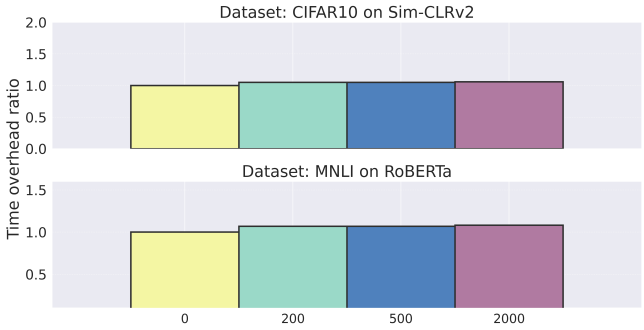

Figure 8: Efficiency Experiments on Subspace Identification of DC-DPSGD.

are consistent with our discussion on CIFAR10 in main text. To investigate the effect of p, we have added a set of new experiments by varying $p \in [0.01, 0.2]$. The results are presented in Table 13. We observe that the test accuracy is minimally affected when p is less than 0.1, but shows a negative impact at around 0.2. We believe that the proportion of heavy-tailed samples aligns with statistical expectations. Assigning larger clipping thresholds to more light-body samples introduces more noise, while conservatively estimating heavy-tails does not fully exploit the algorithm's potential. Additionally, we acknowledge that since ImageNette-HT has only 2,345 training data, which is one-fifth of ImageNette, it is difficult to support the convergence of the model. In the future, we will improve this aspect in our work.

Time Overhead. In addition, since we employ random projections instead of performing expensive principal component analysis, our identification method has a time complexity of $\mathbb{O}(dk)$ and introduces only a modest computational overhead. We evaluate this overhead across different model architectures by varying the projection dimension k from 0 to 2000, where $k = 0$ serves as the baseline without subspace identification. Empirically, for smaller models, our method incurs an additional overhead of around 5%, while larger models exhibit higher yet still acceptable computational overhead (about 8%) due to their increased dimensionality. This trend is expected, as the cost of random projection scales linearly with both the ambient dimension d and the chosen subspace dimension k. Nevertheless, even for large-scale models, the observed overhead remains within a practical range and does not dominate the overall training cost. Throughout all experiments, the trigger frequency is fixed to 1 to ensure consistent and fair comparisons across different settings.

Table 11: Effects of parameters on test accuracy with MNIST and FMNIST with $\varepsilon = 8$.

Dataset	Subspace-k				ε_{tr} / ε			sub-Weibull-θ		
	None	100	150	200	0.2/8	0.4/8	0.8/8	1/2	1	2
MNIST	97.33	97.86	97.95	98.14	97.97	98.14	98.02	97.90	98.06	98.14
FMNIST	83.56	84.62	84.70	84.76	84.62	84.76	84.72	84.05	84.41	84.76

Table 12: Effects of parameters on test accuracy with ImageNette and ImageNette-HT with $\varepsilon = 8$.

Dataset	Subspace-k				ε_{tr} / ε			sub-Weibull-θ		
	None	100	150	200	0.2/8	0.4/8	0.8/8	1/2	1	2
ImageNette	64.98	65.34	66.52	67.66	65.23	67.66	66.12	65.91	66.28	67.66
ImageNette-HT	31.33	35.44	36.17	36.72	35.65	36.72	36.11	35.75	36.37	36.72

Table 13: Effects of parameter on p with ImageNette and $\varepsilon = 8$.

Dataset	Heavy tail Proportion-p				
	0.2	0.1	0.05	0.02	0.01
ImageNette	66.82	67.66	66.02	66.14	65.89

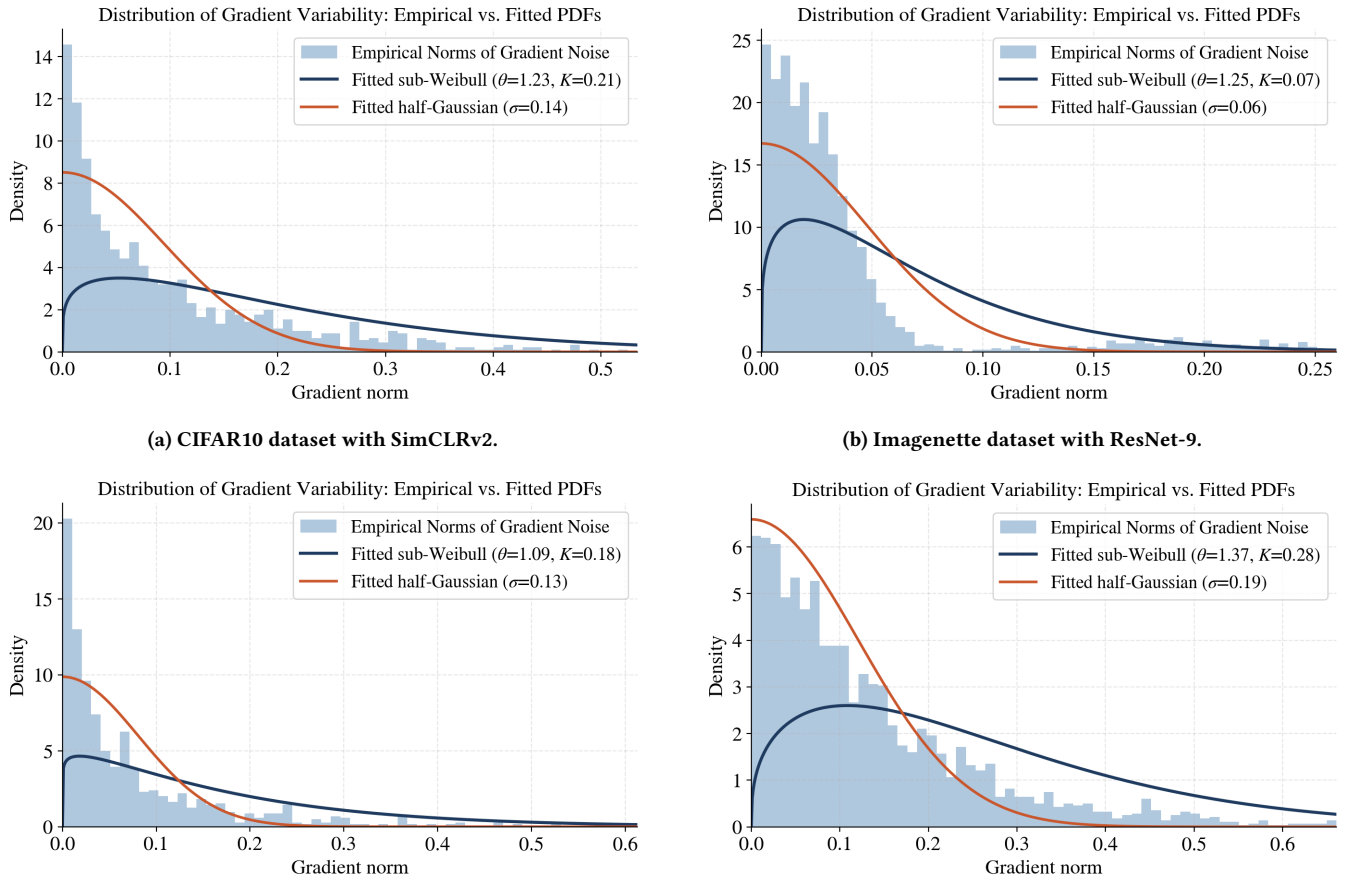

(a) CIFAR10 dataset with SimCLRv2.

(b) Imagenette dataset with ResNet-9.

(c) Credit card dataset with MLP.

(d) E2E dataset with GPT-2.

Figure 9: Sub-Weibull simulation of gradient variability.

H.5 Simulation Experiment

In the appendix, we conduct the simulation experiment to characterize the empirical distribution of gradient variability $\|\nabla \ell(\mathbf{w}_t, z_{j_t}) - \nabla L_S(\mathbf{w}_t)\|_2$ on several realistic datasets, including CIFAR-10, Imagenette, tabular datasets, and E2E. We emphasize that these quantities correspond to the L_2 norm of gradient variability rather than raw gradients, and are therefore non-negative. As a result, the empirical distribution is one-sided, with its upper tail reflecting the magnitude of gradient deviations. In our experiments, we fit the per-sample gradient variability using a sub-Weibull distribution, with parameters estimated from the upper tail via quantile-initialized maximum likelihood estimation, and compare the results against a sub-Gaussian fit. The estimated shape parameter θ and scale parameter K quantify the degree of tail heaviness. All simulations are conducted at the early stages of training, as gradient clipping and parameter updates during this phase have a disproportionate impact on the overall optimization trajectory and final model performance.

As shown in Figure 9, across most datasets and model architectures, the empirical gradient variability exhibits a clear transition from light-tailed to heavy-tailed behavior. Specifically, the centrally concentrated region aligns closely with a sub-Gaussian fit, while this fit progressively deviates in the tail region, which is more accurately captured by a sub-Weibull distribution with $\theta > 1$. Relying solely on a sub-Gaussian assumption would overlook a substantial number of tail outliers, potentially leading to insufficient training and excessive clipping loss. These observations provide empirical evidence supporting the practical validity of our sub-Weibull assumption. Moreover, since the sub-Weibull family naturally subsumes the sub-Gaussian distribution as a special case, it enables us to optimize clipped DPSGD within a unified theoretical framework.